Photoinduced dynamics in hydrogen-bonded rotaxanes

Wurpel, G.W.H.

Publication date
2001
Document Version
Final published version

Photoinduced Dynamics in Hydrogen-Bonded Rotaxanes

Photoinduced Dynamics in Hydrogen-Bonded Rotaxanes

ACADEMISCH PROEFSCHRIFT

ter verkrijging van de graad van doctor
aan de Universiteit van Amsterdam
op gezag van de Rector Magnificus Prof. Dr. J.J.M. Franse
ten overstaan van een door het College voor Promoties
ingestelde commissie, in het openbaar te verdedigen
in de Aula der Universiteit
op 3 juli 2001 te 11.00 uur

door

George Willem Hendrik Wurpel
geboren te Den Helder

Promotiecommissie

Promotor	Prof. Dr. J.W. Verhoeven
Co-Promotor	Dr. A.M. Brouwer
Overige leden	Prof. Dr. D.A. Leigh
	Dr. C. Frochot
	Prof. Dr. R.J.M. Nolte
	Prof. Dr. J.W. Hofstraat
	Prof. Dr. W.J. Buma
	Prof. Dr. L. De Cola
	Dr. R.M. Williams

Het onderzoek beschreven in dit proefschrift werd uitgevoerd in het Laboratorium voor Organische Scheikunde binnen de faculteit der Natuurwetenschappen, Wiskunde en Informatica van de Universiteit van Amsterdam.

Dit werk kwam tot stand met financiële ondersteuning van de Nederlandse Organisatie voor Wetenschappelijk Onderzoek (NWO) en een Training and Mobility of Researchers (TMR) programma van de Europese Unie: het Development of Rotaxane-based Unconventional Materials (DRUM) project.

Omslagontwerp: Paula van der Heijdt, De Grafische Werkkamer, Amsterdam

Drukwerk: Ponsen & Looijen, Wageningen

ISBN 90-9014806-X

Contents

1 ROTAXANES **1**
From chemical curiosities to molecular machines

1.1 The Rediscovery of the Wheel 1
1.2 Early Synthetic Approaches 3
1.3 Catenanes in Nature. 4
1.4 Supramolecular Chemistry 5
1.5 Template Directed Synthesis 6
1.6 Rotaxanation Effects 9
1.7 Shuttling and Pirouetting. 10
1.8 Molecular Machines: an Intermezzo. 11
1.9 Rotaxanes as Molecular Machines 13
1.10 Photoaddressable Rotaxanes 16
1.11 Biomolecular Machines 18
1.12 Scope of this Thesis 22
1.13 References 23

2 BIXIN ROTAXANES **31**
Electronic effects caused by rotaxanation of a natural polyene

2.1 Introduction. 31
2.2 Experimental 33
2.3 Electronic Structure 33
2.4 Bixin Solvatochromism 35
2.5 Conclusions 38
2.6 References 38

3 ELECTRON TRANSFER IN ROTAXANES **41**
Signalling of the macrocycle's position by electron transfer quenching of a fluorescent stopper

3.1 Introduction. 41
3.2 Experimental 45
3.2.1 Fluorescence Measurements 45

3.2.2 Synthesis . . . 45
3.2.3 Irradiation Experiments . . . 46
3.3 Solvent-Switchable Rotaxanes . . . 47
3.3.1 Structural Characteristics . . . 47
3.3.2 Electron Transfer Thermodynamics and Kinetics . . . 48
3.3.3 Steady State Fluorescence . . . 51
3.3.4 Time Resolved Fluorescence . . . 53
3.3.5 Solvent Induced Switching . . . 57
3.4 Photocleavable Rotaxane . . . 58
3.4.1 Solution Phase Irradiation . . . 59
3.4.2 Solid Support Irradiation . . . 61
3.5 Conclusions . . . 62
3.6 References . . . 63

4 ANTHRACENE ROTAXANES **67**
Sub-nanosecond excited state dynamics in a peptide based, hydrogen-bonded molecular shuttle

4.1 Introduction . . . 67
4.2 Experimental . . . 68
4.3 Results and Discussion . . . 69
4.3.1 Structural Characteristics . . . 69
4.3.2 Steady State Fluorescence . . . 71
4.3.3 Temperature and Matrix Effects . . . 74
4.3.4 Time Resolved Fluorescence . . . 75
4.3.5 Mechanism . . . 77
4.4 Conclusions . . . 78
4.5 References . . . 79

5 STOCHASTIC DYNAMICS SIMULATIONS **81**
Analysis of hydrogen bond patterns and steric effects in an anthracene stoppered, peptide based rotaxane

5.1 Introduction . . . 81
5.2 Computational Details . . . 83
5.3 Conformational Searches . . . 86
5.3.1 Introduction . . . 86
5.3.2 The MMFFs Force Field . . . 88
5.3.3 The OPLS-AA Force Field . . . 90

5.3.4 The AMBER* Force Field . . . 92
5.3.5 Comparison of Conformations . . . 92
5.4 Stochastic Dynamics Simulations . . . 94
5.5 Effect of Anthracene-Carbonyl Dihedral Angle . . . 97
5.6 Discussion of the Model . . . 100
5.7 Conclusions . . . 101
5.8 References . . . 102

6 NAPHTHALIMIDE ROTAXANES **105**
Photoinduction of Fast, Reversible Translational Motion in a Hydrogen-Bonded Molecular Shuttle

6.1 Introduction . . . 105
6.2 Experimental . . . 107
6.3 Results and Discussion . . . 108
6.3.1 Structural Characteristics . . . 108
6.3.2 Electrochemistry . . . 110
6.3.3 Photoreduction Strategy . . . 112
6.3.4 Naphthalimide Photophysics . . . 112
6.3.5 Electron Transfer to Triplet Naphthalimide . . . 116
6.3.6 Transient Absorption Shift . . . 119
6.3.7 Solvent and Temperature Effects . . . 120
6.3.8 Mechanism . . . 122
6.4 Conclusions . . . 124
6.5 Appendix: Relation Between Peak Shift and Population Change . . . 125
6.6 References . . . 128

SUMMARY **133**

SAMENVATTING **137**

DANKWOORD **141**

Chapter 1

ROTAXANES

From chemical curiosities to molecular machines

> *"What I want to talk about is the problem of manipulating and controlling things on a small scale. As soon as I mention this, people tell me about miniaturization, and how far it has progressed today. They tell me about electric motors that are the size of the nail on your small finger. And there is a device on the market, they tell me, by which you can write the Lord's Prayer on the head of a pin. But that's nothing; that's the most primitive, halting step in the direction I intend to discuss. It is a staggeringly small world that is below. In the year 2000, when they look back at this age, they will wonder why it was not until the year 1960 that anybody began seriously to move in this direction."*
>
> – Richard P. Feynman, There's Plenty of Room at the Bottom (1959)

1.1 The Rediscovery of the Wheel

Chemists have always tried to rebuild well known forms and shapes on a molecular level: basketene, cubane, diamantane, helicene, and twistane are only a few of the many aesthetically pleasing molecules that have been created in the past.[1] In this Thesis, the fascinating properties of structures that resemble a wheel will be discussed. This class of compounds is called *rotaxanes*, after the Latin words for wheel (*rota*) and axle (*axis*), and in contrast to the aforementioned structures, rotaxanes are not defined by one single molecule, but consist of at least

two molecules. It is the specific 3-dimensional entanglement of an axle molecule with one or more wheel molecules that makes rotaxanes unique.

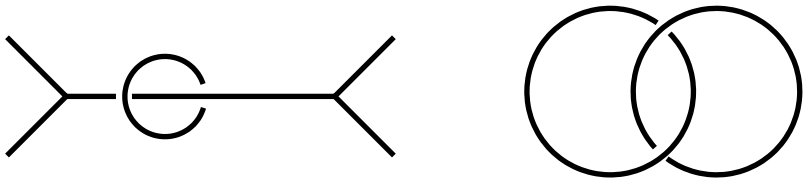

Rotaxane Catenane

Consideration of rotaxane structure brings us within the realm of *chemical topology*, a concept that was introduced in the 1960s by Frisch and Wasserman.[2] They realised that the structure of a molecule is *not* described sufficiently by (i) the order in which given numbers of specific atoms are joined, (ii) the types of bonds which connect them, and (iii) the spatial arrangement around rigid centres such as asymmetric atoms and double bonds. One should also make a *topological* distinction between molecules or molecular assemblies. Two macrocyclic molecules, *e.g.* can form several topoisomers: these rings can exist separately or can be interlocked. In the latter case, they are said to be mechanically bonded in a structure known as catenane (from the Latin *catena*, which means chain). A single macrocycle in its own right can furthermore exist as a simple loop or as a knot within a loop, in the simplest case a trefoil.

In rotaxanes, there is a mechanical bond between an acyclic molecule (thread), and one or more molecular rings. For such an interlocked system to be thermally stable, the ring must be prevented from slipping off the thread by endcapping the thread with bulky groups. Because in principle the macrocycle can still slip over the stoppers without breaking bonds, formally a rotaxane is not a topological isomer of its separate constituents. Without these stoppers the system is sometimes referred to as *pseudo-rotaxane*, even though it can just as well be named a pseudo-catenane, and strictly speaking, there is no difference with a molecular complex. For both catenanes and rotaxanes, a number in square brackets indicates the number of molecular entities in the nomenclature: a [2]catenane, *e.g.* consists of two rings and a [3]rotaxane of one thread and two macrocycles. Since in this Thesis only [2]rotaxanes are discussed, it is convenient to omit this index and refer to them as "rotaxanes".

Figure 1-1. Two cycloenantiomeric forms of a [2]rotaxane. The different atom sequence of the macrocycle with respect to the thread creates this type of chirality.

A special property that can occur in intertwined and knotted structures is *topological chirality*.[2] A molecule or molecular assembly is topologically chiral if and only if no contin-

uous deformation in three dimensional space converts it to its mirror image.[3] This is illustrated for rotaxanes in Figure 1-1: the macrocycle and thread are not chiral themselves, but the mechanically connected assembly is. These rotaxanes are said to be *cycloenantiomers*. Synthesis and separation of a cycloenantiomeric [2]rotaxane[4] and a [3]rotaxane[5] was first accomplished by Vögtle and co-workers.

The world of molecular topology contains an endless reservoir of appealing structures, providing an everlasting source of inspiration for chemist and mathematicians alike. More complex structures can be constructed by interlocking more rings, but also by twisting (Möbius ladders) or knotting.[3,6,7] To actually synthesise these structures, of course, remains a formidable challenge to the chemist, and we will now look at the synthetic approaches that have been used to create these structures.

1.2 Early Synthetic Approaches

Historically, the development of synthetic strategies to make a rotaxane has always been preceded by the synthesis of a similar catenane. The higher symmetry and the biological relevance (see Section 1.3) of catenanes is likely to be the reason for this. In order to understand the routes that lead to rotaxanes, we will also discuss catenane synthesis.

The first successful synthesis of a catenane (**1**), was accomplished using a statistical approach:[8] a cyclisation of a 34-membered ring was performed in the presence of a deuterium labelled 34-membered ring. Structural evidence that indeed a catenane was formed, included IR, chromatographic behaviour, m.p. and mixed m.p. of **1** and its degradation products.

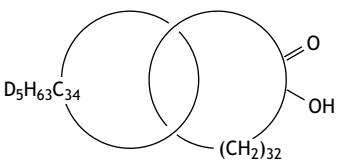

1

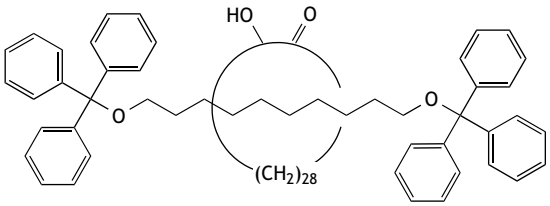

2

Using the same statistical approach Harrison and Harrison synthesised the first rotaxane* (**2**).[9] They demonstrated that a C_{30} ring bound to a Merrifield resin could be threaded by a decane-1,10-diol, and consecutively locked by reacting it with triphenylmethyl chloride to the 1,10-diether. After repeating this threading and locking treatment 70 times, they achieved a yield of rotaxanation of 6%. The statistical threading approach was further developed to gain yields of approximately 10%.[10,11]

*They suggested the name *hooplane*, but this was not adopted by others.

The simplicity and versatility of the statistical approach, makes it a useful synthetic strategy that is only hampered by inherently low yields. To overcome this problem Schill and coworkers developed target directed syntheses for rotaxanes and catenanes.[12] The first rotaxane made by this method (**4**) was formed from a pre-rotaxane (**3**) that was synthesised in 18 steps (overall yield 0.07%).[13]

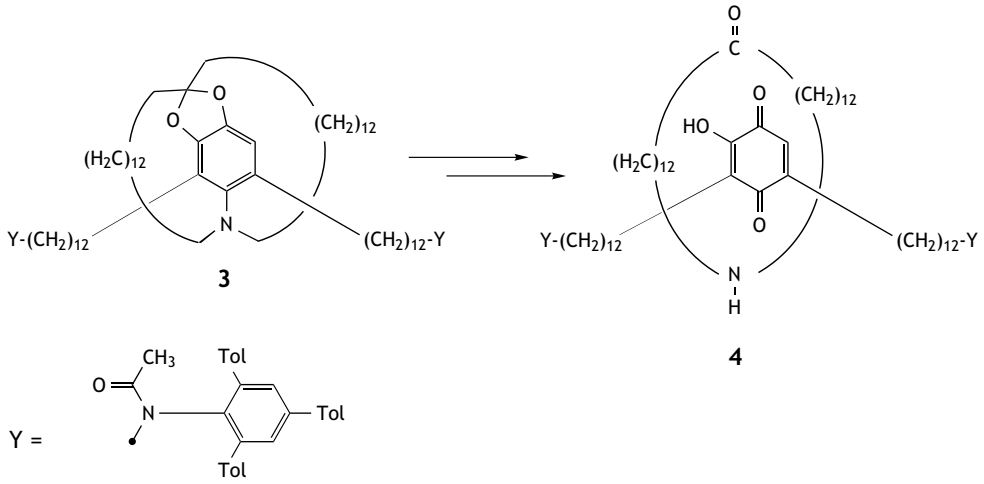

Although the yield of the total synthesis of a rotaxane can be improved, and in principle allows for easy derivation, this method has not been copied by other researchers, because simpler, and more efficient methods became available (Section 1.5).

1.3 Catenanes in Nature

When Wasserman reported the first synthesis of a catenane in 1960[8] this system seemed nothing more than a curiosity. However, already in 1963 it was found that DNA in bacteriophage λ could form macrocycles with a contour length of *circa* 170,000 Å.[14] Such a large ring can easily be interpenetrated, and indeed in 1967 the first example of catenated closed circles of DNA were discovered in HeLa cell mitochondria.[15,16] Soon thereafter catenane structures were found in many other circular DNA molecules.[17]

It was quickly realised that catenanes could be formed upon replication of circular DNA.[18] The implications for the biological function of DNA are clear: if parent and daughter circular DNA are mechanically trapped as a catenane after the replication process, the genetic information can not be moved into a new cell. To solve this problem, nature invented a family of enzymes termed *DNA topoisomerases*, that catalyse the interpenetration of DNA strands or double helices.[19] In their presence, DNA strands and double helices can go through one another as if there were no physical boundaries in between. This function is essential to solve the topological problems associated with DNA replication, because cate-

nated DNA is only one of the possible topoisomers of DNA: it can also be knotted or supercoiled,[6] much like a telephone cord.

Besides naturally occurring topological structures in DNA, linear DNA has also been used as a building block for the synthesis of artificial topologically complex molecules. Seeman and co-workers have utilised the fact that DNA can form well-behaved right-handed (B) or left-handed (Z) double helical structures to build a variety of catenanes, knots and larger geometrical shapes.[7,20-22]

1.4 Supramolecular Chemistry

The catenanes and rotaxanes described thusfar have one thing in common: the separate molecules that form the interlocked assembly do not interact in a way that significantly affects their chemical properties. One could say that they are holding each other, but do not feel it. The IR spectra of **1** and **2** *e.g.* are indistinguishable from the sum of their constituents; the only property that really changes upon interlocking is the molecular mass. The notion evolved that when the separate molecules would have some (directional) interactions, much more efficient synthesis, based on molecular recognition, could be developed. But more importantly, these molecules could be made to perform certain unique functions.

The inspiration for this line of thought came from *supramolecular chemistry*, a concept that was introduced in 1978 by Jean-Marie Lehn.[23] The objects of supramolecular chemistry are supramolecular entities, *supermolecules* possessing features as well defined as those of molecules themselves. Supramolecular species are characterised both by the spatial arrangement of their molecular components, their architecture or superstructure, and by the nature of the intermolecular bonds that hold these components together.[24]

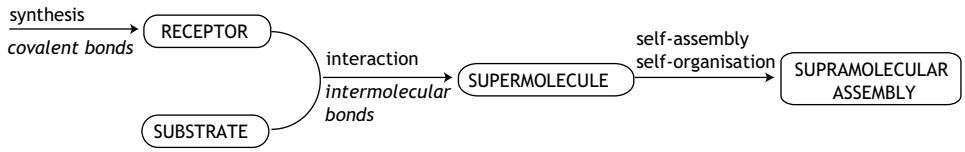

Figure 1-2. From molecular to supramolecular chemistry: the intermolecular interaction between receptor and substrate molecules gives rise to a supermolecule, which in turn can self-assemble into supramolecular structures. Adopted from Lehn.[24]

The hierarchy of this "chemistry beyond the molecule" is depicted in Figure 1-2. The nomenclature of substrate and receptor clearly is reminiscent of the early days of supramolecular chemistry, when major attention was paid to molecular recognition. Usually the larger of the two molecules that form intermolecular bonds is considered the receptor. Obviously for catenanes and rotaxanes this convention is less useful.

According to the diagram in Figure 1-2 catenanes and rotaxanes should be considered *supermolecules*, since they are well-defined, discrete oligomolecular species that result from the intermolecular association of a few components. Vesicles, micelles, films, and solid state

structures, then are examples of *supramolecular assemblies*, characterised by the spontaneous association of a large number of components.

1.5 Template Directed Synthesis

To synthesise rotaxanes or catenanes using supramolecular concepts, one needs to organise the molecular components in a specific 3-dimensional configuration. This so-called template directed synthesis can use a variety of intermolecular interactions. The common feature for all these rotaxanes is the binding site that is present on the thread molecule: the *station*. This provides a preferential position for the macrocycle, which at the same time assists in the synthesis.

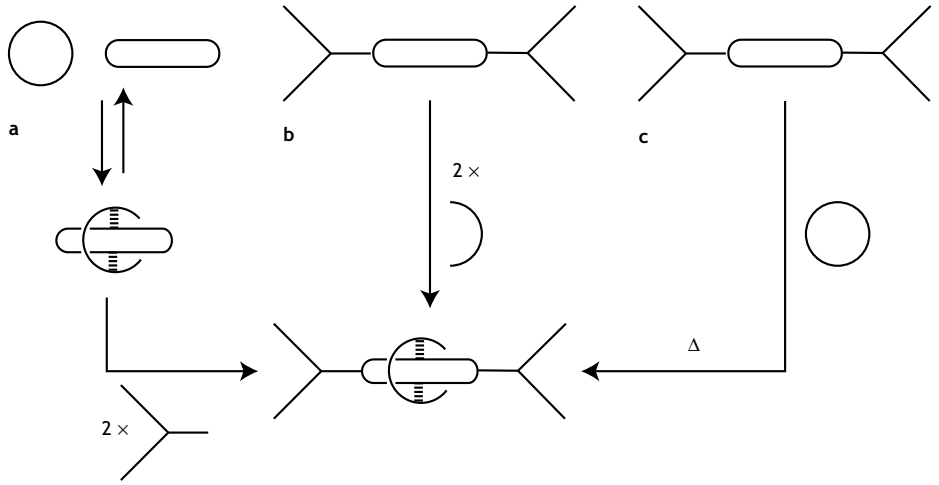

Figure 1-3. Synthetic template directed approaches to rotaxanes: *threading* (a), *clipping* (b), and *slipping* (c).

In the absence of stoppers, the macrocycle and station will form an intermolecular assembly. Because of the intermolecular interactions, the chances that such a complex is present in solution are much higher than they are based on purely statistical encounters (see Section 1.2). Endcapping the thread by bulky groups then affords a rotaxane (Figure 1-3a). This synthetic approach is called *threading*, as opposed to *clipping* (Figure 1-3b) and *slipping* (Figure 1-3c), where the macrocycle is formed around or slided onto a dumbbell-shaped thread.

Several types of intermolecular interactions have been employed in rotaxane synthesis, each of which is more or less associated with certain research groups.[7] The group of Stoddart has made extensive use of π-stacking between electron deficient and electron rich aromatic groups (Figure 1-4a),[25-29] whereas the Sauvage group has employed metal to ligand co-ordination (Figure 1-4b).[30-33] Hydrogen-bonding interactions have been put to use by Vögtle

(Figure 1-4c),[34,35] and Stoddart and Balzani (Figure 1-4d).[36-38] A fourth type of rotaxanes (not shown), made by several groups, is based on hydrophobic interactions, using mainly cyclodextrin macrocycles.[39]

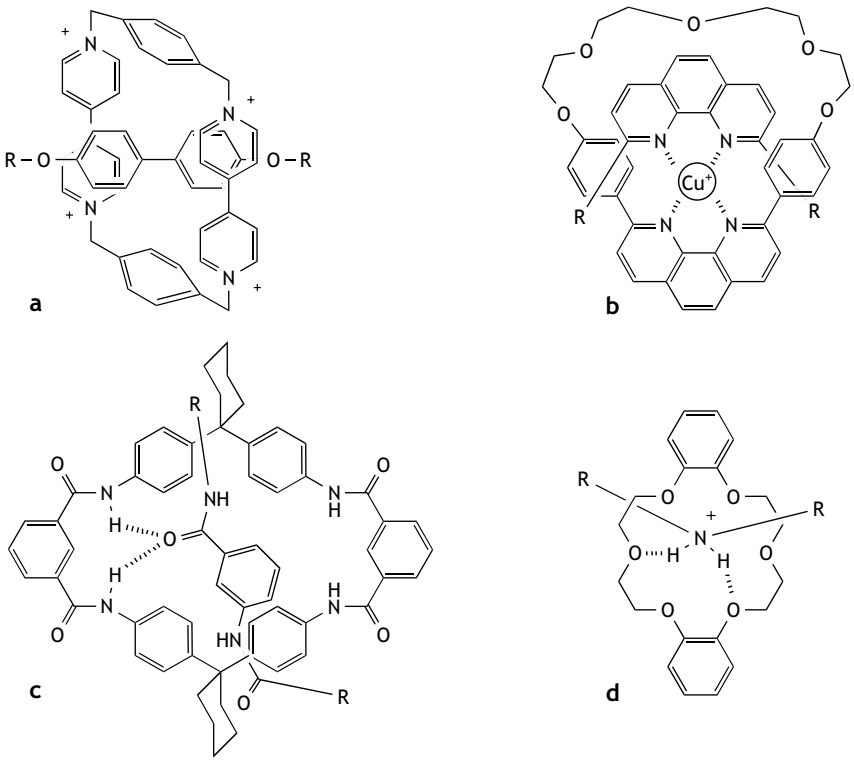

Figure 1-4. Examples of intermolecular binding motifs between a station and a macrocycle: π-stacking between electron rich and electron deficient aromatic moieties (a), metal to ligand co-ordination (b), and hydrogen bonds (c and d).

The rotaxanes discussed in this Thesis are also of the hydrogen-bonding type, and are synthesised by the group of Leigh.[40] The hydrogen-bonding motifs they use to synthesise both catenanes and rotaxanes, were discovered by serendipity in 1995. A condensation reaction between *p*-xylylenediamine and isophthaloyl dichloride was carried out to make a macrocycle (Figure 1-5, **5**) as a potential receptor for CO_2. Instead, the reaction yielded a catenane (**6**) as the sole isolable product, the tetra-amide macrocycle being intractable from a precipitate of cyclic oligomers and polymers.[41,42] By adding a dumbbell-shaped thread with a glycylglycine binding station to the reaction mixture, the macrocycle was found to be formed around the binding site in a 5-component clipping reaction (Figure 1-5, **7**).[43] This rotaxanation prevents the tetra-amide ring from forming intermolecular hydrogen-bonding net-

works, and can thus be used to enhance the solubility of the macrocycle. Thus, macrocycle **5** could be isolated after all by selectively cleaving the thread in a suitable rotaxane.[44]

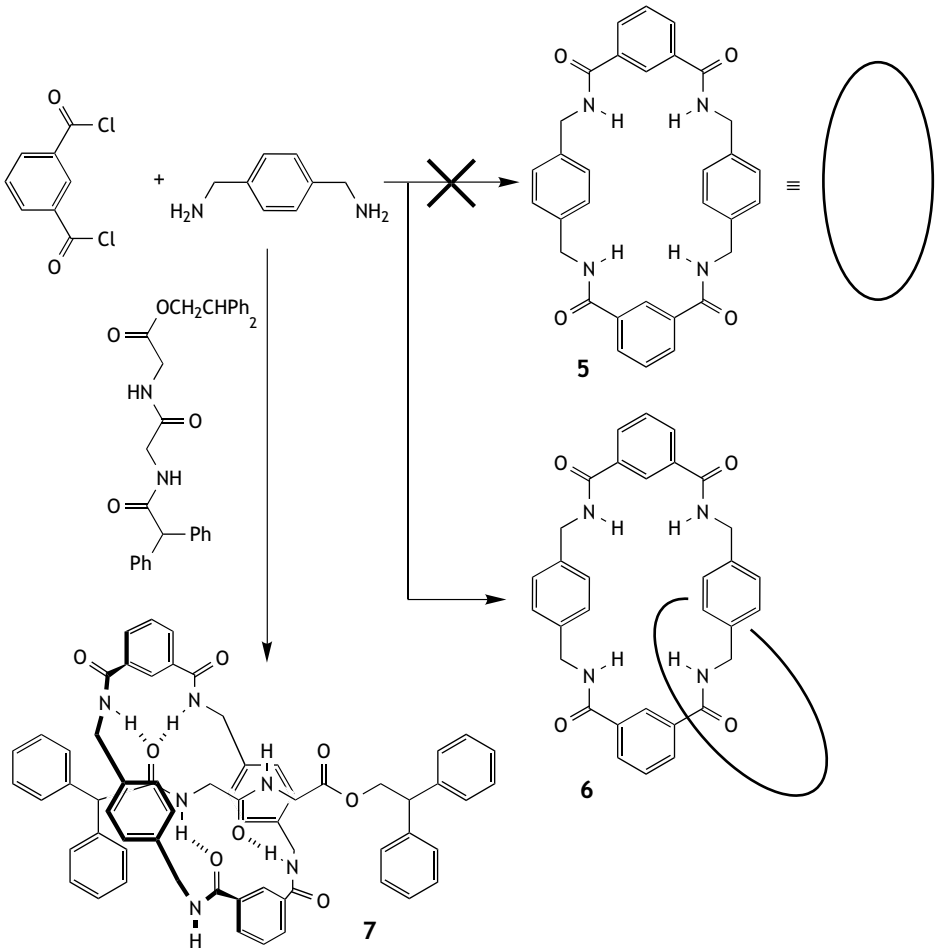

Figure 1-5. [2]catenane **6** is the only product isolable from the condensation of *p*-xylylenediamine and isophthaloyl dichloride. The tetra-amide macrocycle **5** is intractable from a mixture of other precipitated cyclic oligomers and polymers.[41,42] When a thread containing a glycylglycine binding station is present, a rotaxane (**7**) is formed.[43]

This synthetic method to form rotaxanes is simple and versatile at the same time, but is critically dependent on the binding station. For it to function as a good template in the rotaxanation reaction, it must satisfy the hydrogen-bonding needs of the macrocycle. It has been shown that specifically the hydrogen-bond-accepting sites in the thread are important.[43] Two carbonyl or nitrone groups, separated by three bonds, and pointing in opposite direction (Figure 1-6) promote high rotaxane yields, for they allow in principle two sets of bifur-

cated hydrogen bonds to the macrocycle's N-H groups to be formed. Hydrogen-bonds between the macrocycle's C=O groups and the thread can also be formed, but these are usually fewer and are not essential for the rotaxanation step.[45]

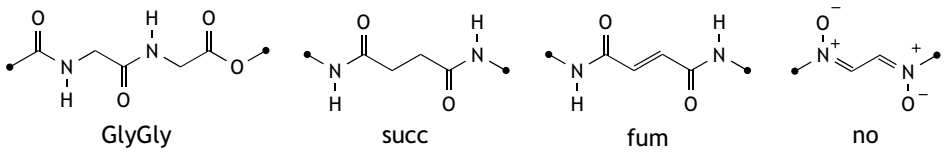

Figure 1-6. Efficient binding stations for rotaxane formation: glycylglycine (GlyGly),[43] succinamide (succ, see Chapter 6), fumaramide (fum), and nitrone (no).[46]

Derivatisation of the macrocycle in a rotaxane can be accomplished by substituting *p*-xylylenediamine or isophthaloyl dichloride for other diamines or diacid chlorides. In the compounds described in this Thesis only the diacid chlorides were varied, and some typical derivatives are shown in Figure 1-7. Further transformations after formation of the rotaxane include protonation and alkylation of the pyridine group.

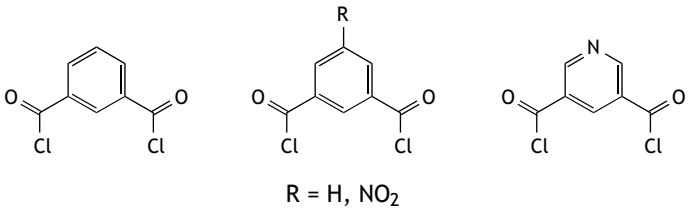

Figure 1-7. The isophthaloyl dichloride building block and some variations.

1.6 Rotaxanation Effects

A number of physical properties change upon rotaxanation. One was already mentioned in Section 1.5, namely the increased solubility of a hydrogen-bonded rotaxane with respect to its separate constituents.[44] Due to the formation of intercomponent H-bonds, the tendency to aggregate is diminished. In other ways the macrocycle can also protect the thread from the environment: rotaxanes where one or two cyclodextrin macrocycles interlocked with polyene chromophores have been shown to enhance fluorescence and photostability of the thread, by shielding it from the surrounding water molecules.[47,48] A cucurbituril macrocycle could even act as a catalyst in a 1,3-dipolar polymerisation reaction by providing a hydrophobic interior for a self-threading reaction that forms a polyrotaxane.[49]

Another physical property that usually changes significantly upon rotaxanation is the chemical shift in NMR spectra. This so-called complexation induced shift (CIS)[50] derives *e.g.* from aromatic shielding effects or hydrogen bonding between separate components of the rotaxane. Such effects are short ranged and therefore can be used to determine the relative

position and orientation of the macrocycle with respect to the thread. Because in many cases dynamic processes in rotaxanes such as shuttling and pirouetting (see Section 1.7) take place at time scales comparable to those of NMR, this technique can also provide information on the kinetics of rotaxanes.

Electrochemical measurements can give similar, albeit less detailed information. The redox potentials of units incorporated in rotaxanes will change upon macrocycle complexation, thus showing whether the macrocycle is on or off the station.[51,52] The interpretation of these changes is crucial in understanding the behaviour of electrochemical shuttles (see Section 1.9).

If both macrocycle and thread contain chromophores, the interaction between the two can cause photophysical effects in rotaxanes that would normally be much weaker or absent because the components would diffuse apart. The mechanical bond between thread and macrocycle thus makes rotaxanes attractive systems to study energy transfer[38,53-55] and electron transfer.[32,33,53,56] Both energy and electron transfer cause changes in the (time resolved) absorption and emission spectra.

A spectacular example showing the influence of rotaxanation on the electronic properties is found in measurements of the electro-optical Kerr effect, where the birefringence of hydrogen-bonded rotaxanes was found to be completely different from the uninterlocked components,[46] an effect that was ascribed to the pirouetting motion (see Section 1.7) of the macrocycle.

1.7 Shuttling and Pirouetting

All the changes in physical properties that were described in Section 1.6 can be used to establish the structure of the rotaxane, but what is even more important: the dynamics. Together with the first template-directed rotaxane synthesis, it was immediately recognised that the noncovalent interactions between macrocycle and station allowed for a unique type of conformational freedom, where the separate molecules can have different dispositions and orientations with respect to each other.[25,57] The term *co-conformation* has been advocated to describe this special type of isomers.[58] Two important types of motions that can interconvert such co-conformers are shown in Figure 1-8.

In a rotaxane containing two binding sites, there will be an equilibrium between rotaxanes where the macrocycle occupies station 1 and rotaxanes where the macrocycle is located on station 2. The relative populations then are determined by the relative binding strength between macrocycle and either station. These two co-conformers can interconvert by a process which is called *shuttling*. If the macrocycle can adopt different rotational orientations with respect to the thread, the interconversion of the co-conformers is referred to as *pirouetting* (Figure 1-8).

In rotaxanes where the intercomponent interactions between macrocycle and station are dominated by π-stacking or hydrogen-bonding interactions, shuttling is readily observed

using variable temperature ^{1}H NMR. For π-stacking rotaxanes (see Figure 1-4) in $(CD_3)_2CO$, free energy barriers for shuttling between equivalent stations have been determined, and range from ~13 kcal mol^{-1} ($k \approx 2000$ s^{-1}) at room temperature[57] to 9.9 kcal mol^{-1} at 198 K (corresponding to $k \approx 300{,}000$ s^{-1} at 298 K).[59] For hydrogen-bonded rotaxanes the shuttling barrier, $\Delta G^{\ddagger}$, has been found to be 11.2 ± 0.3 kcal mol^{-1} at 298 K in $CDCl_3$ or CD_2Cl_2 for a rotaxane with a benzylic macrocycle (**5**) and two GlyGly stations (Figure 1-6) separated by a C_8 alkyl chain.[60] Elongating the chain to a 16-carbon analogue increased the barrier by 1.2 kcal mol^{-1}, whilst adding up to 5% CD_3OD lowered the shuttling barrier by 2.3 kcal mol^{-1} as a consequence of the weakened hydrogen bonds between macrocycle and station.[60]

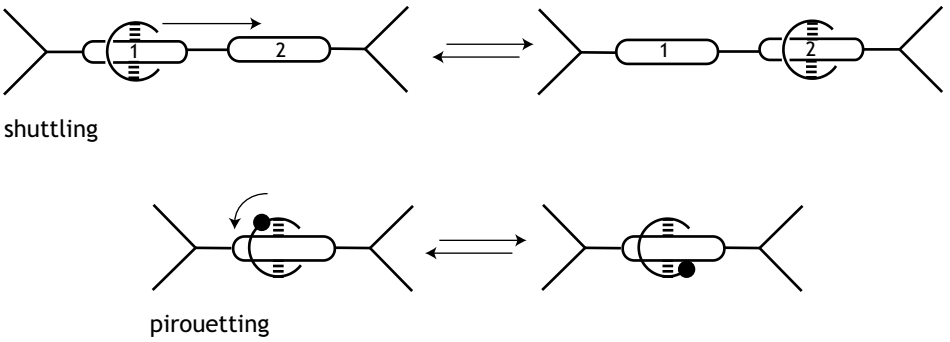

Figure 1-8. Co-conformations can be interconverted by a translational motion of the macrocycle with respect to the thread (*shuttling*), or by a rotational motion (*pirouetting*).

1.8 Molecular Machines: an Intermezzo

The intermolecular large amplitude motions that are possible in rotaxanes have infused the idea that such assemblies could function as *molecular machines*.[26,28,29] This notion has certainly inspired a lot of new research, but is potentially confusing since molecular machines do not and can not function in the same way as their macroscopic analogues. In a mechanical sense, a *machine* is defined as: any arrangement of stationary and moving mechanical parts that affects the force, needed to do a certain amount of work. The standard group of six simple machines includes the *lever, pulley, inclined plane, wheel and axle, wedge,* and *screw,* that each function in different ways, but all change the direction or the amount of force put into them. By combining them, more complex machines such as combustion engines or generators can be constructed. Since axle and wheel are listed as machines it is tempting to immediately classify rotaxanes as molecular machines, but how would it differ from an everyday machine?

An important realisation in this respect is that molecular machines must be *isothermal* engines, not *heat* engines (which operate by drawing heat from a source which is at thermal

equilibrium at some temperature T, and delivering useful work).[61] They are obliged to operate at a single temperature because they do not have any way to insulate themselves from the heat bath that they are embedded in. In other words: molecular machines are constantly subjected to random thermal movements, causing the well-known Brownian motion. Because of the statistical nature of this motion there is no overall directionality and the thermal background noise thus cannot be used to do work, in accordance with the Second Law of thermodynamics.

Still the living world is filled with examples of molecular machines (see also Section 1.11) that make muscles contract, or duplicate our genetic material. These do not violate the laws of thermodynamics (although in a rigorous treatment of heat and work on the molecular level, time must be introduced in the Second Law[62]) so how can molecular machines operate? Let us take our muscles as an example: they manage to contract, *not* because the muscle's molecular assembly draws its energy from some heat reservoir, but because a chemical reaction activates the muscle's molecules. Nature has found a way to capture the activation energy and convert it into motion, before it has a chance to spread out over many vibrational degrees of freedom, producing only heat. Externally applied chemical energy in the form of ATP generates the necessary conformational changes that can generate a force to move one molecule with respect to the other.

This is how molecular machines work: external energy (*input*) is applied to a molecule or molecular assembly, which dissipates the energy and performs a mechanical function (*output*). Such a molecular machine can "run" on chemical energy (like most biomolecular motors), light or an electrical potential. Its functions can be as diverse as translating, rotating, splicing, or joining different parts of the assembly. However, it is not essential that the applied energy *directly* generates a force; the energetic stimulus can also be used to bias the motion of molecules by an appropriately designed external modulation.[63-68] Note that in our description there is no assumption on directionality: the molecular machine may randomly turn clockwise or counter-clockwise on each operation, as long as it does so in response to the appropriate stimulus.

The definition of a molecular machine, thus is quite broad and would also include for example the photoisomerisation of stilbene (but *not* the thermal isomerisation). Balzani *et al.* therefore restrict the definition to systems whose component parts undergo movement with relatively large amplitudes.[29] This of course introduces some unwanted arbitrariness: in the macroscopic world a pair of tweezers is still a machine even though the amplitude of movement is much smaller than say a crane. In analogy with real world examples, it seems more sensible to define a set of *simple molecular machines* from which all other molecular machines can be built.

As mentioned earlier, our bodies form the workplace of many different types of molecular machines, the working of which we are only beginning to grasp (see Section 1.11). The notion, however, that such molecular-level machines could also be constructed artificially is

a quite recent one. The birth of this topic –since then called *nanotechnology*– was in 1959, when Richard Feynman, Nobel laureate in physics, gave his famous lecture, entitled "There's plenty of room at the bottom".[69] He realised that by storing information in atoms or molecules, "(…)all of the information that man has carefully accumulated in all the books in the world can be written in this form in a cube of material one two-hundredth of an inch wide –which is the barest piece of dust that can be made out by the human eye." But his greatest vision showed when he speculated about "(…) the possibility that we [too] can make a thing very small which does what we want –that we can manufacture an object that manoeuvres at that level".

By now, many of Feynman's predictions have come true, as is most dramatically shown by the development of probe microscopies that allow us to visualise and manipulate atoms and molecules.[70,71] The development of artificial molecular machines has also shown great progress: unidirectional molecular rotors, driven by chemical energy[72,73] or light,[74] are two exciting examples of the current possibilities. We will now return to the rotaxanes to show how they can be applied as molecular machines.

1.9 Rotaxanes as Molecular Machines

The criteria for molecular machines as laid out in Section 1.8, should also be applied to rotaxanes. The mechanical functions that are most suitable for rotaxanes are obviously the shuttling or pirouetting movements as described in Section 1.7. Now we will discuss how such movements can be induced by an external stimulus.

Since most effort has been devoted to induce shuttling in rotaxanes, we will confine our discussion to this, but the same principles hold for pirouetting. Consider a rotaxane with two different binding stations (Figure 1-9a), and let us assume that station 1 binds the macrocycle more strongly than station 2. In other words the Gibbs free energy for the co-conformation shown in Figure 1-9a where the macrocycle resides on station 1 is lower in energy than that of a co-conformer where the macrocycle surrounds station 2, so ΔG is positive.

Now, an appropriate external stimulus is applied to either station 1 or station 2 that temporarily changes the relative binding strength of the stations so that ΔG becomes negative (Figure 1-9b). The stimulus might weaken the binding to station 1 or strengthen the binding to station 2, but the result is the same: the macrocycle will move to station 2 (Figure 1-9c), provided the life time of the new state is longer than the time it takes to shuttle. The movement in itself can be the result of the force that the stimulus has generated, for instance, an attractive electrostatic force between macrocycle and station 2. This will lower the barrier ($\Delta G^{\ddagger}$) for shuttling, making the rate of this process faster. This, however, is not essential: in the absence of a directing force, thermal motions will eventually drive the macrocycle to station 2, because thermodynamically this is now the most stable co-conformer. In this case we speak of biased Brownian motion (see Section 1.8).

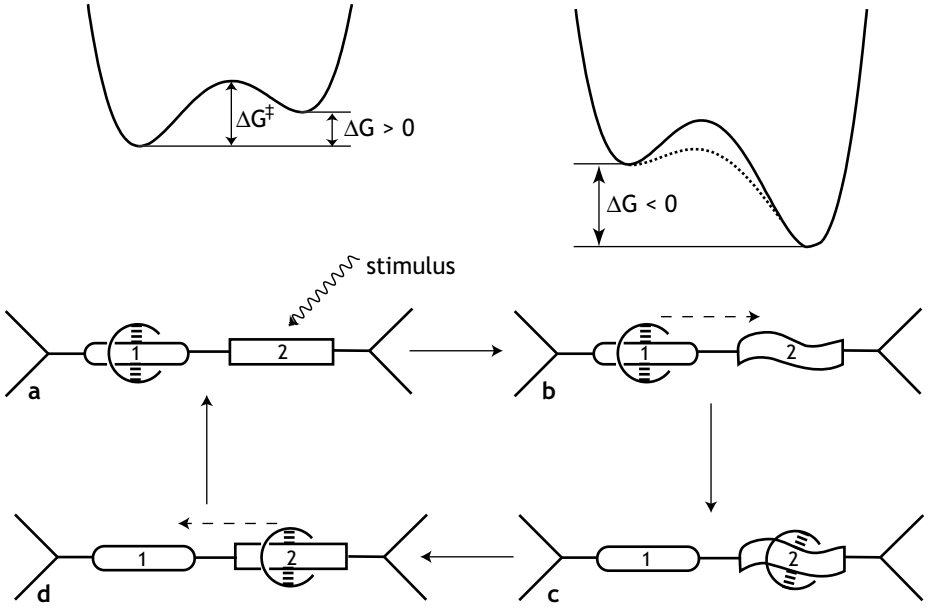

Figure 1-9. A rotaxane as a molecular machine, showing the work cycle together with the associated potential energy curves. The lowered barrier (dotted curve) indicates the case of an attractive force between the macrocycle and the altered station 2. See text for further explanation.

If the stimulus has irreversibly altered the relative binding strength of the stations, this is the endpoint of the mechanical work cycle of the molecular machine, and the original state can only be restored by a second stimulus. If on the other hand the change in binding strength is transient, the original stations are spontaneously restored (Figure 1-9d) and the cycle is complete.

All molecular machines based on rotaxanes in literature work along these principles.[26-29,31,33,53,75-78] The major differences lie in the type of stimulus that is applied: chemical, electrical, or photonic. Nondestructive chemical stimuli such as solvent changes[60] or pH-changes[36,37,79-82] are relatively easy to apply and can induce large changes in binding strength between macrocycle and station. To operate them, however, requires manipulation with solutions, which is less elegant from a practical point of view. Therefore, a lot of effort has been put into manipulating the redox states of station or macrocycle in order to alter the relative binding strengths. Because redox states can be changed electrochemically, but also photochemically, this provides a "cleaner" operation. Since in π-stacking and metal-ligand rotaxanes (see Figure 1-4) the stations can readily be oxidised or reduced at low voltages, redox-active rotaxanes in literature are almost exclusively found for these types of rotaxanes,[32,51-55,75,79,83-88] which does not mean that hydrogen-bonded rotaxanes cannot use these stimuli as will be shown in this Thesis.

Before discussing how rotaxanes can be controlled photochemically, we will first have a look at two examples of electrochemically addressable rotaxanes, for these will aid in the understanding of the photoactive rotaxanes. In a rotaxane from the Stoddart group (**8**),[79] the macrocycle contains a π-electron-accepting tetracationic cyclophane comprising two bipyridinium units bridged by two *p*-xylyl spacers. The thread contains two π-electron-donating units: a biphenyl ether and a benzidine station. At room temperature in CD_3CN, the macrocycle resides 84% of the time on the station with the lowest oxidation potential, *viz.* benzidine (Figure 1-10).

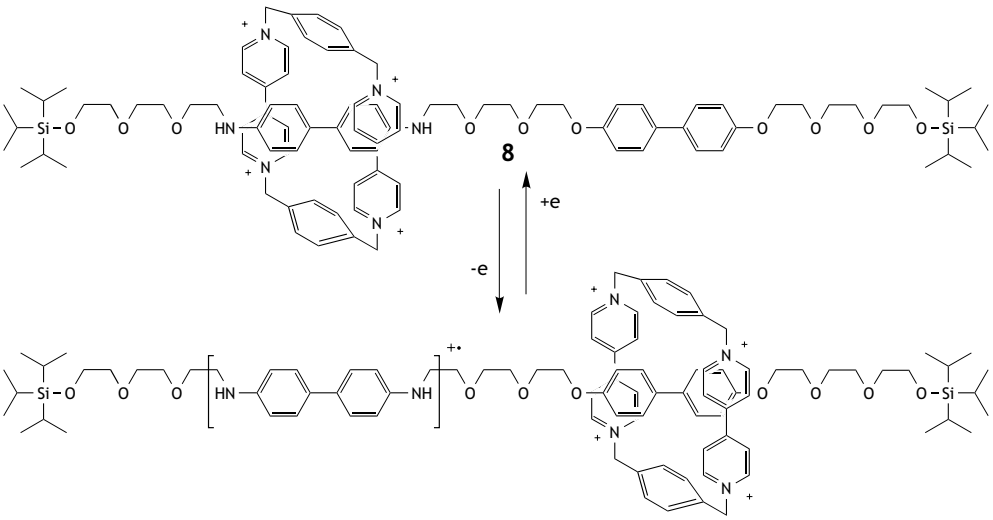

Figure 1-10. Electrochemically controllable molecular shuttle, based on π-stacking interactions.

Upon oxidation of the benzidine station in **8**, the intermolecular binding between cyclophane and benzidine radical cation is weakened and the macrocycle moves to the biphenyl ether station. Proof for this mechanism comes from cyclic voltammetry: the unfavourable electrostatic repulsion between the tetracationic macrocycle and the benzidine radical cation cause the first oxidation wave to occur at higher potential than that of the free thread. The second oxidation wave of benzidine however is unaltered, whereas in a rotaxane containing *only* a benzidine station, this wave is also shifted to higher potential. The conclusion must be that when the second oxidation of **8** takes place, the macrocycle no longer influences the benzidine station, because it has shuttled away.

The Sauvage group used the different preferred coordination environments of Cu(I) and Cu(II) to make a redox-active shuttle (**9**).[85] The macrocycle contains a 1,10-phenantroline (phen) bidentate ligand, which is also present as one of the binding stations on the thread. The second binding station is formed by a terdendate ligand: 2,2',6',2"-terpyridine (terpy). Copper(I) has a strong tendency to be four-coordinate, and thus in this oxidation state **9** will

exclusively exist in a co-conformation where the phen groups of the macrocycle and the thread are complexed (Figure 1-11).

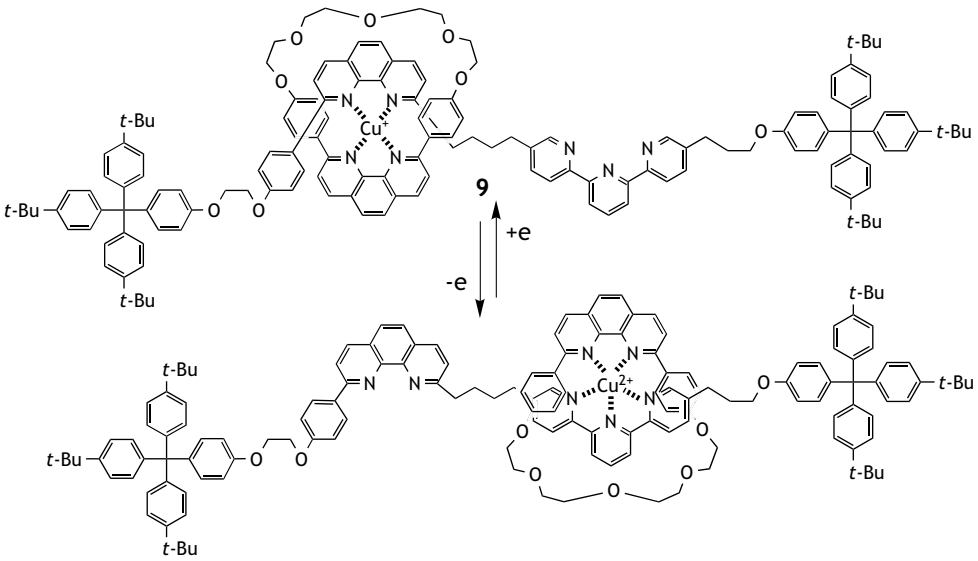

Figure 1-11. Electrochemically controllable molecular shuttle, based on metal-ligand interactions.

The stable tetrahedral Cu(I) complex can be oxidised to Cu(II), but in this oxidation state of the metal, a pentacoordinated complex is more stable, and the macrocycle rearranges to form a complex with the terpy station. Again the shuttling of this molecular machine was proven by cyclic voltammetry. Note that when the thread incorporates only phen, and the macrocycle contains both phen and terpy, the same principles lead to electrochemically induced pirouetting.[89]

1.10 Photoaddressable Rotaxanes

The earliest attempts to use light as a fuel for molecular shuttles were carried out by Benniston and Harriman using π-stacking rotaxanes.[56,90] The binding between the macrocycle and station in these rotaxanes is due to π-π interactions between electron donating and electron accepting aromatic groups, and therefore a low lying charge transfer (CT) state might be present. Indeed, **10** shows a charge transfer absorption centred around 467 nm.

Photoexcitation in this CT band leads to electron transfer from the dialkoxybenzene station to the bipyridinium containing macrocycle, as witnessed by the picosecond transient absorption spectrum of the bipyridinium radical cation. The radical ion pair thus created has a very short lifetime (20 ps), but 10% of the molecules decay more slowly (480 ns), because the dialkoxybenzene radical cation oxidises the ferrocene ($Fe(Cp)_2$) stopper. It was proposed that electrostatic repulsion between the ferrocenium radical cation and the positively charged

macrocycle could lead to shuttling, although no spectroscopic evidence could be found.[90] In a later, more elaborate study including also rotaxanes with two binding stations it was concluded that it was unlikely that the cyclophane translates before reverse electron transfer takes place.[56]

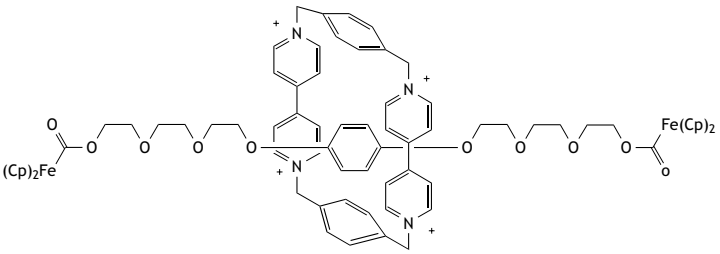

10

A charge-transfer state with a much longer lifetime was created in a rotaxane containing an electron-donor-acceptor-acceptor (D^{2+}-$A_1{}^{2+}$-$A_2{}^{2+}$) system (**11**.6PF_6), using a ruthenium(II) trisbipyridyl donor and two different bipyridinium acceptors.[77] In the ground state the π-electron donating macrocyclic polyether resides over the station furthest from the ruthenium(II)trisbipyridyl stopper, *i.e.* $A_2{}^{2+}$. Selective photoexcitation of the ruthenium complex led to stepwise electron transfer, affording the D^{3+}-$A_1{}^{2+}$-$A_2{}^{+}$ state with a decay time of 4100 ns (MeCN, 298 K). Despite this long lifetime of the charge-separated state, the macrocycle was not observed to leave the $A_2{}^{+}$ station.

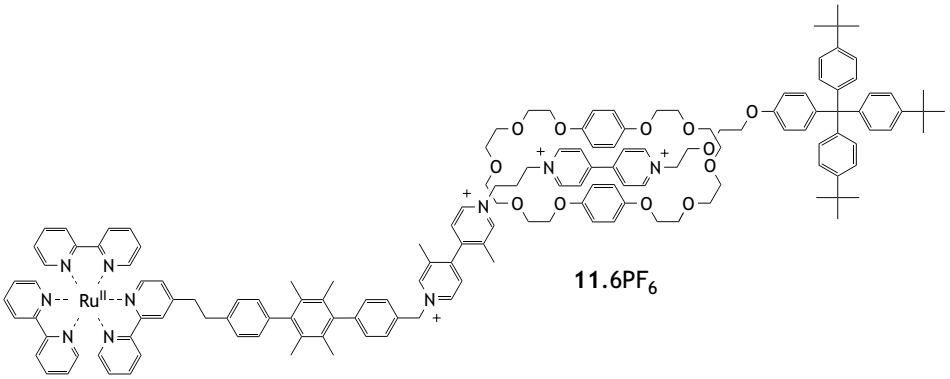

11.6PF_6

Reverse electron transfer seems to be the biggest enemy of these types of photodriven machines. Intramolecular charge-transfer states have lifetimes in the order of picoseconds to nanoseconds which is too short in general for translation of the macrocycle over several Ångstrøms. How can this problem be overcome? Most trivially by not relying on photoinduced electron transfer: Murakami *et al.* have used trans-cis photoisomerisation of an azobenzene station to move a cyclodextrin macrocycle (**12**.4ClO_4).[91] As a trans-isomer the rotaxane

adopts a co-conformation where the macrocycle resides over the azobenzene unit, but this is sterically impossible for the cis-isomer and thus the macrocycle moves away after irradiation.

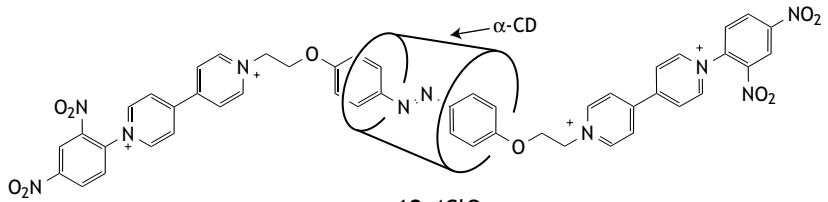

12.4ClO_4

Another workaround is to use intermolecular charge transfer with an external, sacrificial electron donor or acceptor. Electron transfer to the sacrificial compound will cause it to decompose and thus render it unavailable for reverse electron transfer. By continuous irradiation of a redox-active rotaxane in the presence of a suitable sacrificial donor or acceptor a steady state concentration of reduced or oxidised rotaxanes will build up that function in the same way as electrochemically activated systems (see Section 1.9). This strategy has been used successfully for a number of rotaxanes and pseudo-rotaxanes.[54,75,77,85,92,93]

1.11 Biomolecular Machines

The achievements in the field of artificial molecular machines, discussed in the preceding sections, look impressive, but compared to what nature realises it is still child's play. To appreciate the differences between artificial and natural molecular motors, we will now discuss the working of biomolecular systems.

There are many different types of molecular motors that perform vital functions. Muscles as well as intracellular transports are driven by molecular motors that move unidirectionally along protein polymers. But motor proteins also play a role during *e.g.* cell division, where they perform the tasks of unwinding DNA, replicating and dividing the genetic material over two new cells. Table 1-1 shows some examples of biomolecular machines that have been recognised,[94] most of which have been reviewed.[95-97] We will confine our discussion to ATPase and kinesin, since for these the most detailed information is available. This increase in knowledge in the last decade is owed to X-ray structures and single molecule optical techniques.[71,98-100]

For the cytoskeletal motor proteins, two classes of tracks have been identified: actin filaments and microtubules. Motors of the myosin superfamily (responsible for muscle movement) interact with and move along actin. Motors of the kinesin and dynein superfamilies interact with and move along microtubules. A few basic concepts underlie the action of all three types of motor molecules: movement of the molecule along the track involves repeated cycles of motor domain attachment, force generation and detachment. This cycle of interactions is coupled to ATP hydrolysis.[95]

Table 1-1. Examples of proteins that are believed to act as molecular motors.[94]

motor	force generating partner	energy source	motion	role and features
Cytoskeletal motors				
kinesin	microtubule	ATP	linear	Mitosis/organelle transport, microtubule dynamics
myosin	actin	ATP	linear	Muscle contraction/organelle transport/cytokinesis
dynein	microtubule	ATP	linear	Ciliary beating/organelle transport/mitosis. Motor has 4 ATP-binding sites
Polymers				
actin	none	ATP	extend/shrink	Cell motility/cortical organisation
microtubule	none	GTP	extend/shrink	Mitosis/cytoplasmic organisation
dynamin	membranes	GTP	pinching	Endocytosis/vesicle budding
spasmin/centrin	none?	Ca^{2+}	contraction	Contraction
G proteins				
EfG	Ribosome	GTP	lever	Movement of peptidyl-tRNA, mRNA in the ribosome
Rotary motors				
F_1 ATPase	F_0 complex	ATP	rotary	ATP synthesis/hydrolysis, reversible/100% efficient
bacterial flagellar	many proteins	H^+/Na^+	rotary	Bacterial propulsion, rapidly reversible motor
Rings				
AAA proteins	various partners	ATP	twisting	Disruption of protein-protein interactions
GroEl	GroES, unfolded	ATP	prying	Protein folding
Nucleic acid motors				
polymerase	DNA/RNA	ATP	linear	Template replication
helicases	DNA/RNA	ATP	linear	Unwinding activity
SMC proteins	DNA, condensins	ATP	condensation	Chromosome formation

Kinesin is the smallest biomolecular motor known, and is structurally related to myosin, although it is thought to operate very differently. It advances at random times through fixed

distances, moving in discrete steps of 80 Å, which corresponds directly to the lattice spacing of tubulin dimers along the microtubule. Individual molecules typically make ~100 steps before disengaging, and do so at speeds of ~800 nm/s in vitro. In one step an amount of mechanical work of 48 pN·nm is done, corresponding to 60% or more of the available energy in a single ATP molecule.[101]

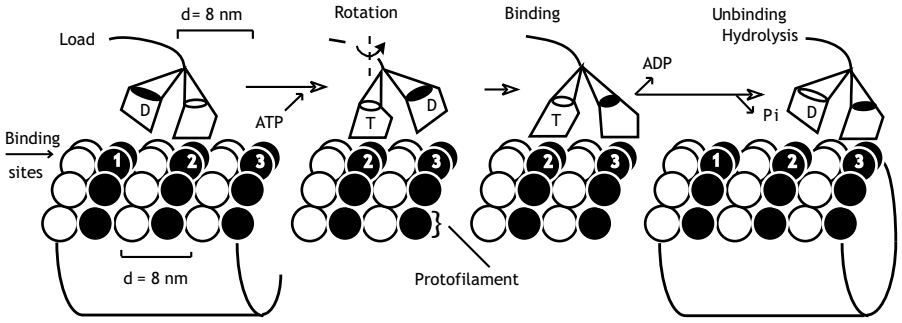

Figure 1-12. The motion of conventional kinesin along the microtubule surface.[102] Kinesin's path follows one of the protofilaments. The rear head, which was initially bound at site 1 (left panel), skips over the other head attached at site 2, and binds at site 3 to become the new leading head (right panel). The middle panels show the chemical and structural transitions that probably drive the motion: the binding of ATP (T) to the bound head is thought to produce a rotation in this head that swings the second head towards its next binding site. The second head then binds and accelerates ADP (D) release. During this time, the trailing head hydrolyses ATP to ADP-Pi.

Exactly how kinesin functions on a molecular level is still a matter of debate,[101] but most data seem to support a hand-over-hand model.[95,100] We will describe the model proposed by Howard[102] and Vale and Milligan,[95] schematically depicted in Figure 1-12 (animated models are also available on the world wide web[103]). The kinesin motor contains two head groups that work in a co-ordinated manner to move processively along the track. When the leading head binds ATP, it throws its rear partner 160 Å forward to the next tubulin binding site. The tight binding of the partner head to its new tubulin site then locks the step in place and produces a force that pulls kinesin's cargo forward by 80 Å.

Table 1-1 shows that there are many linear motors beside kinesin, but there are only two rotary motors known in the biological world: F_1-ATPase and the bacterial flagellar motor. F_1-ATPase, a portion of ATP synthase (see Figure 1-13), is the smallest, and best understood of the two. ATP synthase is found in mitochondrial membrane where it synthesises ATP in the presence of a proton gradient. This enzyme is composed of a membrane embedded, proton-conducting portion, F_0, and a part that protrudes into the inside of the mitochondrium, F_1. When protons flow through F_0, ATP is synthesised in F_1. The reverse process, hydrolysis of ATP into ADP and Pi in F_1, is also possible, and is the only process observed in isolated F_1.[104-106]

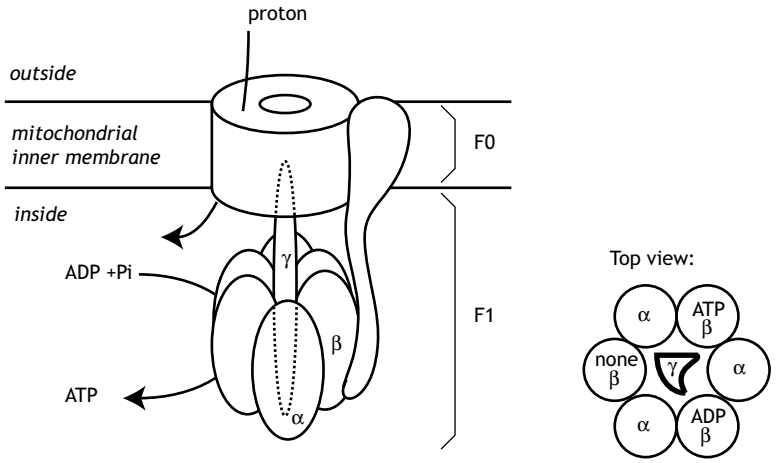

Figure 1-13. Simplified structure of ATP Synthase.[105]

The coupling of proton flow and ATP synthesis/hydrolysis was already proposed to occur *via* a rotation of a common shaft (γ) penetrating F_0 and F_1 long before it was actually detected.[107] This rotary motion could be deduced from the fact that F_1 contains a 3-fold symmetric $\alpha_3\beta_3$ hexamer (Figure 1-13), having three catalytic sites, one on each β, which on average participate equally in ATP synthesis/hydrolysis. The γ-subunit in the centre of the hexamer, however, lacks 3-fold symmetry and must therefore rotate in order to treat all binding sites alike (Figure 1-14).

Figure 1-14. F_1-ATPase mode of operation, during ATP hydrolysis viewed from the F_0 side.[105] The three β-subunits are static with respect to the membrane, leaving only the central γ-subunit (thick lines) to rotate. When bound ATP is hydrolysed to ADP by catalytic action of the central γ-subunit, the new nucleotide in the binding site dictates a different conformation of β, just as releasing ADP from the binding site causes yet another conformational change in the β-subunit. To accommodate these changes the central γ-subunit must rotate 120°.

This working model for F_1-ATPase has recently been confirmed by direct observation of the rotation of the gamma subunit with an epifluorescent microscope.[108] The β-subunits were immobilised on a glass surface and a fluorescently labelled actin filament was attached to the γ-subunit for observation. When ATP was added, the filament started to rotate (video movies of rotating actin filament are available[109]). Further studies have shown that a discrete

120° rotation is associated with one ATP binding event.[110] Moreover it was estimated that the work required to rotate the filament against viscous loads had to be as much as 80 pN·nm, which is approximately the free energy liberated by hydrolysis of a single ATP molecule under physiological conditions. Thus, F_1-ATPase can couple nearly 100% of chemical energy into mechanical work.

The kinesin and ATPase examples serve to show the important points for the design of artificial molecular machines. Nature has found mechanisms to create unidirectional motion from chemical energy with high efficiency. We are only beginning to understand these molecular machines, let alone make artificial model systems that have the same speed, efficiency, or directionality. Efforts in that direction using hydrogen-bonded rotaxanes that are fuelled by light are described in this Thesis.

1.12 Scope of this Thesis

The heart of this Thesis is formed by Chapters 4 and 6 where we describe the photoinduced translation of a macrocycle along a thread in hydrogen-bonded rotaxanes. Upon photoexcitation with a short laser pulse the preferential binding station in the rotaxane is changed after which thermal motions drive the macrocycle over the thread. The altered binding station is spontaneously restored causing the macrocycle to return to its original position. These rotaxanes therefore constitute the first examples of fully *reversible*, artificial molecular shuttles.

The translation of the macrocycle in Chapter 4 was induced by changing the hydrogen-bonding properties of the stopper chromophore in the singlet excited state. Because this change lasts only a few nanoseconds, the macrocycle can only be translated over a relatively short distance (~3Å). The changes in the fluorescence behaviour because of this macrocycle translation are nevertheless sizable and were used to elucidate the excited state dynamics. Based on these fluorescence measurements a working hypothesis was formulated that was consistent with the experimental findings. The experiments, however, could not give insight into the detailed changes in the hydrogen-bond pattern in the excited state of the rotaxane.

For this system, we therefore performed a number of molecular modelling calculations, described in Chapter 5. In accordance with our working hypothesis, Stochastic Dynamics simulations confirmed the preferential H-bond pattern of the rotaxane in the ground state. We were furthermore able to show that in the singlet state the change in steric demand of the chromophore is likely to be important in the excited state mechanism.

The rotaxane described in Chapters 4 and 5 is attractive in that no additional external assistance besides photons is needed to induce macrocyclic motion. The displacement caused however is not particularly large. In order to make a photonic molecular machine where the macrocycle travels over longer distances, the photoinduced changes must persist longer. In Chapter 6, a rotaxane is described in which this goal was achieved using triplet electron transfer with an external electron donor. Following a nanosecond laser pulse, the macrocycle moves reversibly between two hydrogen-bonding stations over a distance of approximately

1.5 nm. Observation of transient changes in the optical absorption spectrum after photoexcitation allowed direct, quantitative monitoring of the submolecular translational process.

In the remaining Chapters (2 and 3) photons are not used to fuel artificial molecular machines but solely as spectroscopic tools. Chapter 2 introduces a rotaxane that is sometimes referred to as an "impossible rotaxane", because the thread does not contain a binding station for the macrocycle, but rather a natural polyene: bixin. We studied the absorption solvatochromism of this rotaxane and its corresponding thread and found that the macrocycle has a profound influence on the electronic properties of the polyene thread because it shields the chromophore from the solvent.

The solvent also plays an important role in Chapter 3, where the rotaxane's thread contains two regions: a hydrogen-bonding station and a long alkyl chain. Here, fluorescence spectroscopy was used as a tool to probe the position of the macrocycle on the thread as a function of solvent. The average distance from one stopper to the macrocycle could be inferred, because the macrocycle contains an electron-accepting group that quenches the fluorescence of this stopper by electron transfer. The same chromophores were used to construct a rotaxane based device that is nonfluorescent, but will become fluorescent under irradiation. For this, one stopper is replaced by a photocleavable group. Under irradiation this group splits off, releasing the macrocycle and restoring the fluorescence of the other stopper. We succeeded in incorporating this rotaxane on a solid support, and writing a fluorescent pattern in it.

1.13 References

1. Anand, N., Bindra, J.S., and Ranganathan, S. *Art in Organic Synthesis* Holden-Day Inc.: San Francisco, 1970.
2. Frisch, H.L., and Wasserman, E. Chemical topology. *J. Org. Chem.* **83**, 3789-3795 (1961)
3. Walba, D.M. Topological Stereochemistry. *Tetrahedron* **41**, 3161-3212 (1985)
4. Schmidt, T., Schmieder, R., Müller, W.M., Kiupel, B., and Vögtle, F. Chiral amide rotaxanes with glucose stoppers. Synthesis, chiral properties and wheel-axle interactions. *Eur. J. Org. Chem.* 2003-2007 (1998)
5. Schmieder, R., Hubner, G., Seel, C., and Vögtle, F. The first cyclodiasteromeric [3]rotaxane. *Angew. Chem.-Int. Edit.* **38**, 3528-3530 (1999)
6. Breault, G.A., Hunter, C.A., and Mayers, P.C. Supramolecular topology. *Tetrahedron* **55**, 5265-5293 (1999)
7. Sauvage, J.P., and Dietrich-Buchecker, C. *Molecular catenanes, rotaxanes and knots: a journey through the world of molecular topology* Wiley-VCH: Weinheim, 1999.
8. Wasserman, E. The preparation of interlocking rings: a catenane. *J. Am. Chem. Soc.* **82**, 4433-4434 (1960)
9. Harrison, I.T., and Harrison, S. The synthesis of a stable complex of a macrocycle and a threaded chain. *J. Am. Chem. Soc.* **89**, 5723-5724 (1967)
10. Harrison, I.T. Preparation of rotaxanes by the statistical method. *J. Chem. Soc.-Perkin Trans. 1* 301-304 (1974)

11. Schill, G., Beckmann, W., Schweickert, N., and Fritz, H. Untersuchungen zur statistischen synthese von rotaxanen. *Chem. Ber.* **119**, 2647-2655 (1986)
12. Schill, G. *Catenanes, rotaxanes and knots* Academic Press: New York, 1971.
13. Schill, G., and Zollenkopf, H. Rotaxan-verbindungen, I. *Liebigs Ann. Chem.* **721**, 53-74 (1969)
14. Hershey, A.D., Burgi, E., and Ingraham, L. Cohesion of DNA molecules isolated from phage lambda. *Proc. Natl. Acad. Sci. U. S. A.* **49**, 748-755 (1963)
15. Hudson, B., and Vinograd, J. Catenated circular DNA molecules in HeLa cell mitochondria. *Nature* **216**, 647-652 (1967)
16. Clayton, D.A., and Vinograd, J. Circular dimer and catenate forms of mitochondrial DNA in human lukaemic leucocytes. *Nature* **216**, 652-657 (1967)
17. Kreuzer, K.N., and Cozzarelli, N.R. Formation and resolution of DNA catenanes by DNA gyrase. *Cell* **20**, 245-254 (1980)
18. Wang, J.C. Interlocked deoxyribonucleic acid rings. *Acc. Chem. Res.* **6**, 252-256 (1973)
19. Wang, J.C. Moving one DNA double helix through another by a type II DNA topoisomerase: the story of a simple molecular machine. *Q. Rev. Biophys.* **31**, 107-144 (1998)
20. Mao, C.D., Sun, W.Q., Shen, Z.Y., and Seeman, N.C. A nanomechanical device based on the B-Z transition of DNA. *Nature* **397**, 144-146 (1999)
21. Seeman, N.C. Nucleic acid nanostructures and topology. *Angew. Chem.-Int. Edit.* **37**, 3220-3238 (1998)
22. Seeman, N.C. DNA nanotechnology: Novel DNA constructions. *Annu. Rev. Biophys. Biomolec. Struct.* **27**, 225-248 (1998)
23. Lehn, J.-M. Cryptates: inclusion complexes of macrocyclic receptor molecules. *Pure Appl. Chem.* **50**, 871-892 (1978)
24. Lehn, J.-M. *Supramolecular Chemistry. Concepts and Perspectives* VCH: Weinheim, 1995.
25. Anelli, P.L., Ashton, P.R., Ballardini, R., Balzani, V., Delgado, M., Gandolfi, M.T., Goodnow, T.T., Kaifer, A.E., Philp, D., Pietraszkiewicz, M., Prodi, L., Reddington, M.V., Slawin, A.M.Z., Spencer, N., Stoddart, J.F., Vicent, C., and Williams, D.J. Molecular Meccano. 1. [2]Rotaxanes and a [2]catenane made to order. *J. Am. Chem. Soc.* **117**, 193-218 (1992)
26. Gomez-Lopez, M., Preece, J.A., and Stoddart, J.F. The art and science of self-assembling molecular machines. *Nanotechnology* **7**, 183-192 (1996)
27. Anelli, P.L., Asakawa, M., Ashton, P.R., Bissell, R.A., Clavier, G., Gorski, R., Kaifer, A.E., Langford, S.J., Mattersteig, G., Menzer, S., Philp, D., Slawin, A.M.Z., Spencer, N., Stoddart, J.F., Tolley, M.S., and Williams, D.J. Toward controllable molecular shuttles. *Chem.-Eur. J.* **3**, 1113-1135 (1997)
28. Balzani, V., Gomez-Lopez, M., and Stoddart, J.F. Molecular machines. *Acc. Chem. Res.* **31**, 405-414 (1998)
29. Balzani, V., Credi, A., Raymo, F.M., and Stoddart, J.F. Artificial molecular machines. *Angew. Chem.-Int. Edit.* **39**, 3349-3391 (2000)
30. Dietrich-Buchecker, C.O., and Sauvage, J.P. Interlocking of molecular threads: from the statistical approach to the templated synthesis of catenands. *Chem. Rev.* **87**, 795-810 (1987)
31. Sauvage, J.P. Transition metal-containing rotaxanes and catenanes in motion: Toward molecular machines and motors. *Acc. Chem. Res.* **31**, 611-619 (1998)
32. Chambron, J.C., and Sauvage, J.P. Functional rotaxanes: From controlled molecular motions to electron transfer between chemically nonconnected chromophores. *Chem.-Eur. J.* **4**, 1362-1366 (1998)

33. Blanco, M.J., Jimenez, M.C., Chambron, J.C., Heitz, V., Linke, M., and Sauvage, J.P. Rotaxanes as new architectures for photoinduced electron transfer and molecular motions. *Chem. Soc. Rev.* **28**, 293-305 (1999)
34. Vögtle, F., Jager, R., Handel, M., and OttensHildebrandt, S. Catenanes and rotaxanes of the amide type. *Pure Appl. Chem.* **68**, 225-232 (1996)
35. Vögtle, F., Dunnwald, T., and Schmidt, T. Catenanes and rotaxanes of the amide type. *Acc. Chem. Res.* **29**, 451-460 (1996)
36. Ashton, P.R., Ballardini, R., Balzani, V., GomezLopez, M., Lawrence, S.E., MartinezDiaz, M.V., Montalti, M., Piersanti, A., Prodi, L., Stoddart, J.F., and Williams, D.J. Hydrogen-bonded complexes of aromatic crown ethers with (9-anthracenyl)methylammonium derivatives. Supramolecular photochemistry and photophysics. pH-controllable supramolecular switching. *J. Am. Chem. Soc.* **119**, 10641-10651 (1997)
37. Ashton, P.R., Ballardini, R., Balzani, V., Baxter, I., Credi, A., Fyfe, M.C.T., Gandolfi, M.T., Gomez-Lopez, M., Martinez-Diaz, M.V., Piersanti, A., Spencer, N., Stoddart, J.F., Venturi, M., White, A.J.P., and Williams, D.J. Acid-base controllable molecular shuttles. *J. Am. Chem. Soc.* **120**, 11932-11942 (1998)
38. Ishow, E., Credi, A., Balzani, V., Spadola, F., and Mandolini, L. A molecular-level plug/socket system: Electronic energy transfer from a binaphthyl unit incorporated into a crown ether to an anthracenyl unit linked to an ammonium ion. *Chem.-Eur. J.* **5**, 984-989 (1999)
39. Nepogodiev, S.A., and Stoddart, J.F. Cyclodextrin-based catenanes and rotaxanes. *Chem. Rev.* **98**, 1959-1976 (1998)
40. Leigh, D.A., and Murphy, A. Molecular tailoring: the made-to-measure properties of rotaxanes. *Chemistry & Industry* 178-183 (1999)
41. Johnston, A.G., Leigh, D.A., Pritchard, R.J., and Deegan, M.D. Facile synthesis and solid-state structure of a benzylic amide [2]catenane. *Angew. Chem.-Int. Edit.* **34**, (1995)
42. Johnston, A.G., Leigh, D.A., Nezhat, L., Smart, J.P., and Deegan, M.D. Structurally diverse and dynamically versatile benzylic amide [2]catenanes assembled directly from commercially available precursors. *Angew. Chem.-Int. Edit.* **34**, (1995)
43. Leigh, D.A., Murphy, A., Smart, J.P., and Slawin, A.M.Z. Glycylglycine rotaxanes - The hydrogen bond directed assembly of synthetic peptide rotaxanes. *Angew. Chem.-Int. Edit. Engl.* **36**, 728-732 (1997)
44. Johnston, A.G., Leigh, D.A., Murphy, A., Smart, J.P., and Deegan, M.D. The synthesis and solubilization of amide macrocycles via rotaxane formation. *J. Am. Chem. Soc.* **118**, 10662-10663 (1996)
45. Leigh, D.A., (University of Warwick) personal communication.
46. Bermudez, V., Capron, N., Gase, T., Gatti, F.G., Kajzar, F., Leigh, D.A., Zerbetto, F., and Zhang, S.W. Influencing intramolecular motion with an alternating electric field. *Nature* **406**, 608-611 (2000)
47. Anderson, S., Aplin, R.T., Claridge, T.D.W., Goodson, T., Maciel, A.C., Rumbles, G., Ryan, J.F., and Anderson, H.L. An approach to insulated molecular wires: synthesis of water- soluble conjugated rotaxanes. *J. Chem. Soc.-Perkin Trans. 1* 2383-2397 (1998)
48. Buston, J.E.H., Young, J.R., and Anderson, H.L. Rotaxane-encapsulated cyanine dyes: enhanced fluorescence efficiency and photostability. *Chem. Commun.* 905-906 (2000)
49. Tuncel, D., and Steinke, J.H.G. Catalytically self-threading polyrotaxanes. *Chem. Commun.* 1509-1510 (1999)
50. Schneider, H.-J., and Yatsimirsky, A. *Principles and Methods in Supramolecular Chemistry* Wiley: Chichester, UK, 2000.

51. Cordova, E., Bissell, R.A., and Kaifer, A.E. Synthesis and Electrochemical Properties of Redox-Active [2]Rotaxanes Based On the Inclusion Complexation of 1,4- Phenylenediamine and Benzidine By Cyclobis(Paraquat-P- Phenylene). *J. Org. Chem.* **60**, 1033-1038 (1995)
52. Devonport, W., Blower, M.A., Bryce, M.R., and Goldenberg, L.M. A redox-active tetrathiafulvalene [2]pseudorotaxane: Spectroelectrochemical and cyclic voltammetric studies of the highly-reversible complexation/decomplexation process. *J. Org. Chem.* **62**, 885-887 (1997)
53. Collin, J.P., Gavina, P., Heitz, V., and Sauvage, J.P. Construction of one-dimensional multicomponent molecular arrays: Control of electronic and molecular motions. *Eur. J. Inorg. Chem.* 1-14 (1998)
54. Ashton, P.R., Ballardini, R., Balzani, V., Constable, E.C., Credi, A., Kocian, O., Langford, S.J., Preece, J.A., Prodi, L., Schofield, E.R., and Spencer, N. Ru-II polypyridine complexes covalently linked to electron acceptors as wires for light-driven pseudorotaxane-type molecular machines. *Chem.-Eur. J.* **4**, 2413-2422 (1998)
55. Ballardini, R., Balzani, V., Dehaen, W., Dell'Erba, A.E., Raymo, F.M., Stoddart, J.F., and Venturi, M. Molecular meccano, 56 - Anthracene-containing [2]rotaxanes: Synthesis, spectroscopic, and electrochemical properties. *Eur. J. Org. Chem.* 591-602 (2000)
56. Benniston, A.C., Harriman, A., and Lynch, V.M. Photoactive [2]Rotaxanes - Structure and Photophysical Properties of Anthracene-Stoppered and Ferrocene-Stoppered [2]Rotaxanes. *J. Am. Chem. Soc.* **117**, 5275-5291 (1995)
57. Anelli, P.L., Spencer, N., and Stoddart, J.F. A molecular shuttle. *J. Am. Chem. Soc.* **113**, 5131-5133 (1991)
58. Fyfe, M.C.T., Glink, P.T., Menzer, S., Stoddart, J.F., White, A.J.P., and Williams, D.J. Anion-assisted self-assembly. *Angew. Chem.-Int. Edit.* **36**, 2068-2069 (1997)
59. Ashton, P.R., Philp, D., Spencer, N., and Stoddart, J.F. A new design strategy for the self assembly of molecular shuttles. *J. Chem. Soc.-Chem. Commun.* 1124-1128 (1992)
60. Lane, A.S., Leigh, D.A., and Murphy, A. Peptide-based molecular shuttles. *J. Am. Chem. Soc.* **119**, 11092-11093 (1997)
61. Jaynes, E.T. In *Maximum-Entropy and Bayesian Methods in Science and Engineering*; Erickson, G. J., Smith, C. R., Eds.; Kluwer Academic Publishers: Dordrecht, The Netherlands, 1988; Vol. 1, pp 267-281.
62. Blumenfeld, L.A., and Tikhonov, A.N. *Biophysical Thermodynamics of Intracellular Processes. Molecular Machines of the Living Cell* Springer-Verlag: New York, 1994.
63. Astumian, R.D. Thermodynamics and kinetics of a Brownian motor. *Science* **276**, 917-922 (1997)
64. Keller, D., and Bustamante, C. The mechanochemistry of molecular motors. *Biophys. J.* **78**, 541-556 (2000)
65. Lipowsky, R. Universal aspects of the chemomechanical coupling for molecular motors. *Phys. Rev. Lett.* **85**, 4401-4404 (2000)
66. Marchesoni, F. Conceptual design of a molecular shuttle. *Phys. Lett. A* **237**, 126-130 (1998)
67. Porto, M., Urbakh, M., and Klafter, J. Atomic scale engines: Cars and wheels. *Phys. Rev. Lett.* **84**, 6058-6061 (2000)
68. Stratopoulos, G.N., Dialynas, T.E., and Tsironis, G.P. Directional Newtonian motion and reversals of molecular motors. *Phys. Lett. A* **252**, 151-156 (1999)
69. Feynman, R.P. There's plenty of room at the bottom. *Eng. Sci.* **23**, 22-36 (1960)
70. Binnig, G., and Rohrer, H. Scanning tunneling microscopy - from birth to adolescence (Nobel lecture). *Angew. Chem.-Int. Edit.* **26**, 606-614 (1987)

71. Gimzewski, J.K., and Joachim, C. Nanoscale science of single molecules using local probes. *Science* **283**, 1683-1688 (1999)
72. Kelly, T.R., De Silva, H., and Silva, R.A. Unidirectional rotary motion in a molecular system. *Nature* **401**, 150-152 (1999)
73. Kelly, T.R., Silva, R.A., De Silva, H., Jasmin, S., and Zhao, Y.J. A rationally designed prototype of a molecular motor. *J. Am. Chem. Soc.* **122**, 6935-6949 (2000)
74. Koumura, N., Zijlstra, R.W.J., van Delden, R.A., Harada, N., and Feringa, B.L. Light-driven monodirectional molecular rotor. *Nature* **401**, 152-155 (1999)
75. Benniston, A.C. Photo- and redox-active [2]rotaxanes and [2]catenanes. *Chem. Soc. Rev.* **25**, 427-436 (1996)
76. Amabilino, D.B., Ashton, P.R., Boyd, S.E., GomezLopez, M., Hayes, W., and Stoddart, J.F. Translational isomerism in some two- and three-station [2]rotaxanes. *J. Org. Chem.* **62**, 3062-3075 (1997)
77. Ashton, P.R., Ballardini, R., Balzani, V., Credi, A., Dress, K.R., Ishow, E., Kleverlaan, C.J., Kocian, O., Preece, J.A., Spencer, N., Stoddart, J.F., Venturi, M., and Wenger, S. A photochemically driven molecular-level abacus. *Chem.-Eur. J.* **6**, 3558-3574 (2000)
78. Gale, P.A. Supramolecular chemistry: from complexes to complexity. *Philos. Trans. R. Soc. Lond. Ser. A-Math. Phys. Eng. Sci.* **358**, 431-453 (2000)
79. Bissell, R.A., Cordova, E., Kaifer, A.E., and Stoddart, J.F. A Chemically and Electrochemically Switchable Molecular Shuttle. *Nature* **369**, 133-137 (1994)
80. Ashton, P.R., Ballardini, R., Balzani, V., Fyfe, M.C.T., Gandolfi, M.T., Martinez-Diaz, M.V., Morosini, M., Schiavo, C., Shibata, K., Stoddart, J.F., White, A.J.P., and Williams, D.J. Selective self-assembly and acid-base controlled de- /rethreading of pseudorotaxanes constructed using multiple recognition motifs. *Chem.-Eur. J.* **4**, 2332-2341 (1998)
81. Matthews, O.A., Raymo, F.M., Stoddart, J.F., White, A.J.P., and Williams, D.J.R. Acid/Base-controlled supramolecular switch. *New J. Chem.* **22**, 1131-1134 (1998)
82. Jun, S.I., Lee, J.W., Sakamoto, S., Yamaguchi, K., and Kim, K. Rotaxane-based molecular switch with fluorescence signaling. *Tetrahedron Lett.* **41**, 471-475 (2000)
83. Ashton, P.R., Ballardini, R., Balzani, V., Belohradsky, M., Gandolfi, M.T., Philp, D., Prodi, L., Raymo, F.M., Reddington, M.V., Spencer, N., Stoddart, J.F., Venturi, M., and Williams, D.J. Self-assembly, spectroscopic, and electrochemical properties of [n]rotaxanes. *J. Am. Chem. Soc.* **118**, 4931-4951 (1996)
84. Asakawa, M., Ashton, P.R., Balzani, V., Credi, A., Mattersteig, G., Matthews, O.A., Montalti, M., Spencer, N., Stoddart, J.F., and Venturi, M. Electrochemically induced molecular motions in pseudorotaxanes: A case of dual-mode (oxidative and reductive) dethreading. *Chem.-Eur. J.* **3**, 1992-1996 (1997)
85. Armaroli, N., Balzani, V., Collin, J.P., Gavina, P., Sauvage, J.P., and Ventura, B. Rotaxanes incorporating two different coordinating units in their thread: Synthesis and electrochemically and photochemically induced molecular motions. *J. Am. Chem. Soc.* **121**, 4397-4408 (1999)
86. Ashton, P.R., Balzani, V., Becher, J., Credi, A., Fyfe, M.C.T., Mattersteig, G., Menzer, S., Nielsen, M.B., Raymo, F.M., Stoddart, J.F., Venturi, M., and Williams, D.J. A three-pole supramolecular switch. *J. Am. Chem. Soc.* **121**, 3951-3957 (1999)
87. Clegg, W., Gimenez-Saiz, C., Leigh, D.A., Murphy, A., Slawin, A.M.Z., and Teat, S.J. "Smart" rotaxanes: Shape memory and control in tertiary amide peptido[2]rotaxanes. *J. Am. Chem. Soc.* **121**, 4124-4129 (1999)
88. Balzani, V., Credi, A., Mattersteig, G., Matthews, O.A., Raymo, F.M., Stoddart, J.F., Venturi, M., White, A.J.P., and Williams, D.J. Switching of pseudorotaxanes and catenanes incorporat-

ing a tetrathiafulvalene unit by redox and chemical inputs. *J. Org. Chem.* **65**, 1924-1936 (2000)
89. Raehm, L., Kern, J.M., and Sauvage, J.P. A transition metal containing rotaxane in motion: Electrochemically induced pirouetting of the ring on the threaded dumbbell. *Chem.-Eur. J.* **5**, 3310-3317 (1999)
90. Benniston, A.C., and Harriman, A. A Light-Induced Molecular Shuttle Based On a [2]Rotaxane- Derived Triad. *Angew. Chem.-Int. Edit. Engl.* **32**, 1459-1461 (1993)
91. Murakami, H., Kawabuchi, A., Kotoo, K., Kunitake, M., and Nakashima, N. A light-driven molecular shuttle based on a rotaxane. *J. Am. Chem. Soc.* **119**, 7605-7606 (1997)
92. Ballardini, R., Balzani, V., Gandolfi, M.T., Prodi, L., Venturi, M., Philp, D., Ricketts, H.G., and Stoddart, J.F. A Photochemically Driven Molecular Machine. *Angew. Chem.-Int. Edit. Engl.* **32**, 1301-1303 (1993)
93. Ashton, P.R., Balzani, V., Kocian, O., Prodi, L., Spencer, N., and Stoddart, J.F. A light-fueled "piston cylinder" molecular-level machine. *J. Am. Chem. Soc.* **120**, 11190-11191 (1998)
94. Vale, R.D. Millennial musings on molecular motors. *Trends Biochem.Sci.* **24**, M38-M42 (1999)
95. Vale, R.D., and Milligan, R.A. The way things move: Looking under the hood of molecular motor proteins. *Science* **288**, 88-95 (2000)
96. Minireviews on Molecular Motors. *Cell* **93**, 1-24 (1998)
97. Reviews on Macromolecular Machines. *Cell* **92**, 291-390 (1998)
98. Moerner, W.E., and Orrit, M. Illuminating single molecules in condensed matter. *Science* **283**, 1670-1676 (1999)
99. Weiss, S. Fluorescence spectroscopy of single biomolecules. *Science* **283**, 1676-1683 (1999)
100. Mehta, A.D., Rief, M., Spudich, J.A., Smith, D.A., and Simmons, R.M. Single-molecule biomechanics with optical methods. *Science* **283**, 1689-1695 (1999)
101. Block, S.M. Kinesin: What Gives? *Cell* **93**, 5-8 (1998)
102. Howard, J. Molecular motors: structural adaptations to cellular functions. *Nature* **389**, 561-567 (1997)
103. Science Online, Supplementary Material, http://www.sciencemag.org/feature/data/1049155.shl
104. Allison, W.S. F-1-ATPase: A molecular motor that hydrolyzes ATP with sequential opening and closing of catalytic sites coupled to rotation of its gamma subunit. *Accounts Chem. Res.* **31**, 819-826 (1998)
105. Kinosita, K., Yasuda, R., Noji, H., Ishiwata, S., and Yoshida, M. F1-ATPase: a rotary motor made of a single molecule. *Cell* **93**, 21-24 (1998)
106. Pedersen, P.L., Ko, Y.H., and Hong, S.J. ATP syntheses in the year 2000: Evolving views about the structures of these remarkable enzyme complexes. *J. Bioenerg. Biomembr.* **32**, 325-332 (2000)
107. Boyer, P.D. The ATP synthase-a splendid molecular machine. *Annu. Rev. Biochem.* **66**, 717-749 (1997)
108. Noji, H., Yasuda, R., Yoshida, M., and Kinosita, K. Direct observation of the rotation of F1-ATPase. *Nature* **386**, 299 (1997)
109. Direct observation of the rotation of F1-ATPase, http://www.res.titech.ac.jp/seibutu/nature/f1rotate.html
110. Yasuda, R., Noji, H., Kinosita, K., and Yoshida, M. F1-ATPase Is a Highly Efficient Molecular Motor that Rotates with Discrete 120° Steps. *Cell* **93**, 1117-1124 (1998)

Chapter 2

Bixin Rotaxanes

Electronic effects caused by rotaxanation of a natural polyene[*]

Als je goed om
je heen kijkt
zie je dat alles
gekleurd is.

– K. Schippers

2.1 Introduction

The carotenoids, present in many fruits and vegetables like carrots and tomatoes, form a class of natural pigments that perform a number of biologically relevant functions.[1] In photosynthetic organisms, the extremely high molar absorption coefficient (*circa* 1.5×10^5 $M^{-1}cm^{-1}$) of these polyenes is used to harvest light. Certain carotenoids are also very efficient triplet quenchers and so can protect an organism from photodegradation initiated by singlet oxygen that is produced by the triplet state of biological dyes. In a more general sense, carotenoids are thought to have protective abilities against cancer, and were shown to posses antimutagenic properties.[2]

---

*Brouwer, A.M., Buma, W.J., Fanti, M., Futterer, T., Leigh, D.A., Wurpel, G.W.H., and Zerbetto, F. *in preparation*

Polyenes, especially those carrying a push-pull pair of substituents, are also of interest for their nonlinear optical (NLO) properties. For example, the hyperpolarisability (β) of molecules is directly related to efficiency in optical frequency doubling and to the Pockels effect. Experimentally, there are two common strategies for optimising β: (1) changing the donor and/or acceptor strength of substituents on the polyene and (2) changing the solvent polarity and/or polarisability. Both alter the local field at the polyene chain, leading to a change in bond-order alternation and in NLO properties, including β.[3] Alternatively, rotaxanation can be used to alter the properties of a linear molecule (thread). This change might be considered to lie in between a substituent and solvent change. The changes in the NLO properties with respect to the separate constituents can be quite dramatic, as was demonstrated for the quadratic electro-optic (Kerr) effect.[4]

In this Chapter, we will address how the interlocked macrocycle influences the energy levels of a natural polyene by looking at its solvatochromic behaviour. It will be shown that the macrocycle can decrease the energy gap for the first allowed electronic transition, but also that the macrocycle shields the polyene from the polarisation effects of the surrounding solvent.

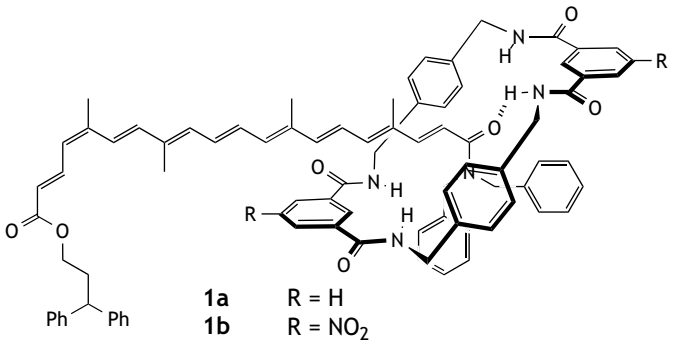

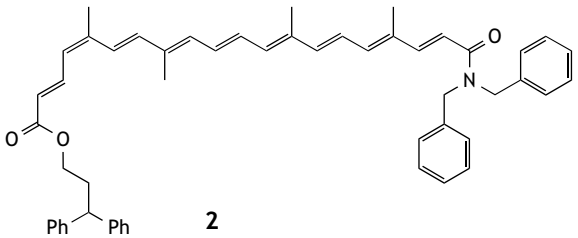

The carotenoid studied here is a derivative of bixin ((9'Z)-6,6'diapo-Ψ-Ψ'-carotenedioic acid monomethyl ester), which is the main constituent of annatto, a widely used orange red colourant for dairy and other food products, extracted from the seed coat of the tree *Bixa orellana*.[5] Direct rotaxanation of this linear compound by template directed synthesis is impossible, since it does not contain the right recognition motif for the formation of a tetraamide macrocycle. Therefore, thread **2** was first extended with a dipeptide recognition motif

using an ester linkage (synthetic scheme not shown here). This temporary binding station was subsequently rotaxanated. In polar, hydrogen bonding solvents the macrocycle is to a large extent displaced towards the hydrophobic polyene chain, and transesterification of the binding site for a stopper in DMSO afforded rotaxanes **1a** and **1b**.

2.2 Experimental

Fluorescence spectra were recorded on a Spex Fluorolog 3 emission spectrometer, using an Oxford Instrument liquid nitrogen cryostat DN 1704 with an ITC4 control unit to control the temperature of the samples. The samples were degassed by at least three freeze-pump-thaw cycles and allowed to thermally equilibrate for at least 30 minutes prior to data collection. At 77 K, weak emission was detected, but the corresponding excitation spectra did not resemble the characteristic bixin absorption and were therefore ascribed to (minor) fluorescent impurities.

Absorption spectra were recorded on a Cary 3E spectrophotometer, using 2 nm spectral bandwidth. All solvents were of spectrograde quality (Merck, UvaSol).

2.3 Electronic Structure

The basic electronic properties of longer polyenes are well understood:[6,7] the electronic structure of polyenes is almost entirely determined by their π electrons. These occupy molecular orbitals that are classified by the D_{2h} symmetry of all-trans polyenes, even when the polyene has a lower symmetry. They are classified by noting whether or not the orbital changes sign upon inversion at the symmetry centre (symmetry labelled u and g) or under 180° rotation around the symmetry axis (symmetry labelled b and a). This restricts the π-electron orbitals to only two symmetry classes, a_u and b_g, which appear alternately when ordered with respect to energy. Thus the overall symmetry of the $2n$ electron state of a polyene is either A_g or B_u.*

Since in the ground state all orbitals are doubly occupied, this configuration is of A_g symmetry. Promoting one electron from the highest occupied molecular orbital (HOMO) to the lowest unoccupied molecular orbital (LUMO) will always produce a configuration of B_u symmetry. The first excited A_g state will come from either promotion of one electron by an even number of orbitals or by the promotion of two electrons by an odd number of orbitals. If electron correlation is neglected, the ordering of the first three electronic states would be $1A_g$, $1B_u$, $2A_g$. For one-photon processes, the transitions between A_g and B_u are allowed, whilst those between states of the same symmetry are forbidden.

*The full description of the state includes the spin multiplicity (*e.g.* ^1A_g), but this will be omitted since in this Chapter only singlet states are discussed.

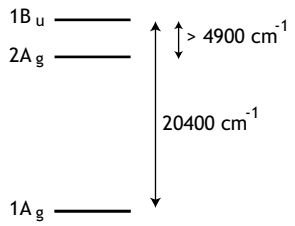

Figure 2-1. State ordering in polyenes, showing the relevant energies of **2** in MeCN.

The absorption spectra of linear polyenes are very similar, displaying a strongly allowed, structured band, ascribed to the $1B_u \leftarrow 1A_g$ transition. The fluorescence that is observed in octatetraene and longer polyenes, however, does not derive from the $1B_u$ state, as is evident from the large Stokes shift and long radiative lifetime of the fluorescence. The $2A_g$ state is lower in energy than $1B_u$ and is responsible for the emission (as shown in Figure 2-1). Only by taking electron correlation into account is this finding reproduced theoretically.

The absorption spectrum of the bixin thread **2** (9 double bonds) in acetonitrile shows a typical polyene absorption (Figure 2-2), with the lowest allowed electronic transition located at 20400 cm^{-1} (490 nm). For comparison, the 1^1B_u 0-0 transition of octadecaoctaene (8 double bonds) in *n*-hexadecane at 4.2 K occurs around 22770 cm^{-1}.[8] The high molar absorption coefficient indicates that it is a strongly allowed transition in agreement with the expectation that it is an $1B_u \leftarrow 1A_g$-like transition. The oscillator strength, f_0 = 1.6 was calculated from the integrated absorption[9] and corresponds to a transition dipole moment of 13 D.

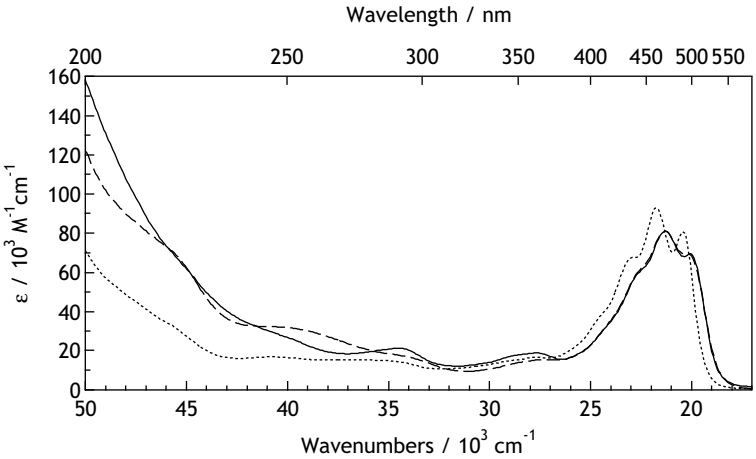

Figure 2-2. Electronic absorption spectra of thread **2** (dotted) and rotaxanes **1a** (continuous) and **1b** (dashed) in MeCN. For **1a** the molar absorption coefficient could not be determined due the limited amount of compound. Therefore, the intensity of **1a** was scaled to the same maximum as that of **1b**.

With increasing chain length of a polyene, the difference in energy between the $1B_u$ and the $2A_g$ states increases: for a polyene with 4 double bonds it is 3540 cm^{-1}, while for 8 double bonds it is 4900 cm^{-1}.[8] So the onset of the fluorescence of bixin (9 double bonds) should be located around 15500 cm^{-1} (645 nm) or lower energy (see also Figure 2-1). Attempts to

detect this $2A_g \rightarrow 1A_g$ fluorescence in the bixin thread or rotaxanes were hampered by fluorescent impurities. Because for longer polyenes the fluorescence quantum yield is known to be very low,[10] extremely pure materials are required to detect the fluorescence from the $2A_g$ state. Since these could not be obtained for the thread and rotaxanes, fluorescence measurements in 2-methyl-tetrahydrofuran at 77 K failed to reveal the energy of this state.

As shown in Figure 2-2, rotaxanation causes a broadening and a red-shift of *circa* 500 cm^{-1} of the $1B_u \leftarrow 1A_g$ absorption in acetonitrile. This is ten times less than the expected energy gap between the $1B_u$ and $2A_g$ state, so it is unlikely that rotaxanation of bixin causes a change in the order of excited states. Rotaxanation, however, *does* have an effect on the solvatochromic behaviour of the absorption spectrum and this will be discussed in the next section.

2.4 Bixin Solvatochromism

In general, the influence of the solvent on spectral properties is treated with a continuum model in which the solute is considered as a sphere of isotropic polarisability with a point dipole in the centre.[11] The sphere is surrounded by the solvent which is represented as a dielectric continuum, characterised by its dielectric constant and refractive index. Stabilisation or destabilisation of electronic states of a solute may derive from purely electronic effects, *i.e.* induction polarisation, and from a different arrangement of the solute environment (orientation polarisation). We used the McRae-Bayliss model for solvatochromism to analyse our data.[12-15] This model contains two variables, f_1 and f_2 (Equation 2-1), which are functions of the refractive index (n) and the dielectric constant (ε) of the solvent. These represent the electronic polarisation and reorganisational factors, respectively. The A and B parameters give the sensitivity towards these terms, while the offset $\tilde{\nu}_0$ is the extrapolated gas phase absorption maximum.

$$\tilde{\nu} = \tilde{\nu}_0 + A f_1 + B f_2$$

$$f_1 = \frac{n^2 - 1}{2n^2 + 1} \qquad \text{(Eq. 2-1)}$$

$$f_2 = \frac{\varepsilon - 1}{\varepsilon + 2} - \frac{n^2 - 1}{2n^2 + 1}$$

For nonpolar polyenes, the solute-solvent interactions are governed by mutual polarisability interactions, and thus are expected to depend solely on f_1. Indeed, it has been shown that the solvatochromism of the $1B_u \leftarrow 1A_g$ transition in a series of linear polyenes is well described by a function of the refractive index alone.[16] The bixin thread and rotaxane have a non-zero dipole moment and thus the use of a more elaborate model (Equation 2-1) is justified. The spectral variations induced by different solvents are reported in Table 2-1. Because the 0-0 transition in the absorption spectrum could not be resolved in all solvents, the next vibronic

peak ($\tilde{\nu}_{01}$) is reported. The vibronic spacing (~1360 cm^{-1}), however remains constant in all solvents, so the 0-0 energies can always be deduced.

Table 2-1. Solvatochromism of thread and rotaxane absorption, showing the relevant solvent parameters for analysis with Equation 2-1.

solvent	n	ε_r	f_1	f_2	$\tilde{\nu}_{01}$ / cm^{-1}		
					2	**1a**	**1b**
methanol	1.3284	32.7	0.169	0.710	21786	21231	21186
acetonitrile	1.3441	37.5	0.175	0.712	21739	21322	21277
diethyl ether	1.3524	4.2	0.178	0.300	21882	21368	21459
ethanol	1.3614	24.6	0.181	0.666	21645	21097	21097
n-hexane	1.3749	1.9	0.186	-0.002	22026	[a]	[a]
di-*n*-propyl ether	1.3805	3.4	0.188	0.212	21834	21322	21459
di-*n*-butyl ether	1.3992	3.1	0.195	0.170	21739	21231	21368
1,4-dioxane	1.4224	2.2	0.203	0.031	21459	20964	21097
dichloromethane	1.4242	8.9	0.203	0.470	21368	20790	20921
cyclohexane	1.4262	2.0	0.204	-0.004	21786	[a]	[a]
chloroform	1.4457	4.7	0.21	0.286	21231	20619	20790
cis-decalin	1.481	2.2	0.222	0.001	21505	[a]	[a]
benzene	1.5011	2.3	0.228	0.004	21231	20747	20833
benzonitrile	1.5282	25.2	0.235	0.582	21053	20619	20747
dichlorobenzene	1.5515	9.9	0.242	0.429	20921	20450	20534

a. Insoluble.

From Table 2-1 it is immediately clear that the absorption in the rotaxanes **1a** and **1b** is always at lower energy than that of the corresponding thread **2**. Overall, rotaxanation red-shifts the absorption maximum by ~800 cm^{-1} irrespective of the solvent. This is a sizable amount, corresponding to the solvent shift in the noninterlocked system **2** going from *n*-hexane to chloroform.

The experimental data were fitted to the two-parameter model of Equation 2-1. In agreement with previously reported trends for polyenes,[15] both for the bixin and the rotaxanated derivatives, the dominant contribution originates from the electronic polarisation term f_1. In Figure 2-3 we plot the experimental absorption maxima $\tilde{\nu}_{01}$ *vs.* f_1 (+), together with the predicted values from Equation 2-1 (open circles). The 1-dimensional crosscut of the fit at $B = 0$ visualises the minor importance of the f_2 contribution (Figure 2-3). The B term in

Equation 2-1 serves therefore merely as a correction factor. This is the typical situation for polyenes, which have a small dipole moment in both ground and excited states.

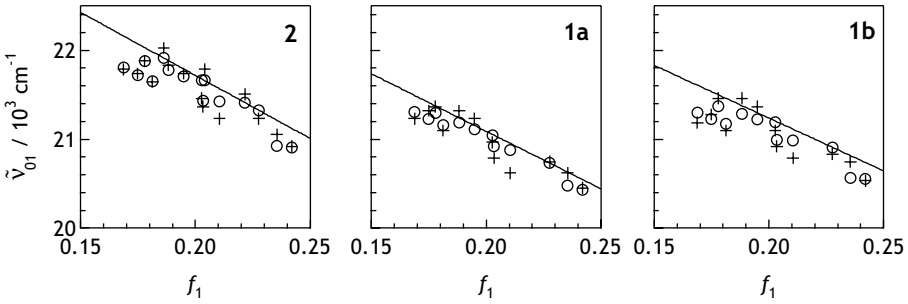

Figure 2-3. Experimental absorption maxima $\tilde{\nu}_{01}$ (+) plotted against f_1. The predicted values from the two parameter fit (Equation 2-1) are indicated by open circles. The straight line shows the crosscut of the fit plane at $B = 0$.

Table 2-2 summarises the fit results. The extrapolated gas-phase absorption maxima, $\tilde{\nu}_0$, show that in the absence of solvent, the macrocycle causes a red-shift of almost 900 cm^{-1}. It can be envisaged that this is caused by hydrogen bonding interactions of the macrocycle with the (conjugated) carbonyl group of one of the stoppers (see also Chapter 4). Although neither of the stoppers forms a good binding site for the ring (free shuttling was observed on the ^{1}H NMR time-scale down to -30°C)[17] most of the time the macrocycle will form a H-bond with one of the carbonyl groups, causing a red-shift of the absorption. The presence of the NO_2-group in the macrocycle hardly influences this value.

Table 2-2. Fit results (see Equation 2-1). Standard deviations in parentheses.

compound	$\tilde{\nu}_0$ [a] / 10^4 cm^{-1}	A / 10^4 cm^{-1}	B / 10^4 cm^{-1}
thread **2**	2.32 (0.03)	-1.4 (0.1)	-0.05 (0.01)
rotaxane **1a**	2.23 (0.04)	-1.3 (0.2)	-0.03 (0.02)
rotaxane **1b**	2.23 (0.04)	-1.2 (0.2)	-0.04 (0.02)

a. The gas phase 0-0 energy was obtained by subtracting 1360 cm^{-1} from the fit result, to compensate for using experimental $\tilde{\nu}_{01}$ data.

In terms of sensitivity to polarisation changes of the solvent (A term) the thread appears to be more affected than rotaxane **1a**, which in turn is more sensitive than the NO_2-rotaxane **1b**. This could be interpreted as a shielding of the polarisation effect of the solvent by the macrocycle or, in other words, as the insulation of the chromophore. Even if the effect of the macrocycle on the electronic states would have been nil, *i.e.* $\tilde{\nu}_0$ is unaffected by rotaxanation, this phenomenon could occur. The solvent cavity in which rotaxanes **1a** and **1b** reside is

enlarged due to the presence of the macrocycle. The polyene thus responds less to the polarisability of the solvent, because the macrocycle on average keeps the solvent at a larger distance. The same effect is responsible for the observed increase in photostability and fluorescence quantum yield of rotaxanated dyes in water. By keeping the solvent away from a chromophore, its quenching effects are diminished.[18,19]

2.5 Conclusions

Rotaxanation with the tetra-amide macrocycle of a natural polyenic system induces a red-shift of the $1B_u \leftarrow 1A_g$ transition of hundreds of wavenumbers, which is comparable to solvent induced shifts. Hydrogen bonding of the macrocycle to the terminal carbonyl groups of the carotenoid thread is considered to be responsible for this difference between thread and rotaxane. The solvatochromism of the absorption band of thread and rotaxanes was fitted with the McRae-Bayliss model, which showed that solvent polarisability accounts for the largest part of the solvent induced shift. We observed a decrease in sensitivity towards the solvent polarisability going from thread to rotaxane to NO_2-rotaxane, indicating that the macrocycle is capable of shielding the polyene electronic transition from the solvent field.

The 2^1A_g state could not be detected by fluorescence methods, but there are no indications that the state ordering in bixin or its rotaxanated compounds is any different from analogous long polyenes.

Acknowledgements. We thank Dr. T. Futterer, working in the group of Prof. Dr. D.A. Leigh at the University of Warwick, for performing the formidable syntheses of the bixin compounds. We thank Prof. W.J. Buma for useful discussions.

2.6 References

1. Mellor, J. In *Light, chemical change and life: a source book in photochemistry*; Coyle, J. D., Hill, R. R., Roberts, D. R., Eds.; The Open University Press: Walton Hall, Milton Keynes, 1982, pp 61-72.
2. Rauscher, R., Edenharder, R., and Platt, K.L. In vitro antimutagenic and in vivo anticlastogenic effects of carotenoids and solvent extracts from fruit and vegetables rich in cartenoids. *Mutation Research* **413**, 129-142 (1998)
3. Locknar, S.A., Peteanu, L.A., and Shuai, Z. Calculation of Ground and Excited State Polarizabilities of Unsubstituted and Donor/Acceptor Polyenes: A Comparison of the Finite-Field and Sum-Over-States Methods. *J. Phys. Chem. A.* **103**, 2197-2201 (1999)
4. Bermudez, V., Capron, N., Gase, T., Gatti, F.G., Kajzar, F., Leigh, D.A., Zerbetto, F., and Zhang, S.W. Influencing intramolecular motion with an alternating electric field. *Nature* **406**, 608-611 (2000)
5. Häberli, A., and Pfander, H. Synthesis of bixin and three minor cartenoids from annatta (*Bixa orellana*). *Helv. Chim. Acta* **82**, 696-706 (1999)
6. Orlandi, G., Zerbetto, F., and Zgierski, M.Z. Theoretical Analysis of Spectra of Short Polyenes. *Chem. Rev.* **91**, 867-891 (1991)

7. Hudson, B.S., Kohler, B.E., and Schulten In *Excited States*; Lim, E. C., Ed., 1982; Vol. 6, pp 1-95.
8. Kohler, B.E., Spangler, C., and Westerfield, C. The 2 ^1A_g State in the Linear Polyene 2,4,6,8,10,12,14,16- Octadecaoctaene. *J. Chem. Phys.* **89**, 5422-5428 (1988)
9. Turro, N.J. *Modern Molecular Photochemsitry* The Benjamin/ Cummings Publishing Company, Inc.: Menlo Park, California, 1978.
10. D'Amico, K.L., Manos, C., and Christensen, R.L. Electronic energy levels in a homologous series of unsubstituted linear polyenes. *J. Am. Chem. Soc.* **102**, 1777-1782 (1980)
11. Suppan, P., and Ghoneim, N. *Solvatochromism* The Royal Society of Chemistry: Cambridge, 1997.
12. Bayliss, N.S., and McRae, E.G. Solvent effects in organic spectra: dipole forces and the Franck-Condon principle. *J. Phys. Chem.* **58**, 1002-1006 (1954)
13. McRae, E.G. Theory of solvent effects on molecular electronic spectra. Frequency shifts. *J. Phys. Chem.* **61**, 562-572 (1957)
14. McRae, E.G. Solvent effects on merocyanine spectra. *Spectrochim. Acta* **12**, 192-210 (1958)
15. Cooper, T.M., Natarajan, L.V., Sowards, L.A., and Spangler, C.W. Investigation of solvatochromism in the low-lying singlet states of dithienyl polyenes. *Chem. Phys. Lett.* **310**, 508-514 (1999)
16. Sklar, L., Hudson, B., Petersen, M., and Diamond, J. Conjugated Polyene Fatty Acid fluorescent Probes: Spectroscopic Characterization. *Biochemistry* **16**, 813-819 (1977)
17. Leigh, D.A., (University of Warwick) personal communication.
18. Anderson, S., Aplin, R.T., Claridge, T.D.W., Goodson, T., Maciel, A.C., Rumbles, G., Ryan, J.F., and Anderson, H.L. An approach to insulated molecular wires: synthesis of water- soluble conjugated rotaxanes. *J. Chem. Soc.-Perkin Trans. 1* 2383-2397 (1998)
19. Buston, J.E.H., Young, J.R., and Anderson, H.L. Rotaxane-encapsulated cyanine dyes: enhanced fluorescence efficiency and photostability. *Chem. Commun.* 905-906 (2000)

Chapter 3

Electron Transfer in Rotaxanes

Signalling of the macrocycle's position by electron transfer quenching of a fluorescent stopper

How is it that we know so little, given that we have so much information.

– Noam Chomsky

3.1 Introduction

The architecture of rotaxanes offers unique possibilities to explore light driven processes between noncovalently bound entities, because the mechanical bond between the macrocycle and the thread allows the study of intermolecular processes that would otherwise be completely controlled by diffusion. From a photophysical perspective, electron transfer is one of the interesting processes that could take advantage of this property of the rotaxane molecular assembly. Rotaxanes can, for instance, be used to simulate the influence of natural cofactors on photoinduced electron transfer in the bacterial photosynthetic reaction centre. For this reason, Sauvage and co-workers studied the influence of the macrocycle on the electron transfer rates in rotaxanes with zinc(II) and gold(II) porphyrin stoppers.[1]

Electron transfer in rotaxanes has furthermore been used as a tool to change the binding interactions between the macrocycle and thread in order to induce a translation of the macrocycle.[2-7] Electron transfer, however, can also be employed to signal the position of the macrocycle on the thread by using its distance dependence. In this Chapter we will show that this can lead to a solvent polarity effect that is opposite to the normal intermolecular electron

transfer behaviour, where fluorescence quenching *via* electron transfer is faster and more efficient in more polar solvents. In the rotaxanes studied here, more polar solvents increase the average distance between electron donor (D) and acceptor (A). As a result the solvent effect is reversed.

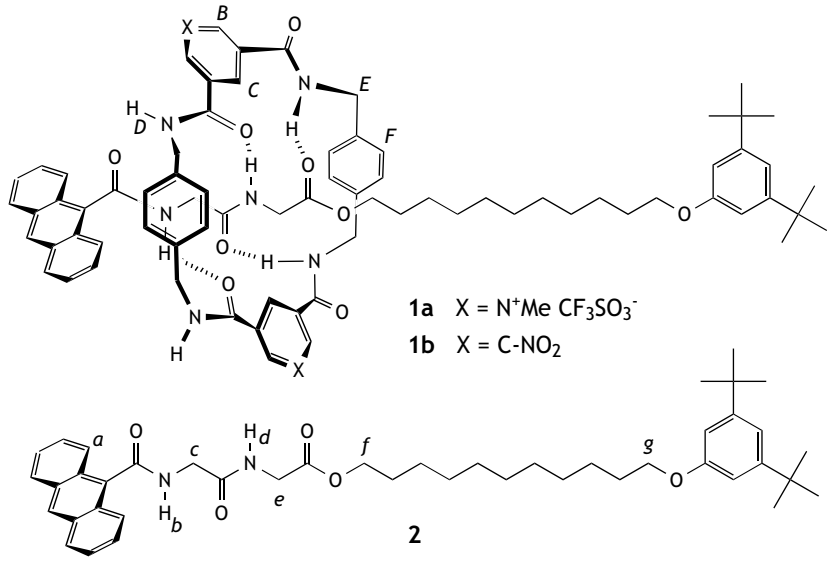

Figure 3-1. Chemical formulae of thread (**2**) and rotaxanes (**1a**-**b**), drawn with the H-bond motif found in the X-ray structure of a related system. The letters identify non-equivalent ^{1}H environments used in the assignment of the ^{1}H NMR spectrum (Figure 3-5). Capitals indicate macrocycle protons and lower case letters indicate thread

Rotaxanes **1a** and **1b** both contain a derivative of the tetra-amide macrocycle described as **5** in Figure 1-5 on page 8. Here the two isophthaloyl groups are replaced by electron accepting units: pyridinium-3,5-dicarboxamide groups in **1a**, and nitrobenzene-3,5-dicarboxamide groups in **1b**. The corresponding thread (**2**), consists of two regions with very different binding properties: a hydrophobic C_{11} alkyl chain, and a hydrogen-bonding dipeptide station (glycylglycine; GlyGly). The latter is covalently bound to a fluorescent stopper, *viz.* anthracene. In nonpolar, non-hydrogen-bonding solvents the macrocycle forms multiple H-bonds with the GlyGly station and thus anthracene and the electron accepting groups are in close proximity. These intercomponent hydrogen bonds are weakened in more polar, hydrogen-bond-disrupting solvents, displacing the macrocycle towards the alkyl chain. In this way, the maximum number of polar groups can be exposed to the solvent. Thus, the average location of the macrocycle on the thread is determined by the solvent properties.

The macrocycle's average position in general can be determined using ^{1}H NMR, but for **1a**-**b**, it can also be deduced from fluorescence measurements. Upon photoexcitation of the anthracene stopper, electron transfer to the electron accepting unit in the macrocycle occurs,

quenching the anthracene fluorescence. Since the rate of electron transfer typically drops exponentially with increasing distance, the amount of quenching is a measure for the distance between the anthracene stopper and the macrocycle (Figure 3-2). Using steady state and time resolved fluorescence techniques, we can form a more detailed picture of the conformational dynamics of hydrogen-bonded rotaxanes.

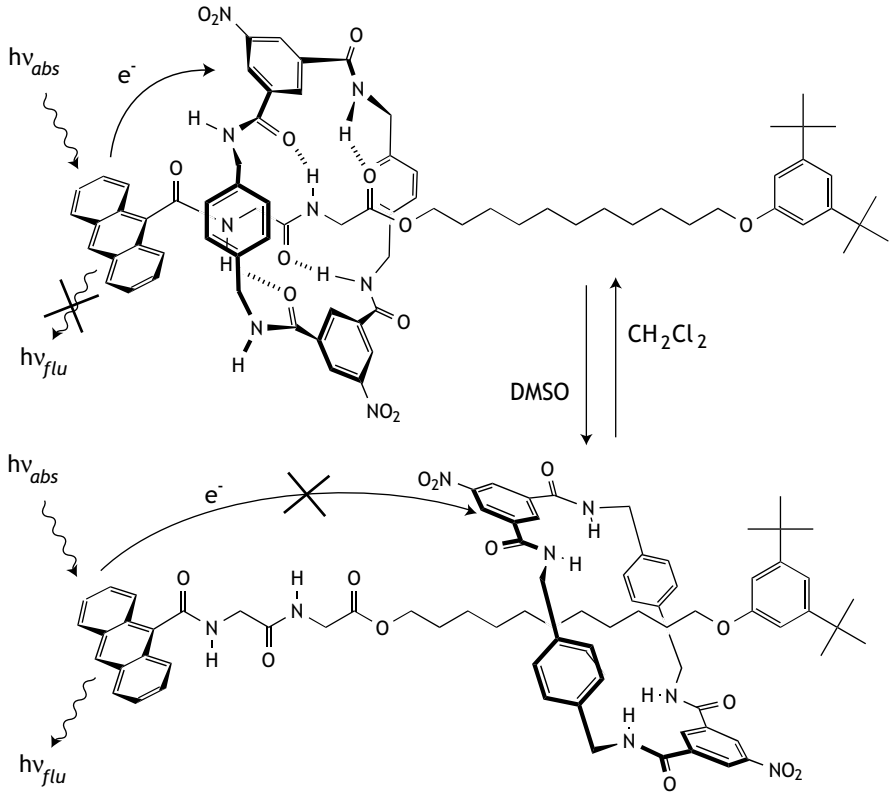

Figure 3-2. In a nonpolar solvent such as dichloromethane, the macrocycle resides on the peptide station. This is close to the anthracene stopper so electron transfer quenching is efficient. In a polar hydrogen-bond-disrupting solvent such as DMSO, the macrocycle surrounds the alkyl chain. This increases the distance to the anthracene stopper, making electron transfer slow and thus the fluorescence of anthracene is restored.

The same principles were used to construct a device in which the fluorescence of the anthracene stopper of the rotaxane is always quenched, because the macrocycle is constrained to be close to the anthracene, until it is released by photocleavage of the other stopper (Figure 3-3). Upon irradiation of **3** with UV light the desyl group is cleaved off the thread as shown in Figure 3-4. Without this stopper, the macrocycle can slip off the thread provided the surrounding matrix allows this molecular movement. After this dethreading, the anthracene flu-

orescence is no longer quenched and the system goes from a nonfluorescent to a fluorescent state as was demonstrated in solution.

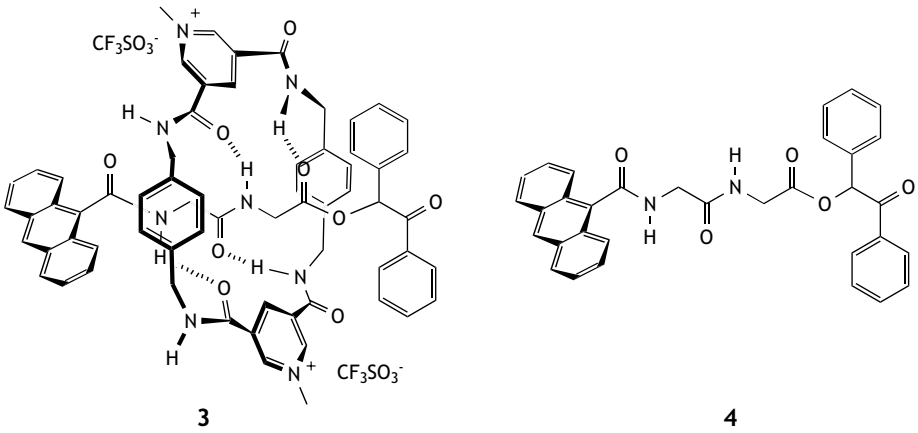

Figure 3-3. Structural formulae of the photocleavable rotaxane **3** and corresponding thread **4**.

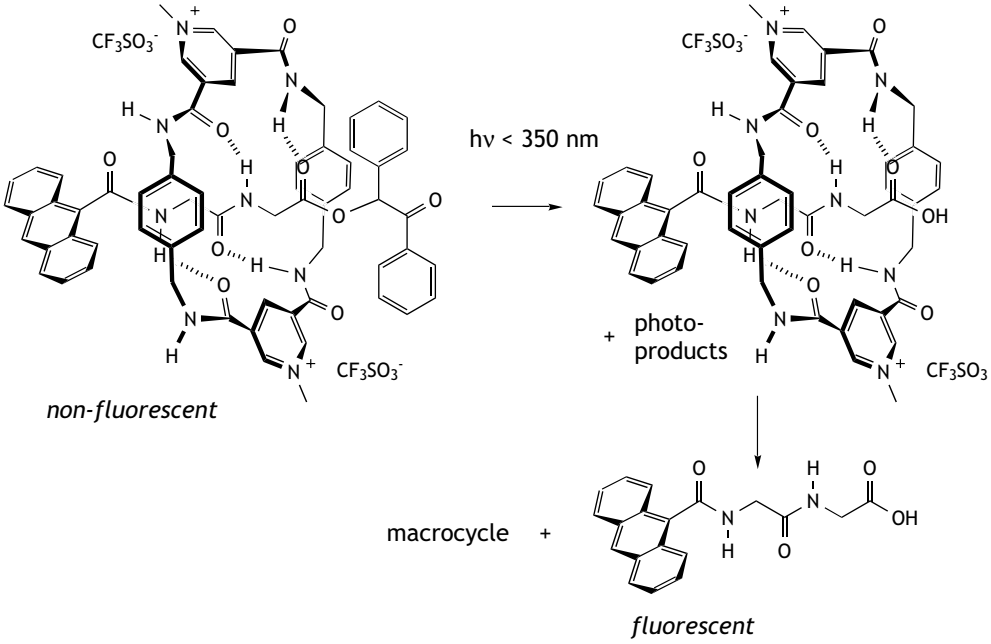

Figure 3-4. Irradiation of **3** with UV light leads to cleavage of the desyl stopper, causing dethreading of the macrocycle. The second stopper (anthracene) is now no longer quenched by the methylpyridinium groups of the macrocycle, and the system goes from a nonfluorescent to a fluorescent state.

The working of such a system is reminiscent of that of a WORM (Write Once Read Many times) device. We therefore tried to incorporate **3** into a solid matrix. Although the photocleavage reaction proceeded smoothly when **3** was mixed into a polymer, dethreading did not occur. Only in the presence of small amounts of solvents, as can be captured in a microporous filter (anodisc), could the rotaxane device be operated. The working of such a system was demonstrated by writing a fluorescent pattern on an anodisc.

3.2 Experimental

3.2.1 Fluorescence Measurements

Steady State. Samples were contained in Hellma 10×10 mm quartz cells. Fluorescence spectra were recorded on a Spex Fluorolog 3 emission spectrophotometer, using a spectral bandwidth of ≤ 2 nm for both excitation and emission. Spectra were corrected for the wavelength dependent response of the detection system and converted to a wavenumber scale: $f(\tilde{\nu}) = \lambda^2\varepsilon(\lambda)$ when an energy scale was needed.[8] Fluorescence quantum yields were determined with reference to a solution of quinine bisulphate in 1 M H_2SO_4 ($\Phi_f = 0.546$)[9] and corrected for the refractive index of the solvent. The samples had an absorbance of *circa* 0.1 (determined with a Cary 3E absorption spectrophotometer) at the excitation wavelength and were degassed by purging with argon for 15 minutes. Commercially available spectrograde solvents were used (Merck, Uvasol) and stored over mol sieves. When the purity of a solvent was found to be insufficient, it was purified by standard procedures.[10]

Time Resolved. Fluorescence decay curves were measured by means of picosecond time-correlated single photon counting (SPC). The experimental setup has been fully described elsewhere.[11] A mode-locked Argon-ion laser (Coherent 486 AS Mode Locker and Coherent Innova 200 laser) was used to pump synchronously a dye-laser (Coherent model 700, Radiant Dye "DCM-special"). The output frequency was doubled with a BBO crystal resulting in 322 nm or 330 nm pulses. The emission was detected under magic angle conditions (54°) with a Hamamatsu microchannel plate photomultiplier (R3809). Time windows (4000 channels) of 5 ns (1.25 ps/channel) - 50 ns (12.5 ps/channel) could be used, enabling the measurement of lifetimes of 5 ps - 40 ns. The instrument response function (fwhm ≈ 17 ps) was obtained by monitoring the Raman band of a cell filled with doubly deionised water. Samples were stirred with a magnetic stirrer, and two adjacent sides of the cell were painted black to avoid reflections at the quartz/air boundary. All samples were degassed by purging with Argon for at least 15 min.

The decay traces were iteratively deconvoluted with the DOS program Fld-Fit[12] to a multiexponential function with a maximum of three components. All fits had a $\chi^2 < 1.6$, evenly spread normalised residuals and a small baseline.

3.2.2 Synthesis

Threads and Rotaxanes. These were synthesised by M.A. Farrán Morales in the group of D.A. Leigh at the University of Warwick. Threads were synthesised in a 5-step reaction, after which a template directed clipping reaction with thread, xylylenediamine, and the appropriate diacid chloride in $CHCl_3$ led to the formation of the corresponding rotaxane.

Benzoin acetate (5). As outlined in literature,[13] 2 ml of concentrated sulfuric acid was added to a stirred mixture of benzoin (21.2 g, 0.1 mol), glacial AcOH (20 ml), and Ac_2O (20 ml). The mixture was refluxed at 80-85°C for 1 hour under the exclusion of light. The solution turned from orange to deep red. After cooling, the solution was added dropwise to ice water and stirred vigorously for 1 hour. A yellow solid precipitated that was filtered and washed with ice water. Recrystalisation from ethanol gave colourless needles. Yield: 24.4 g (96%); m.p: 81°C (lit. 80-82°C)

^{1}H NMR (400 MHz, $CDCl_3$): δ = 7.94 (d, 2H, ArH), 7.51 (t, 1H, ArH), 7.47 (d, 2H, ArH), 7.35-7.40 (m, 5H, ArH), 6.86 (s, 1H, CH), 2.2 (s, 3H, CH_3)

2-Phenylbenzofuran (6). Benzoin acetate (1.64 g, 6.4 mmol) was dissolved in 400 ml CH_2Cl_2 and the solution was irradiated in a quartz tube for 40 min. with a Rayonet reactor (300 nm, bubbling with N_2). The reaction was followed with TLC. 2-phenylbenzofuran was separated from the reaction mixture using column chromatography (petroleum ether:EtOAc 4:1, silica). Evaporation of the solvent afforded colourless crystals.

^{1}H NMR (400 MHz, $CDCl_3$): δ = 7.88 (d, 2H), 7.59 (d, 1H), 7.53 (d, 1H), 7.45 (t, 2H), 7.35 (t, 1H), 7.29 (t, 1H), 7.23 (t, 1H), 7.03 (t, 1H)

3.2.3 Irradiation Experiments

Lamp Irradiation. Samples were placed in front of an Oriel Hg 200 W high pressure lamp, equipped with a 313 nm interference filter.

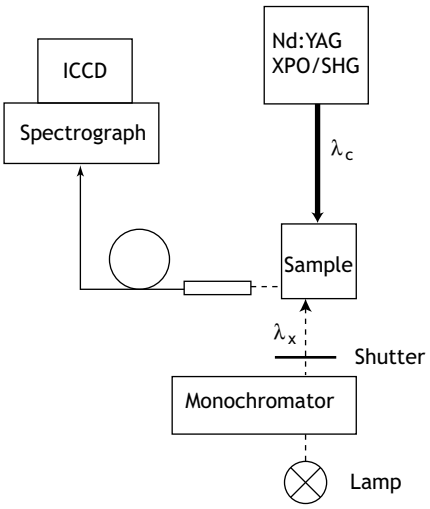

Pulsed Laser Irradiation. A quartz cell containing 1 ml solution (3×10^{-4} M) and a stirring rod was placed in the beam of a pulsed nanosecond laser (Coherent Infinity-XPO Laser with SHG option). The UV light needed for photocleavage (λ_c) was generated by frequency doubling (SHG) of the XPO output, giving a tunable wavelength range of 220-350 nm (30 Hz, pulse duration ~2 ns, typical power used 0.5-2 mJ/pulse).

In order to measure the fluorescence directly after a number of shots, a simple fluorescence setup was built around the cell. A continuous Xe lamp (Müller lamp housing LAX1450, power supply SVX1450) in combination with a monochromator (Oriel 7240) was used as a fluorescence excitation source (λ_x). The fluorescence was picked up by an optical fibre leading into an Acton SpectraPro-150 spectrograph which is coupled to a (Princeton Instruments) ICCD-576-G/RB-EM gated intensified CCD camera (gain 5, gate width 80 ms, 5 accumulations), and transferred to a computer. A shutter blocked the lamp light during the pulsed laser irradiation, and was opened afterwards for only 5 sec. to record the fluorescence spectrum, thus preventing photoreactions during the fluorescence detection.

Anodisc. Whatman's Anodiscs 25 (aluminiumoxide, diameter: 21 mm, thick: 60 μm, pore size 0.2 μm) were used as received. Solutions of rotaxane **3** in CH_2Cl_2 (~10^{-5} M) were added dropwise onto the Anodiscs which absorbed the solution in *circa* 10 min. to give a transparent plate.

3.3 Solvent-Switchable Rotaxanes

3.3.1 Structural Characteristics

The average location of the macrocycle on the thread can be inferred from the ^{1}H NMR spectra of thread and rotaxane in solution. The magnitude and direction of the complexation induced shift (CIS) of a thread signal compared to that of a rotaxane provides clues to the orientation and binding strength of the macrocycle.[14] For thread protons in the vicinity of the aromatic rings of the macrocycle an upfield shift will be observed. Protons involved in hydrogen bonding with the macrocycle are deshielded and thus a downfield shift is expected.

Here, the ^{1}H NMR spectra of **1b** are discussed, but the same trends can be observed in **1a**. In CD_2Cl_2, only the protons of the peptide region of **1b** have a large CIS with respect to thread **2** (Figure 3-5). The methylene protons of the GlyGly unit, H_c and H_e, are shifted upfield, just as the nearby protons *a* and *f*. Also the amide protons of the thread (H_b and H_d) show a large CIS, but only H_d is shifted downfield as one would expect for a hydrogen-bonded NH group. The macrocycle, thus, clearly surrounds the peptide station in CD_2Cl_2, but it does not form a symmetrical hydrogen bond pattern with the two amide groups of the GlyGly unit. The consequences of this asymmetry for the photophysical behaviour in a similar rotaxane will be discussed in Chapters 4 and 5.

In d_6-DMSO, the complexation induced shifts are completely different (Figure 3-5). The macrocycle no longer resides on the peptide station since the resonances of protons *a, b, c, d, e,* and *f* are almost the same in **1b** and **2**. The alkyl chain protons of **1b** on the other hand all display an upfield shift with respect to **2** which means that in d_6-DMSO the macrocycle shuttles over the hydrophobic part of the thread. This solvent induced translation of the macrocycle is a consequence of the fact that d_6-DMSO can better solvate the polar groups of the GlyGly station by hydrogen bonding to the amide NH groups than CD_2Cl_2 as is nicely demonstrated by the downfield shifts of NH_b and NH_d in **2** going from CD_2Cl_2 to d_6-DMSO (Figure 3-5).

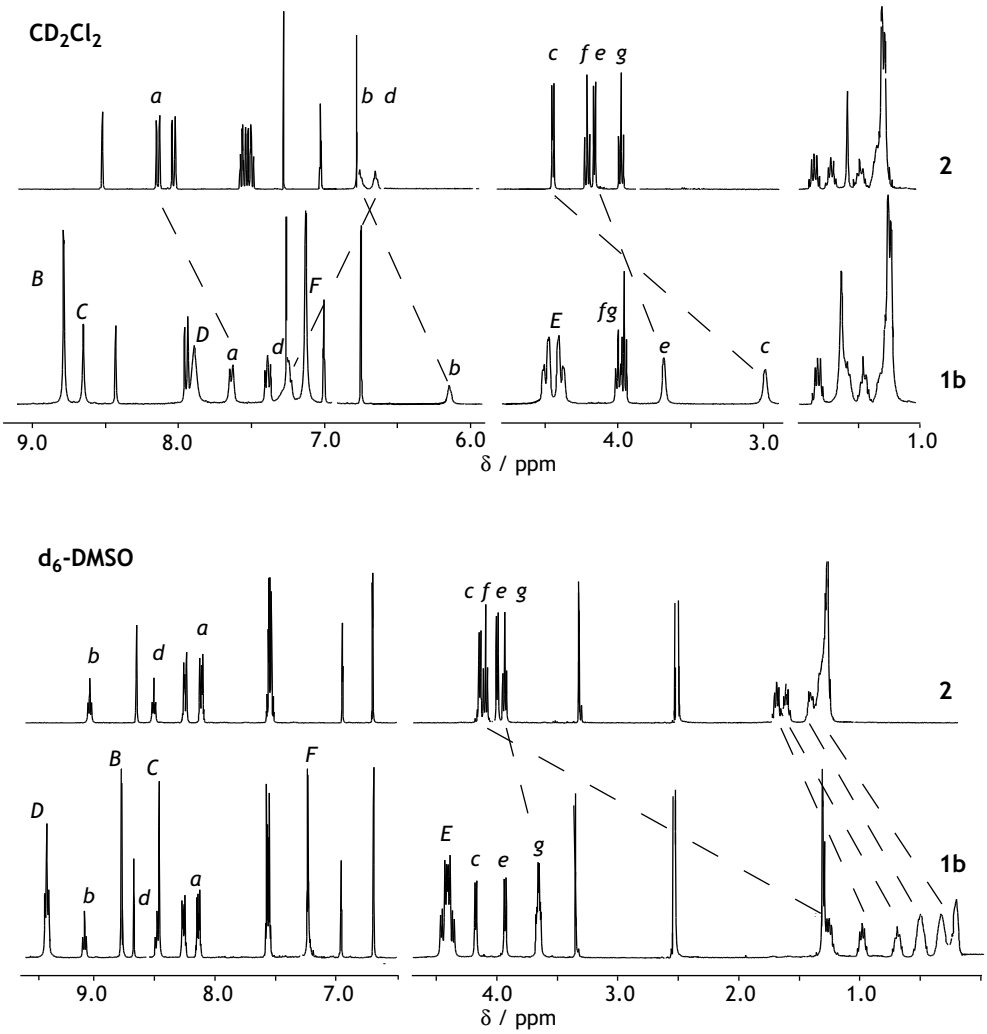

Figure 3-5. ^{1}H NMR (400 MHz) spectra of **2** and **1b** in nonpolar (CD_2Cl_2) and polar, H-bonding (d_6-DMSO) solution. The letters correspond to the assignment of the resonances shown in Figure 3-1.

3.3.2 Electron Transfer Thermodynamics and Kinetics

The fluorescence quenching of the anthracene stopper by the macrocycle in **1a** and **1b** is thought to occur *via* electron transfer. As we will show in this section, this is a reasonable assumption considering the energy levels and redox potentials of the systems. Attempts to detect the charge separated stated by transient absorption spectroscopy unfortunately failed due to a photobleaching reaction of the anthracene.

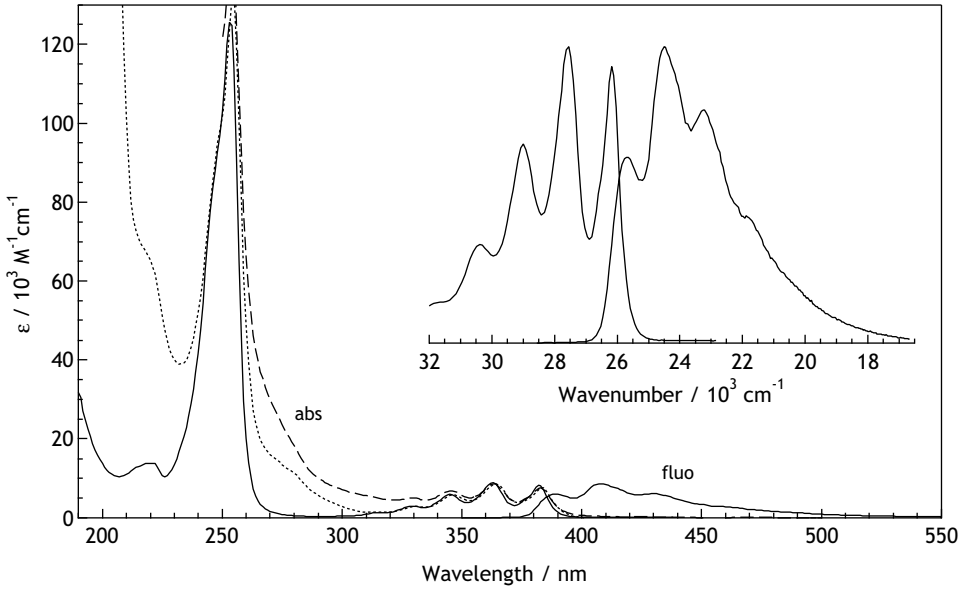

Figure 3-6. Absorption and fluorescence spectra of thread **2** in MeCN. The inset shows an enlargement of the S_0-S_1 transition. Absorption spectra of **1a** (dotted) and **1b** (dashed) are also shown.

The lowest electronic transition in the absorption spectra of all compounds showed the typical anthracene vibrational structure (Figure 3-6). The mirror image shape of the fluorescence spectrum confirms that indeed the lowest excited state is located on the anthracene-9-carboxamide fluorophore. Using the mirror relationship between absorption and fluorescence spectra of **2** in acetonitrile, E_{00} was located at 3.22 eV. Because there are no excited states of lower energy, excitation of the anthracene-9-carboxamide chromophore cannot lead to energy transfer.

The fluorophore in the singlet excited state, however, can easily be oxidised by the macrocycle, since it has a halfwave oxidation potential of $E_{ox}^{1/2}$ = + 1.6 V *vs.* SCE,[15] and the methylpyridinium and nitrobenzene moieties of **1a** and **1b** are reduced at $E_{red}^{1/2}$ = -1.0[16] and -0.95[17] V *vs.* SCE respectively. Since the driving force ($-\Delta G$) for electron transfer in polar solvents is given by

$$-\Delta G = E_{00} - e(E_{ox}^{1/2} - E_{red}^{1/2}) \qquad \text{(Eq. 3-1)}$$

electron transfer is thermodynamically feasible for both rotaxanes, having a $\Delta G \approx$ -0.6 eV. This driving force will make electron transfer fast, provided that there is sufficiently large electronic interaction between the donor and acceptor groups. It is also so large that electron transfer may be expected to remain thermodynamically feasible in much less polar solvents.

Indeed, the anthracene fluorescence of rotaxanes **1a** and **1b** is almost completely quenched in nonpolar solvents such as dichloromethane and benzene (Section 3.3.3). The fact that quenching in nonpolar solvents is still very efficient indicates that the electron transfer process might be close to the Marcus optimal region, where the reorganisation energy (λ) equals $-\Delta G$. In that case the electron transfer process is barrierless and insensitive towards the polarity of the solvent.[18] Indeed, we found that lowering the temperature of a solution of **1a** in CH_2Cl_2 or 2-methyl tetrahydrofuran (MTHF) did *not* result in a large increase of fluorescence. The fluorescence intensity increased only by a factor of 2.5 going from 300 to 180 K (Figure 3-7) which suggests that electron transfer in **1a** is close to barrierless. Only when the MTHF solution was cooled below its glass transition point (136 K) were all dark processes slowed down sufficiently to show a large increase in anthracene fluorescence.

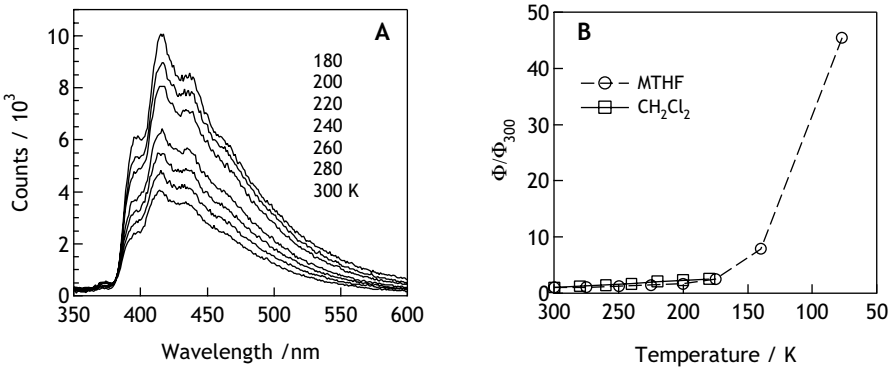

Figure 3-7. (A) Fluorescence spectra of rotaxane **1a** recorded at different temperatures in CH_2Cl_2. (B) The increase of fluorescence quantum yield as a function of temperature relative to its value at 300 K in CH_2Cl_2 and 2-methyl tetrahydrofuran (MTHF).

Thus at fixed donor-acceptor (D-A) distances, the solvent polarity will have little effect on the electron transfer quenching efficiency. In nonpolar solvents, **1b** will have a less negative driving force than in polar solvents due to the bigger Coulomb interaction in the charge separated state. However, since the system is close to the Marcus optimal region this hardly affects the electron transfer rate and thus the quenching efficiency. For rotaxane **1a** the situation is slightly more complicated because the macrocycle contains two cationic electron acceptors. Electron transfer from the anthracene stopper to the macrocycle thus results in a charge shift, which may lead to an increase of the distance between the positive charges. This would make the driving force even more negative. In nonpolar solvents, however, one must assume that the dicationic macrocycle is associated with its $CF_3SO_3^-$ counterions and therefore electron transfer results in a dipolar charge separated state, just like the charge transfer state of **1b**. This makes it difficult to predict the influence of the solvent polarity on the driving force for electron transfer in **1a**.

Because electron transfer occurs under conditions close to the optimum in the sense of Marcus theory, the effects of solvent polarity on electron transfer at fixed distance are likely to be small. The distance dependence of the electron transfer rate is expected to be much more important. Because the electronic coupling between donor and acceptor in general diminishes exponentially with distance, and the electron transfer rate k_{et} is proportional to the square of the electronic coupling matrix element, k_{et} can be described by

$$k_{et} = k_0 \exp(-\beta R_{DA}) \qquad \text{(Eq. 3-2)}$$

in which β is a constant, scaling the distance dependence, R_{DA} is the edge to edge distance between donor and acceptor, and k_0 is the rate at close contact. In well-designed through-bond electron-donor-acceptor systems an increase of D-A distance of 10 Å thus leads to a decrease of k_{et} by a factor of 10^4 (assuming β = 0.9 Å^{-1}).[19] In rotaxanes **1a** and **1b** the electron transfer pathways are not necessarily optimal and therefore the distance effect can be even more pronounced.

3.3.3 Steady State Fluorescence

The solvent can influence the average distance between donor and acceptor in rotaxanes **1a** and **1b** as demonstrated by the ^{1}H NMR experiments (Section 3.3.1). A polar, H-bonding solvent displaces the macrocycle from the peptide station thereby increasing the D-A distance. In nonpolar solvents, the macrocycle forms intercomponent H-bonds to the peptide station which brings the electron donor and acceptor in close proximity. As discussed in Section 3.3.2, at a fixed D-A distance the effect of solvent polarity on the electron transfer rate can be neglected. Thus for rotaxanes **1a** and **1b**, the solvent only influences the electron transfer rate by changing the distance between electron donor and acceptor.

The fluorescence quantum yields Φ_f of the thread **2** and rotaxanes **1a** and **1b** are shown in Table 3-1. In nonpolar solvents such as benzene and dichloromethane, electron transfer is fast enough to completely quench the anthracene fluorescence in both rotaxanes, which can only be explained by fast electron transfer in a close contact electron-donor-acceptor system. The very small residual fluorescence is attributed to a minor impurity, probably the thread (as argued in Section 3.3.4). In polar hydrogen bonding solvents such as methanol, DMF, DMSO, and formamide, the electron transfer quenching is less efficient, which is attributed to a larger average distance between the anthracene stopper and the macrocycle.

This solvent dependence is opposite to what is normally observed in inter- or intramolecular electron-donor-acceptor systems where the solvent in general does not have a significant influence on the distance between the electron donor and acceptor moieties. In the rotaxane, the average distance between the stopper and the macrocycle clearly depends on the solvent: how much of the anthracene fluorescence is regained by displacing the macrocycle from the peptide station depends on the solvent properties. Making the solvent more polar is not enough, as shown for acetonitrile in Table 3-1: even though acetonitrile has a high dielectric

constant (ε = 37.5), which should weaken the intercomponent H-bonds, this is not sufficient to significantly increase the distance between the anthracene stopper and the macrocycle. This is only accomplished by H-bond-disrupting solvents. As shown in Table 3-1, H-bond-*accepting* solvents such as DMSO are more effective in this respect than H-bond-*donating* solvents such as methanol, but the largest effect is found in formamide, an extremely polar solvent that can act both as a H-bond donor and acceptor. The magnitude of these effects is not very different for both rotaxanes, as one would expect for D-A systems with a comparable driving force for electron transfer. The differences that are observed might be due to the different types of charge transfer states that are formed in **1a** and **1b** as discussed in Section 3.3.2.

Table 3-1. Fluorescence quantum yields.

Solvent	Solvent Type[a]	ε	Φ_f			Residual [b]	
			2	**1a**	**1b**	**1a**	**1b**
benzene	aa	2.3	0.26	0.003	0.004	1%	2%
dichloromethane	aa	9.0	0.22	0.004	0.003	2%	1%
acetonitrile	da	37.5	0.17	0.004	0.003	2%	2%
methanol	hd	32.7	0.11	0.008	0.005	7%	5%
DMF	ha	37.0	0.11	0.007	0.013	6%	12%
DMSO	ha	49.7	0.19	0.019	0.032	10%	17%
formamide	hda	109.5	0.13	0.042	0.029	32%	22%

a. apolar aprotic (aa); dipolar aprotic (da), H-bond accepting (ha); H-bond donating (hd), H-bond donating and accepting (hda).

b. $100\% \times \Phi_f$(rotaxane) / Φ_f(thread).

No solvent was found that could displace the macrocycle to such a large distance of the anthracene stopper so as to prevent electron transfer completely. The largest recovery of fluorescence was found for **1a** in formamide where the fluorescence quantum yield of the rotaxane reached a value of 32% of the thread's fluorescence (Table 3-1). Two factors can be responsible for this: (i) electron transfer in the rotaxanes is very fast so that quenching of the anthracene stopper is efficient even if the macrocycle is far away, (ii) the *average* distance between stopper and macrocycle is not changed much, even if the latter is displaced from the peptide station. Using time resolved fluorescence measurements we will try to get a more detailed picture of the electron transfer quenching in rotaxanes **1a** and **1b**.

3.3.4 Time Resolved Fluorescence

Fluorescence decay traces were measured at 420 nm using a single photon counting setup and fitted using iterative deconvolution. Thread **2** had a monoexponential fluorescence decay in all solvents except DMSO and formamide. The rotaxane's decays were multiexponential for a number of reasons: (i) Both rotaxanes **1a** and **1b** may contain a small amount of strongly fluorescent impurities, most likely some unrotaxanated thread, or in the case of **1a**, some unmethylated rotaxane; (ii) Both thread and rotaxanes display excited state dynamics, *viz.* a rotation around the anthracene-carbonyl bond, which can have a dramatic effect on the rotaxane fluorescence even if the macrocycle does not contain electron accepting units (see Chapter 4); (iii) The rotaxane can adopt different (co-)conformations, with different D-A distances, leading to different electron transfer quenching rates.

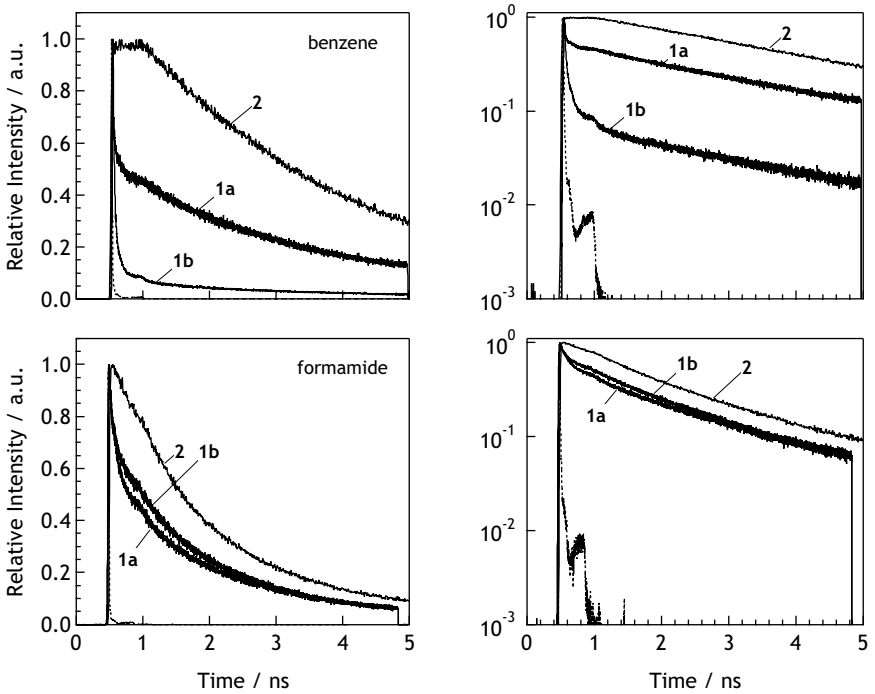

Figure 3-8. Decay traces of thread **2** and rotaxanes **1a** and **1b** recorded at 420 nm in benzene (top) and formamide (bottom). The instrument response function is shown in dots. The traces are plotted against both a linear (left) and a logarithmic (right) axis.

Interpretation of the time-resolved data therefore is difficult, but will aid in the elucidation of the electron transfer quenching mechanism in the rotaxanes. All rotaxane decays could be fitted reasonably well by a sum of three exponential functions. The component with the longest decay time ($\tau_1 \approx$ 1-3 ns) was identified in traces obtained with a 25 ns time window to have approximately the same decay time as the thread. In addition to τ_1, at least two other,

faster components were necessary to describe the data. These were fitted using fluorescence traces recorded with the smallest (5 ns) window, where one component (τ_1) was fixed to the value found in the 25 ns window. The associated decay times for τ_2 lie between 150 ps and 1 ns, and are <100 ps for τ_3 (see also Table 3-2). Typical decay traces for two solvents at the extremes of the polarity range are shown in Figure 3-8.

Visual inspection of the decay traces in benzene and formamide (Figure 3-8) provides important clues for the interpretation of the quantum yields of the rotaxanes with respect to those of the threads as discussed in Section 3.3.3. In benzene, the fluorescence of the rotaxanes (Φ_{rot}) is quenched to 1 or 2% of the thread's fluorescence (Φ_{th}) (see Table 3-1). In the simplest scenario this reduction of fluorescence intensity in the rotaxanes is solely attributed to electron transfer quenching as an additional excited state decay channel. This implies that with a decay time of the thread τ_{th} = 3.25 ns in benzene, the quenching constant k_q is *circa* 1.5×10^{10} s^{-1}, as calculated with the Stern-Volmer relation:

$$\Phi_{th}/\Phi_{rot} = 1 + k_q\tau_{th} \qquad \text{(Eq. 3-3)}$$

Such a quenching rate would correspond to a decay time of approximately 60 ps. Indeed, as can be seen in Figure 3-8, both **1a** and **1b** initially show a very fast decay that almost follows the instrument response (fwhm ≈ 17 ps). The remainder of the trace clearly has the same decay time as the thread, and although this "slow component" is responsible for more than 80% of the *integrated* fluorescence decay, its pre-exponential factor (A_3, see Table 3-2) is relatively unimportant. Such a contribution to the fluorescence decay could either stem from a small population of conformations where the macrocycle is too far from the anthracene stopper to give electron transfer or be attributed to a minor amount of impurity* with a high fluorescence quantum yield, most likely some unrotaxanated thread.

Because of this impurity the quenching efficiency in pure rotaxanes would be larger than the 98-99% observed in fluorescence quantum yield measurements. This, then, would mean that the actual quenching rate should be larger than that based on fluorescence quantum yields. Indeed, the fastest component of the fluorescence decay of the rotaxanes in benzene was found to be 7 ps and 19 ps for **1a** and **1b** respectively, which is almost 10 times faster than the values predicted by fluorescence quantum yield measurements. The corresponding rates (~10^{11} s^{-1}) are typical for a close contact D-A complex.[20]

*The methylpyridinium rotaxane **1a** is very poorly soluble in nonpolar solvents. This compound was therefore sonificated for 1 h which resulted in a finely divided suspension which was filtered. Inspection by its absorption spectrum showed that **1a** was present in this solution. The procedure, however, may well enrich the solution with a much more soluble thread impurity and the measurements of **1a** in benzene and dichloromethane might therefore show a larger contribution of thread-like component.

In formamide, the fluorescence decay traces look very different (Figure 3-8): although there are still fast contributions to the decay, these are less important than in benzene. Clearly, in a polar hydrogen bonding solvent the slower quenching and unquenched contributions are more important. These are attributed to conformations with larger distances between electron donor and acceptor.

The numerical results of the fits to the fluorescence decays in different solvents are shown in Table 3-2. These show the factors that are important in understanding why in rotaxanes **1a** and **1b** fluorescence quenching of the anthracene stopper is more efficient in nonpolar solvents than in polar, H-bond-disrupting solvents.

Table 3-2. Results for the fits of thread and rotaxane fluorescence decays detected at 420 nm. Thread **2** was fitted mono-exponentially. The fit function for the rotaxanes was of the form $A_1\exp(-t/\tau_1) + A_2\exp(-t/\tau_2) + A_3\exp(-t/\tau_3)$. The amplitudes ($A_n$) were scaled so as to give $A_1 + A_2 + A_3 = 1$.

	thread **2**	rotaxane **1a**					
solvent	τ / ns	A_1	τ_1 / ns	A_2	τ_2 / ns	A_3	τ_3 / ps
benzene	3.25	0.28	3.0	0.08	0.16	0.64	7
CH_2CL_2	2.96	0.14	3.2	0.13	0.32	0.73	19
acetonitrile	1.76	0.02	2.0	0.50	0.24	0.48	17
methanol	1.28	0.12	1.2	0.25	0.19	0.63	30
DMF	1.68	0.27	1.4	0.36	0.27	0.37	33
DMSO	2.21[a]	0.29	2.2	0.30	0.59	0.41	54
formamide	2.78[a]	0.13	3.4	0.31	0.94	0.56	89
	thread **2**	rotaxane **1b**					
solvent	τ / ns	A_1	τ_1 / ns	A_2	τ_2 /ns	A_3	τ_3 / ps
benzene	3.25	0.03	3.4	0.09	0.17	0.88	19
CH_2CL_2	2.96	0.06	2.7	0.10	0.12	0.84	13
acetonitrile	1.76	0.03	1.5	0.15	0.18	0.82	17
methanol	1.28	0.05	1.4	0.40	0.40	0.55	46
DMF	1.68	0.18	1.3	0.55	0.51	0.28	56
DMSO	2.21[a]	0.51	1.1	0.30	0.33	0.16	47
formamide	2.78[a]	0.06	5.0	0.46	1.14	0.48	86

a. Decay could not be fitted mono-exponentially. Shown is the longest component of a bi-exponential fit.

We assume that all fluorescent species in solution have the same radiative rate, which is reasonable since all fluorescence originates from the anthracene-9-carboxamide stopper. Also, we assume that the three types of species corresponding to the three decay times are present immediately upon excitation ($t = 0$) *i.e.* they are present in the ground state and are all excited by the laser pulse. Then, the scaled amplitudes A_n are a measure of the populations at $t = 0$ of species with a certain decay time τ_n. We noted, however, that in a tri-exponential fit the separate parameters cannot always be determined reliably. Especially when the decay times get closer in value, mutual compensation of A_n and τ_n is observed.

Although the data can be fit with three decay times, it seems unlikely that each of them corresponds to a single conformation. However, the large differences between τ_1, τ_2, and τ_3 indicates the presence of three rather different *groups* of conformers. In nonpolar solvents, amplitude A_3 is largest and the decay is dominated by the fastest (< 100 ps) component τ_3. Thus, in nonpolar solvents there is a large population of rotaxanes where the anthracene stopper and macrocycle are close enough to form a close contact electron-donor-acceptor complex. In more polar, H-bond-disrupting solvents, A_3 tends to become smaller in favour of the contributions with a longer decay time τ_2. The latter is tentatively assigned to conformations where electron transfer is slower because anthracene and macrocycle are separated a little further apart. For A_1, a less clear trend is observed: in nonpolar solvents, its entire value could be due to fluorescent impurities, while in more polar, H-bonding solvents there are likely to be conformations in which the distance between donor and acceptor is large enough to prevent electron transfer altogether. In that case, contributions to the decay traces are found with time constants that approach those of the thread under the same conditions.

It is furthermore noted that both τ_2 and τ_3 become larger with increasing polarity and H-bonding capacity of the solvent. As discussed in Section 3.3.2 this solvent effect is opposite to what would be expected for a D-A pair at fixed distance. This seems to suggest that within a group of conformations the average distance is also increased, or in other words a tight, close contact D-A pair becomes loser, and D-A pairs that are already separated get further apart.

How should we visualise these groups of conformations? For nonpolar solvents, the picture seems straightforward: the macrocycle resides on the peptide station and is therefore always close enough to the anthracene to give fast electron transfer quenching. In polar, hydrogen-bonding solvents the situation might be more complex. From ^{1}H NMR spectra, we know that in a solvent such as d_6-DMSO, the macrocycle surrounds the alkyl chain, since all alkyl protons of the rotaxane are shielded with respect to those of the thread (see Figure 3-5). By far the largest shift is observed for H_f, the methylene protons directly attached to the peptide station. This suggests that, although polar, hydrogen-bonding solvents displace the macrocycle from the peptide station, *on average* the macrocycle will not be located on the centre of the alkyl chain, but rather on the side closest to the anthracene stopper. Secondly, the alkyl chain is flexible, so that U-shaped conformations are possible in

which the electron accepting units of the macrocycle are very close to the anthracene stopper, whilst the centre of the macrocycle lies on the alkyl chain.

Finally, a dynamic effect should be considered: when a polar, H-bond-disrupting solvent displaces the macrocycle from the peptide station, it will spend most of its time on the alkyl chain. Since the macrocycle interacts with the alkyl chain much like it would with a nonpolar solvent, a quasi-onedimensional diffusional motion of the macrocycle along the alkyl chain of the thread is anticipated. Depending on the viscosity the macrocycle experiences, this process has a typical rate constant of 10^9-10^{11} s^{-1}. Considering the decay time of the anthracene-9-carboxamide excited state (1-3 ns), the macrocycle could thus "visit" the fluorophore several times.

3.3.5 Solvent Induced Switching

The combination of ^{1}H NMR and fluorescence spectroscopy shows that the position of the macrocycle can be switched by a change of solvent. The picture that emerges from fluorescence measurements is not as simple as that of ^{1}H NMR measurements. Due to the relatively long time scale (milliseconds) of the latter, what is observed is an average position of the macrocycle. On a shorter time scale, using picosecond-fluorescence spectroscopy, a more complex picture emerges. The multiexponential decay of the fluorescence shows that there exist probably more (co-)conformers in solution with different distances between the electron donating stopper and the electron accepting macrocycle.

At present the largest difference in fluorescence quantum yield is found when changing from a nonpolar solvent such as benzene or dichloromethane to formamide, using rotaxane **1a**. The rotaxane's fluorescence then goes from almost completely quenched to 32% of the thread's fluorescence. The time resolved measurements reveal why not more of the original fluorescence is recovered in polar, H-bonding solvents: the *average* distance between anthracene stopper and macrocycle does not increase enough. Although the contribution of the fastest component of the multi-exponential fluorescence decay associated with close contact conformers diminishes in polar, H-bond-disrupting solvents, it is still 30-50% of the total amplitude (Table 3-2).

Increasing the donor-acceptor distance by increasing the solvent polarity furthermore has the disadvantage that at the same time electron transfer rate is increased. An optimised rotaxane operating as a solvent induced switch would thus need to (i) have a rigid thread to prevent decreasing the donor-acceptor distance by folding, (ii) have the binding station on the other side of the thread so that increasing the solvent polarity not only closes the gap between stopper and macrocycle, but also increases the electron transfer rate so that both effects work co-operatively, and (iii) have a photostable, highly fluorescent stopper that does not display any excited state dynamics.

3.4 Photocleavable Rotaxane

In the previous section, rotaxanes **1a** and **1b** were discussed in which the fluorescence quenching of the macrocycle could be diminished by changing the solvent and thus changing the average distance between the anthracene stopper and the macrocycle. Here we will discuss the photochemistry of **3** (Figure 3-3) which is an analogue of **1a**: it has the same methylpyridinium macrocycle and anthracene stopper, but it does not have the alkyl chain. Most importantly, the second stopper is a photocleavable desyl group. Since the thread (**4**) of this rotaxane lacks the long alkyl chain, the macrocycle effectively quenches the fluorescence of the anthracene stopper because electron donor and acceptor are in close proximity irrespective of the surrounding medium. By cleaving off the desyl stopper, rotaxane **3** can be dethreaded, and the original thread fluorescence is restored (see Figure 3-4).

The photochemistry of the desyl group was first described by Sheenan and Wilson[21] and the mechanism of its photoreaction has recently been studied in detail.[22,23] This photocleavable group has found applications in the photorelease of biological compounds [24-26] and as a photobase for lithographic use.[27] Here, the desyl group is used to release the macrocycle, and thereby restoring the fluorescence of anthracene. Whether this will work depends on three things: (i) does the photocleavage reaction work, (ii) is the anthracene fluorophore photostable, and (iii) does dethreading take place. In order to study these factors separately, we looked at the rotaxane (**3**), the corresponding thread (**4**) and a reference compound for the photocleavable group, benzoin acetate (**5**).

The photoreaction of **5** is shown in Figure 3-9. Upon irradiation, the RCOOH group splits off and the strongly fluorescent 2-phenylbenzofuran (**6**) is formed in a cyclisation reaction from the triplet state.[22] A number of other Norrish type 1 photoproducts are also formed in the reaction: benzil, benzaldehyde, and dihydrobenzoindiacetate, none of which is fluorescent. Since the reactant, **5**, is also nonfluorescent, the reaction can conveniently be monitored by the increase in fluorescence due to **6**.

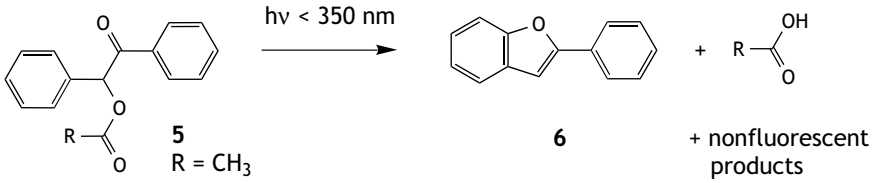

Figure 3-9. Irradiation of the desyl group releases RCOOH. For benzoin acetate **5** photocleavage gives acetic acid, the fluorescent product 2-phenylbenzofuran and other nonfluorescent products.

The absorption and fluorescence spectra of the relevant chromophores in the photoreaction of rotaxane **3** are shown in Figure 3-10. The photocleavable group (**5**) has a characteristic $n\pi^*$ absorption extending to ~350 nm. The other chromophore in **3** is the anthracene group,

which shows the typical vibrational fine structure in both absorption and fluorescence. Note, that between 270 and 320 nm, the anthracene absorption is minimal, so this is a good wavelength region to selectively excite the desyl stopper.

The fluorescent photoproduct of the cleavage reaction is **6**, which has distinct absorption and fluorescent features (Figure 3-10). Like anthracene it has a high fluorescence quantum yield (Φ_f= 0.35 in CH_2Cl_2) and shows vibrational fine structure, but the absorption and fluorescence spectra appear at *circa* 100 nm shorter wavelengths. Thus, after photocleavage of **3**, the progress of the reaction can conveniently be monitored by measuring the fluorescence intensity with excitation wavelengths of λ_x = 304 and 370 nm. These will show the advance of the desyl cleavage and the increase of anthracene fluorescence due to dethreading, respectively.

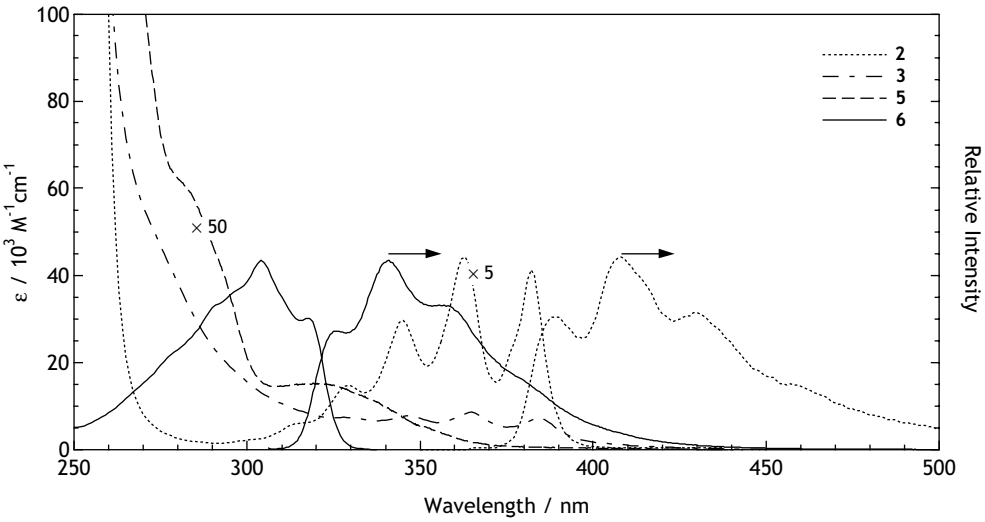

Figure 3-10. Electronic spectra of the chromophores in CH_2Cl_2, relevant in the photocleavage of **3** (dash-dot): The anthracene absorption and fluorescence (**2**, dotted), the desyl absorption (**5**, dashed), and the absorption and fluorescence of 2-phenylbenzofuran (**6**, continuous).

3.4.1 Solution Phase Irradiation

The photocleavage reaction of **5** is not a clean one, giving a number of photoproducts, but it is a fast reaction. Lamp irradiation studies of **5** in CH_2Cl_2 (3 ml; 2×10^{-4} M; 200 W Hg high pressure lamp equipped with a 313 nm interference filter) showed that within 5 min. fluorescence due to 2-phenylbenzofuran (**6**) had risen to its maximum. At this point the fluorescence intensity was compared to that of a solution with a known concentration of **6**. This showed that the mixture of photoproducts contained ~5% 2-phenylbenzofuran.

Having established that the cleavage of **5** in solution proceeds rapidly and can conveniently be monitored using fluorescence spectroscopy, we tried to cleave the desyl stoppers of rotaxane **3** and its corresponding thread **4**. As an excitation source for the cleavage reaction a pulsed nanosecond laser setup was used (see Section 3.2.3) in which the changes in fluorescence can be measured directly after a number of shots. This setup furthermore has the advantage that monochromatic light between 220 and 350 nm can be generated with a known pulse energy. In a typical experiment the laser was operated at λ_c = 285 nm, with 0.3 mJ/pulse energy. After a number of shots, the 2-phenylbenzofuran and anthracene fluorescence were measured using λ_x = 304 and 370 nm respectively. The results for thread **4** in CH_2Cl_2 are shown in Figure 3-11.

In Figure 3-11a we see that within 3000 laser shots the fluorescence due to 2-phenylbenzofuran has reached its maximum. The typical vibrational structure is not observed because large slits were used to improve the signal-to-noise ratio. The anthracene fluorescence shown in Figure 3-11b measured at the same intervals remains more or less constant. This shows that in CH_2Cl_2 solution, cleavage of the desyl stopper can be accomplished without bleaching of the anthracene fluorophore. Note further that photoexcitation of the desyl stopper could give energy transfer to the anthracene chromophore: the anthracene singlet state (see absorption spectra in Figure 3-10) and probably the triplet state (anthracene has a large S-T gap: 1.45 eV[28]) are below that of benzoinacetate, but apparently the photoreaction proceeds fast enough.

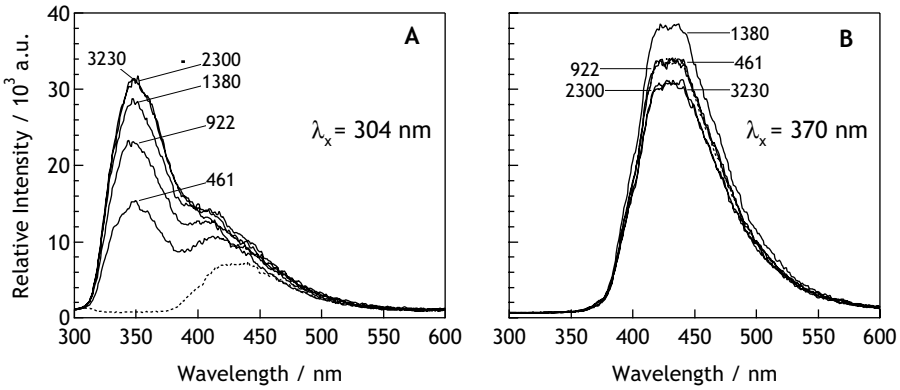

Figure 3-11. Fluorescence spectra of a solution of thread **4** in CH_2Cl_2 (1 ml, 3×10^{-4} M) taken after the indicated number of shots with a nanosecond laser (λ_c = 285 nm, 0.3 mJ/pulse). (A) fluorescence due to 2-phenylbenzofuran is detected using an excitation wavelength of λ_x = 304 nm. The spectrum obtained before laser irradiation (dotted) is due to anthracene fluorescence. (B) Anthracene fluorescence is detected with λ_x = 370 nm.

The results for the thread photocleavage indicate that the same experiment should also work for rotaxane **3**. Indeed, as shown in Figure 3-12a, the desyl group is split off as is evident

from the increase of the 2-phenylbenzofuran fluorescence. With the desyl stopper removed from the thread, the macrocycle can dethread, thus increasing the distance between the anthracene stopper and the quenching units of the macrocycle.

This dethreading of **3** is observed when the fluorescence of the sample is monitored using an excitation wavelength of λ_x = 370 nm (Figure 3-12b). Before pulsed laser irradiation, there is little anthracene fluorescence, because it is quenched by the macrocycle. After 23500 shots (λ_c = 285 nm, 0.3 mJ/pulse) this fluorescence has increased by a factor of 10. Further evidence that the increase in anthracene fluorescence arises from dethreading is found in the increase in scattering of excitation light (Figure 3-12b) that was only observed for rotaxane **3**. The macrocycle is known to be insoluble in nonpolar solvents[29] and since this light scattering was not observed in thread **4** it is likely to be due to precipitation of the macrocycle.

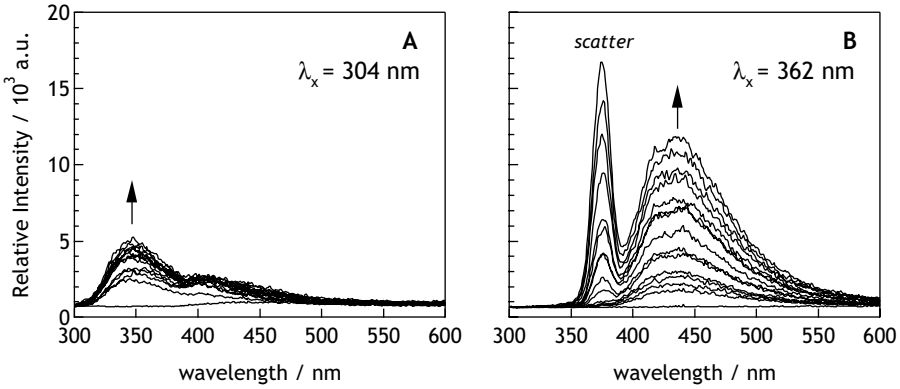

Figure 3-12. Photocleavage of a solution of **3** in CH_2Cl_2 (1 ml, 3×10^{-4} M, λ_c = 285 nm, 0.3 mJ/pulse) with a total of 23500 shots. (A) fluorescence due to 2-phenylbenzofuran is detected using an excitation wavelength of λ_x = 304 nm. (B) Anthracene fluorescence is detected with λ_x = 370 nm.

3.4.2 Solid Support Irradiation

Having established a proof of principle that rotaxane **3** can show photoinduced dethreading monitored by an increase of anthracene fluorescence as laid out in Figure 3-4, we set out to incorporate **3** into a solid matrix. It had been shown that desyl derivatives incorporated in polymethacrylonitrile (PMAN) could be cleaved.[27] Indeed, we were able to show photocleavage of **5** in spin coated thin layers of PMAN as well as in polymethylmethacrylate (PMMA) and polystyrene. When rotaxane **3** was incorporated in the same polymers, however, the solution irradiation behaviour as shown in Figure 3-12 was not reproduced. Apparently, the bottleneck is not the photocleavage of the desyl stopper but the dethreading of the macrocycle.

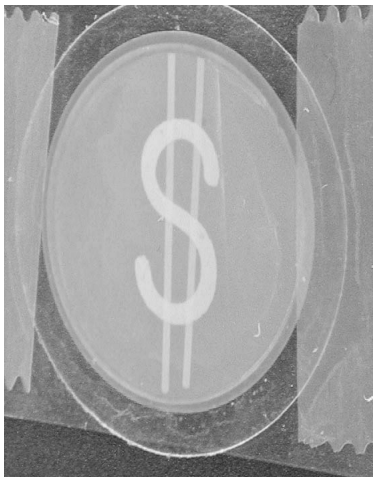

Figure 3-13. Fluorescent $-sign obtained by 313 nm irradiation through a mask of a solution of **3** in CH_2Cl_2 contained in an anodisc.

The large amplitude motion needed for dethreading can only occur when the surrounding medium is not too rigid. Photoinduced dethreading of **3** incorporated in some sort of solid will therefore always be troublesome. The golden mean therefore would be to solvate the rotaxane in a suitable solvent and microencapsulate this in a solid medium. A simple medium in which a liquid phase can be immobilised was found in the anodisc membrane filter which consists of a thin layer of Al_3O_2 with a precise nondeformable honeycomb pore structure of 0.2 μm.

When a solution is dropped onto such an anodisc it is absorbed into the pores of the filter. The solute most probably adsorbs to the aluminium oxide walls, surrounded by solvent. In this way an anodisc was "filled" with a solution of **3** in CH_2Cl_2 and placed in front of a 200 W high pressure Hg lamp (λ_c = 313 nm) with a mask. After 20 min. exposure the anodisc clearly showed the fluorescent imprint when put under "black light" (Figure 3-13). When the solvent was evaporated from the anodisc under vacuum prior to irradiation fluorescent patterning was impossible.

Clearly, the principle of photoinduced dethreading works in a solid support, provided some solvent is present. This could therefore be considered the first step in the direction of a WORM (write once read many times) kind of device based on rotaxanes. At present the system is far from optimised. The desyl group seems to be a very efficient photocleavable group, but its photoreaction is not very clean. With the right substituents, this can be improved a lot.[27] The dethreading step poses a greater challenge: in solution there is no problem, but for practical applications a solid support is necessary. Microencapsulation of rotaxane in solution as provided by the anodiscs could be a solution to the problem.

3.5 Conclusions

Electron transfer in rotaxanes where the electron donor is located at the stopper and the acceptor is incorporated in the macrocycle has been used to signal the location of the macrocycle. In rotaxanes **1a** and **1b** the distance between the anthracene stopper and the macrocycle could be influenced by the solvent. Increasing the average distance between the anthracene stopper and macrocycle was shown to slow down the electron transfer and reduce the quenching of anthracene. No solvent was found to increase this distance so as to completely prevent the electron transfer quenching. The biggest effect was measured for forma-

mide, an extremely polar solvent that is both a H-bond acceptor and H-bond donor so it can most effectively displace the macrocycle from its binding station.

Time resolved fluorescence measurements revealed that in solution at least three groups of rotaxane conformations could be identified: (i) conformations in which the anthracene stopper and the electron accepting units of the macrocycle are in close contact giving rise to fast ($\sim 10^{11}$ s^{-1}) electron transfer, (ii) conformations where they are further apart so electron transfer quenching is slower, and (iii) conformations where the distance between them is so large that electron transfer is prevented. We propose that a change of solvent influences the relative populations of these conformations and thus determines the fluorescence quenching efficiency.

In rotaxane **3** the same macrocycle as used in **1a** could be removed from the thread altogether by photocleavage of the desyl stopper. In dichloromethane solution this led to dethreading of the macrocycle by which its quenching of the second (anthracene) stopper is cancelled out. Using a microporous filter this mechanism could be used to write a fluorescent pattern on a solid support.

Acknowledgements. The compounds discussed in this Chapter were synthesised by Dr. M.A. Farrán Morales in the group of Prof. Dr. D.A. Leigh from the University of Warwick. Drs. S.A. Zoon measured the photocleavable rotaxane and made it work on a solid support. We also thank Ing. D. Bebelaar for technical assistance with the SPC measurements.

3.6 References

1. Chambron, J.C., and Sauvage, J.P. Functional rotaxanes: From controlled molecular motions to electron transfer between chemically nonconnected chromophores. *Chem.-Eur. J.* **4**, 1362-1366 (1998)
2. Benniston, A.C., Harriman, A., and Lynch, V.M. Photoactive [2]Rotaxanes - Structure and Photophysical Properties of Anthracene-Stoppered and Ferrocene-Stoppered [2]Rotaxanes. *J. Am. Chem. Soc.* **117**, 5275-5291 (1995)
3. Ballardini, R., Balzani, V., Gandolfi, M.T., Prodi, L., Venturi, M., Philp, D., Ricketts, H.G., and Stoddart, J.F. A Photochemically Driven Molecular Machine. *Angew. Chem.-Int. Edit. Engl.* **32**, 1301-1303 (1993)
4. Ashton, P.R., Ballardini, R., Balzani, V., Credi, A., Dress, K.R., Ishow, E., Kleverlaan, C.J., Kocian, O., Preece, J.A., Spencer, N., Stoddart, J.F., Venturi, M., and Wenger, S. A photochemically driven molecular-level abacus. *Chem.-Eur. J.* **6**, 3558-3574 (2000)
5. Ashton, P.R., Balzani, V., Kocian, O., Prodi, L., Spencer, N., and Stoddart, J.F. A light-fueled "piston cylinder" molecular-level machine. *J. Am. Chem. Soc.* **120**, 11190-11191 (1998)
6. Ashton, P.R., Ballardini, R., Balzani, V., Constable, E.C., Credi, A., Kocian, O., Langford, S.J., Preece, J.A., Prodi, L., Schofield, E.R., and Spencer, N. Ru-II polypyridine complexes covalently linked to electron acceptors as wires for light-driven pseudorotaxane-type molecular machines. *Chem.-Eur. J.* **4**, 2413-2422 (1998)

7. Brouwer, A.M., Frochot, C., Gatti, F.G., Leigh, D.A., Mottier, L., Paolucci, F., Rofia, S., and Wurpel, G.W.H. Photoinduction of Fast, Reversible Translational Motion in a Hydrogen-Bonded Molecular Shuttle. *Science* **291**, 2124-2128 (2001)
8. Lakowicz, J.R. *Principles of fluorescence spectroscopy* Plenum Press: New York, 1983.
9. Eaton, D.F. International-Union-of-Pure-and-Applied-Chemistry Organic- Chemistry Division Commission On Photochemistry - Reference Materials For Fluorescence Measurement. *J. Photochem. Photobiol. B-Biol.* **2**, 523-531 (1988)
10. Perrin, D., Armarego, W., and Perrin, D. *Purification of Laboratory Chemicals* 2nd ed.; Pergamon Press Ltd.: Oxford, 1980.
11. van Dijk, S.I., Wiering, P.G., Groen, C.P., Brouwer, A.M., Verhoeven, J.W., Schuddeboom, W., and Warman, J.M. Solvent-dependent switching between two dipolar excited states in a rigidly extended trichromophoric system. *J. Chem. Soc.-Faraday Trans.* **91**, 2107-2114 (1995)
12. Gedeck, P., FLDFIT Inst. f. Phys. Chem. I: University of Erlangen-Nürnberg
13. Pei, W., Li, S., Nie, X., Li, Y., Pei, J., Chen, B., Wu, J., and Ye, X. Convenient Syntheses of 2-Alkyl(Aryl)-4,5-diphenyloxazoles and 2-Alkyl(Aryl)-4-phenyloxazoles. *Synthesis* **9**, 1298-1304 (1998)
14. Schneider, H.-J., and Yatsimirsky, A. *Principles and Methods in Supramolecular Chemistry* Wiley: Chichester, UK, 2000.
15. Paolucci, F., (University of Bologna) personal communication.
16. Kuroda, Y., Seshimo, H., Kondo, T., Shiba, M., and Ogoshi, H. Synthesis and redox behavior of novel cyclic hosts having multiple redox centers of NAD+ analogue. *Tetrahedron Lett.* **38**, 3939-3942 (1997)
17. Newkome, G.R., Narayanan, V.V., and Godínez, L.A. Electroactive, Internal Anthraquinonoid Dendritic Cores. *J. Org. Chem.* **65**, 1643-1649 (2000)
18. Kroon, J., Verhoeven, J.W., Paddon-Row, M.N., and Oliver, A.M. Solvent Dependence of Photoinduced Intramolecular Electron- Transfer - Criteria for the Design of Systems with Rapid, Solvent-Independent Charge Separation. *Angew. Chem.-Int. Edit. Engl.* **30**, 1358-1361 (1991)
19. Oevering, H., Paddon-Row, M., Heppener, M., Oliver, A., Cotsaris, E., Verhoeven, J., and Hush, N. Long-range photoinduced through-bond electron transfer and radiative recombination via rigid nonconjugated bridges: distance and solvent dependence. *J. Am. Chem. Soc.* **109**, 3258-3269 (1987)
20. Castner, E.W., Kennedy, D., and Cave, R.J. Solvent as electron donor: Donor/acceptor electronic coupling is a dynamical variable. *J. Phys. Chem. A* **104**, 2869-2885 (2000)
21. Sheenan, J., and Wilson, R. Photolysis of Desyl Compounds. A new Photolytic Cyclization. *J. Am. Chem. Soc.* **86**, 5277-5281 (1964)
22. Rajesh, C.S., Givens, R.S., and Wirz, J. Kinetics and Mechanism of Phosphate Photorelease from Benzoin Diethyl Phosphate: Evidence for Adiabatic Fission to an α-Keto Cation in the Triplet State. *J. Am. Chem. Soc.* **122**, 611-618 (2000)
23. Shi, Y., Corrie, J.E.T., and Wan, P. Mechanism of 3',5'-Dimethoxybenzoin Ester Photochemistry: Heterolytic Cleavage Intramolecularly Assisted by the Dimethoxybenzene Ring Is the Primary Photochemical Step. *J. Org. Chem.* **62**, 8278-8279 (1997)
24. Geibel, S., Barth, A., Amslinger, S., Jung, A., Burzik, C., Clarke, R., Givens, R., and Fendler, K. P^3-[2-(4-hydroxyphenyl)-2-oxo]ethyl ATP for the rapid activation of the Na^+,K^+-ATPase. *Biophys. J.* **79**, 1346-1357 (2000)

25. Gee, K.R., Kueper III, L.W., Barnes, J., Dudley, G., and Givens, R.S. Desyl Esters of Amino Acid Neurotransmitters. Phototriggers for Biologically Active Neurotransmitters. *J. Org. Chem.* **61**, 1228-1233 (1996)
26. Givens, R. Photochemistry of Phosphate Esters: α-Keto Phosphates as a Photoprotecting Group for Caged Phosphate. *J. Am. Chem. Soc.* **115**, 6001 (1993)
27. Cameron, J.F., Willson, C.G., and Frechet, J.M.J. Photogeneration of amines from α-keto carbamates: Photochemical studies. *J. Am. Chem. Soc.* **118**, 12925-12937 (1996)
28. Fukumura, H., Kikuchi, K., Koike, K., and Kokubun, H. Temperature Effect On Inverse Intersystem Crossing of Anthracenes. *J. Photochem. Photobiol. A-Chem.* **42**, 283-291 (1988)
29. Johnston, A.G., Leigh, D.A., Murphy, A., Smart, J.P., and Deegan, M.D. The synthesis and solubilization of amide macrocycles via rotaxane formation. *J. Am. Chem. Soc.* **118**, 10662-10663 (1996)

Chapter 4

ANTHRACENE ROTAXANES

Sub-nanosecond excited state dynamics in a peptide based, hydrogen-bonded molecular shuttle[*]

4.1 Introduction

The mechanically interlocked nature of the molecules that comprise a rotaxane makes it impossible for them to diffuse away from each other. This unique characteristic causes certain small intermolecular effects that would normally occur only under special conditions, to be readily revealed and very prominent. An example of such behaviour will be discussed in this Chapter.

The rotaxane (**1**) studied here contains the same thread (**2**) as the rotaxanes described in Chapter 3. There we saw that when the macrocycle contains a strongly electron accepting group, the fluorescence of the anthracene stopper is quenched. In **1** no such quenching units are present, still the macrocycle has a surprisingly large influence on the fluorescence of the anthracene chromophore.

It will be shown in this Chapter that this is due to a rearrangement of the hydrogen-bond pattern between the binding station and the macrocycle after photoexcitation of the anthracene fluorophore. These changes, that effectively draw the macrocycle closer to the anthracene stopper, are preluded by a fast rotation around the anthracene-carbonyl bond in the excited state. All these dynamical processes take place during the lifetime of the anthracene singlet excited state (2-4 ns), and some of the steps occur on a sub-nanosecond timescale.

---

*Wurpel, G.W.H., Brouwer, A.M., van Stokkum, I.H.M., Morales Farran, M.A., and Leigh, D.A., submitted to *J. Am. Chem. Soc.*

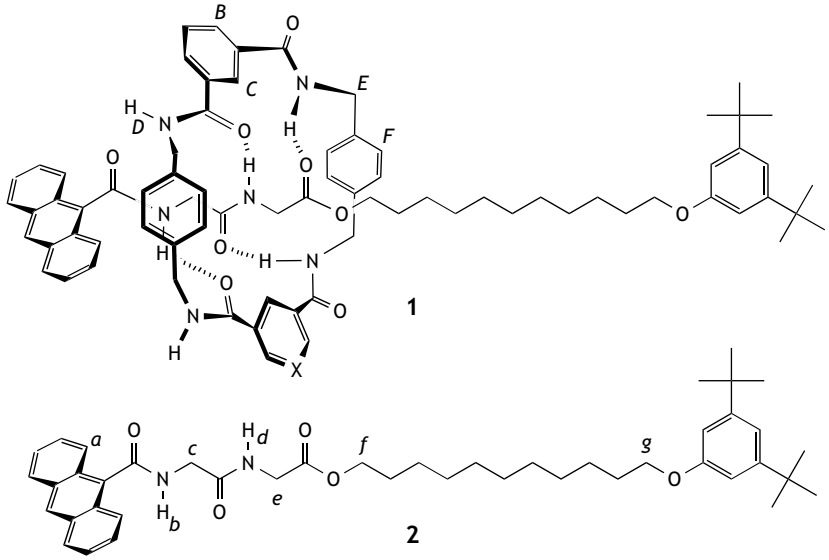

Figure 4-1. Chemical formulae of thread (**2**) and rotaxane (**1**), drawn with the H-bond motif found in the X-ray structure of a related compound. The letters identify nonequivalent ^{1}H environments used in the assignment of the ^{1}H NMR spectrum (Figure 4-2). Capitals indicate macrocycle protons and lower case letters indicate thread protons.

Due to the short lifetime of (singlet) excited states, it has thusfar been impossible to achieve a photoinduced change in the macrocycle position in rotaxanes *intra*molecularly,[1,2] other than by photoisomerisation.[3] Rotaxane **1** constitutes the first example of very fast, reversible switching of the macrocycle upon photoexcitation, without the requirements of external agents (sacrificial reductants, sensitisers, *et cetera*). The distance travelled by the macrocycle, however, is still somewhat limited: ~3Å. In Chapter 6 we will describe a different system, in which reversible switching of conformational states occurs over a longer distance. This switching is still fast, but approximately 1000× slower than in the present case.

4.2 Experimental

Samples. The thread and rotaxane were synthesised by M.A. Farrán Morales in the group of D.A. Leigh at the University of Warwick. Threads were synthesised in a 5-step reaction, after which a template directed clipping reaction with thread, xylylenediamine, and the appropriate diacid chloride in $CHCl_3$ led to the formation of the corresponding rotaxane.

Fluorescence Measurements. Steady state fluorescence and time resolved fluorescence methods are described in Section 3.2.1 on page 45.

Commercially available spectrograde solvents were used (Merck, Uvasol), with the exception of 2,2,2-trifluoroethanol (Aldrich, 99+%), and stored over mol sieves. When the purity of a solvent was found to be insufficient, it was purified by standard procedures.[4] Fluorescence measurements on solid

matrices were performed under front face conditions. 10% polymethyl methacrylate (PMMA) samples were spincoated from toluene. A D(+)-sucrose octaacetate glass (SOA, Aldrich, recrystalised from ethanol) was formed by dissolving both the compound and SOA in a small amount of dichloromethane and casting it on a quartz plate. The sample was then heated above the melting point (87-89°C) under a nitrogen stream with a home built thermostat to evaporate the solvent. After cooling down to room temperature a transparent glass had formed.

Temperature Control. Measurements at low temperature were performed using an Oxford Instrument liquid nitrogen cryostat DN 1704 with an ITC4 control unit. The samples were degassed by at least three freeze-pump-thaw cycles and allowed to thermally equilibrate for at least 30 minutes prior to data collection.

4.3 Results and Discussion

4.3.1 Structural Characteristics

Rotaxane **1** consists of a benzylic amide macrocycle, mechanically interlocked onto the corresponding thread **2**. It contains one region capable of hydrogen bonding to the macrocycle, *viz.* a glycylglycine (GlyGly) dipeptide recognition motif, and one hydrophobic region, *viz.* a C_{11} alkyl chain. The alkyl chain is end-capped with a 2,4-di-*t*-butyl-phenoxy group, whilst the GlyGly station is connected to an anthracene-9-carboxy group.

There is little conjugation between the anthracene and the carboxamide group attached at the 9-position. As is evident from crystal structures, the two groups are nearly perpendicular with respect to each other, because of steric interactions between the *peri*-hydrogens of anthracene and the amide group. The perpendicular orientation of the anthracene stopper prevents the macrocycle from binding to *both* amide carbonyl groups of the GlyGly which is the preferred binding mode in previously studied hydrogen-bonded rotaxanes.[5] This will prove to be important in determining the photophysical properties (see Section 4.3.2 and further).

For the discussion of the bonding motifs between macrocycle and GlyGly unit we will only consider nonpolar solvents, because it is known from ^{1}H NMR[6] and fluorescence (Chapter 3) studies that in polar hydrogen-bonding solvents the macrocycle is (to a large extent) displaced towards the alkyl chain.

Let us therefore consider the ^{1}H NMR spectrum (measured by M.A. Farrán Morales at the University of Warwick, UK) of **1** in $CDCl_3$ (Figure 4-2), which clearly shows the presence of the macrocycle over the peptide motif. The resonances of H_c and H_e of the rotaxane are shifted to higher field with respect to the same signals in thread **2**. This shielding effect is due to the ring current of the aromatic xylylene units of the macrocycle. For the NH protons of the thread the same field effect is operative, but it is opposed by a *deshielding* effect due to hydrogen bonding to the CO groups of the macrocycle.

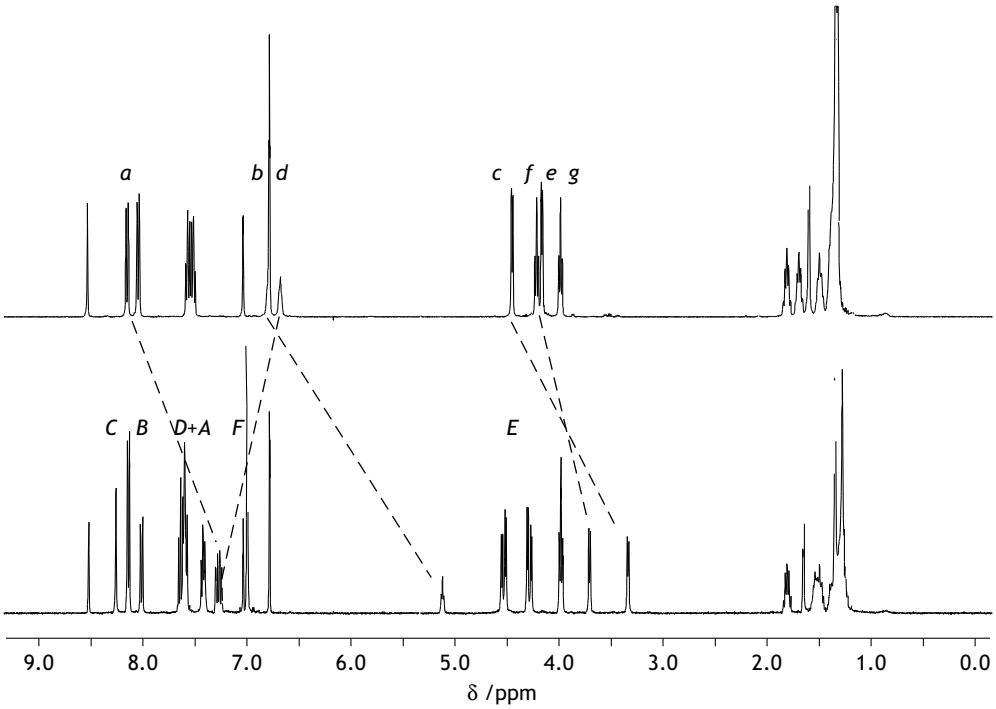

Figure 4-2. ^{1}H NMR spectra (400 MHz) of **1** (bottom) and **2** (top) in $CDCl_3$. The letters correspond to the assignment of the resonances shown in Figure 4-1.

For H_d, which experiences a downfield shift of $\Delta\delta$ = +0.75 ppm, hydrogen-bonding clearly is the dominant contribution. In contrast, H_b is shifted upfield ($\Delta\delta$ = -1.57 ppm), indicating that the NH-group of the amide directly attached to the anthracene is much less involved in hydrogen bonding than the amide group containing NH_d. It is likely that the perpendicular orientation of the anthracene with respect to the amide group directly attached to it, prevents the macrocycle from adopting a conformation that allows the formation of hydrogen bonds to the amide group that is closest to the anthracene.

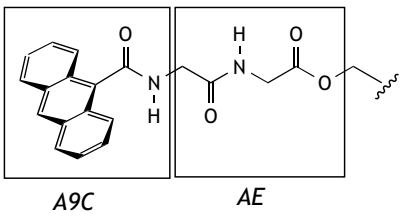

Figure 4-3. The hydrogen-bonding region of thread **2**.

This does not mean that the macrocycle is far away from the anthracene, because a clear shielding effect on the anthracene proton H_a is observed which must be due to the *p*-xylylene units. There is little to no hydrogen bonding from the macrocycle to the amide NH attached closest to the anthracene, and judging from the X-ray structure and molecular modelling calculations (see Chapter 5), there is also no hydrogen bonding to

the carbonyl of this amide group. For the interpretation of the photophysics of **1** it will therefore be useful to discern two potential hydrogen-bonding parts of the thread: the anthracene-9-carboxamide (*A9C*) station which is not involved in hydrogen-bonding in the ground state, and the amide-ester station directly attached to it (*AE*) which *does* form hydrogen-bonds with the macrocycle (Figure 4-3).

4.3.2 Steady State Fluorescence

Both in **1** and **2**, the anthracene-9-carboxamide (*A9C*) group has the lowest excited singlet state, with E_{00} = 3.22 eV. Therefore, when this fluorophore is selectively excited in **1** there will be no energy transfer to any group in the macrocycle. Based on thermodynamic considerations, electron transfer between *A9C* and the macrocycle can also be excluded. In a polar solvent the free energy change upon electron transfer is given by:

$$-\Delta G_{et} = E_{00} - e(E_{ox}^{1/2} - E_{red}^{1/2}) \qquad \text{(Eq. 4-1)}$$

Since *A9C* is oxidised at $E_{ox}^{1/2}$ = +1.6 V *vs.* SCE and the macrocycle is reduced at $E_{red}^{1/2} \approx$ -2.3 V *vs.* SCE,[7] electron transfer is very unfavourable (ΔG_{et} = +0.7 eV) in contrast to the systems described in Chapter 3.

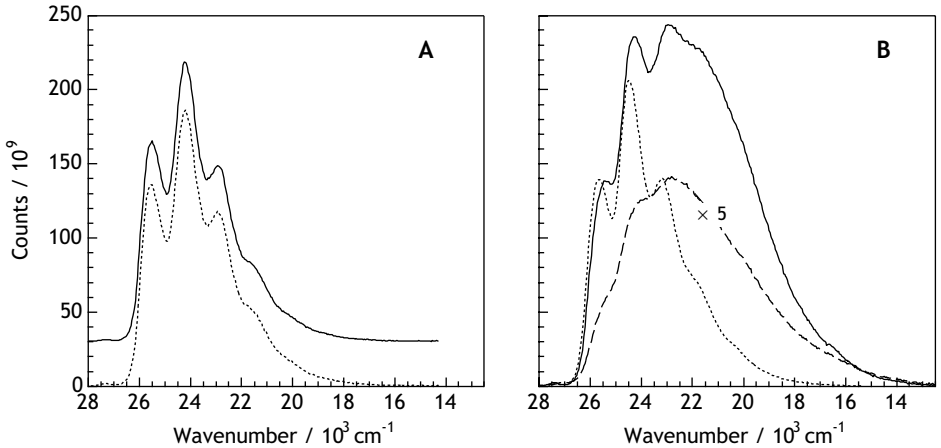

Figure 4-4. (A) Fluorescence spectra of **1** (continuous) and **2** (dotted) in DMSO (notice the vertical offset). (B) Fluorescence spectra of rotaxane **1** (continuous) and thread **2** (dotted) in 1,4-dioxane. For comparison the spectrum of **2** in 2,2,2-trifluoroethanol (dashed) is added. All spectra have been scaled to the same absorbance at the excitation wavelength (330 nm), such that the integrated intensity represents the relative quantum yield.

Because no electron or energy transfer can occur in **1**, its fluorescence is expected to be identical to that of thread **2**. As shown in Figure 4-4a, this is in fact the case in dimethylsulfoxide (DMSO), a solvent in which the hydrogen bonding between the peptide station and the

macrocycle is disrupted. In non-hydrogen-bond-disrupting solvents such as 1,4-dioxane (Figure 4-4b), however, the fluorescence of the rotaxane is considerably broader and more intense. Since some of the vibrational fine structure of the anthracene emission is retained, it seems likely that the broad emission band is composed of two contributions, *viz.* one that resembles the thread spectrum, and an additional broad, red-shifted band.

The presence of this red-shifted band causes the centre of gravity, $\tilde{\nu}_c$, (*i.e.* the position where the integral of the curve reaches half its maximum value) of the emission to shift to lower energy. This is therefore a useful parameter to compare thread and rotaxane in different solvents (Table 4-1).

Table 4-1. Fluorescence properties of thread **2** and rotaxane **1** in different solvents, showing the centre of gravity ($\tilde{\nu}_c$), the shift of rotaxane centre of gravity relative to the thread ($\Delta\tilde{\nu}_c$) and the fluorescence quantum yields (Φ_f).

solvent	ε_r	thread **2**		rotaxane **1**		
		$\tilde{\nu}_c$ / 10^3 cm^{-1}	Φ_f	$\tilde{\nu}_c$ / 10^3 cm^{-1}	$\Delta\tilde{\nu}_c$ / 10^3 cm^{-1}	Φ_f
non-hydrogen-bonding solvents						
1,4-dioxane	2.2	24.0	0.16	22.2	-1.8	0.36
benzene	2.3	23.1	0.26	21.4	-1.7	0.76
ethyl acetate	6.0	23.6	0.17	21.9	-1.7	0.29
dichloromethane	8.9	22.8	0.22	21.1	-1.7	0.22
acetonitrile	37.5	23.5	0.17	22.4	-1.1	0.21
hydrogen-bonding solvents						
methanol	32.7	23.1	0.11	22.7	-0.4	0.13
DMF	37.0	23.8	0.11	23.3	-0.5	0.18
DMSO	46.7	23.9	0.19	23.8	-0.1	0.19
CF_3CH_2OH	26.5	22.1	0.04	21.8	-0.3	0.11

When one examines Table 4-1, a solvent effect can be observed that is similar to that of rotaxanes with a quencher in the macrocycle (Chapter 3): the influence of the macrocycle is strongest in nonpolar, non-hydrogen-bonding solvents. For the rotaxanes from Chapter 3, the nearness of the macrocycle caused a quenching of the anthracene fluorescence, in this case the effect is a centre of gravity shift ($\Delta\tilde{\nu}_c$) of up to 1800 cm^{-1} to lower energy. Additionally, in some solvents a remarkable *increase* of the fluorescence quantum yield is observed. Both these effects are much smaller in hydrogen-bonding solvents, but they do not completely disappear. This is in agreement with the findings of Chapter 3, where there was also no solvent capable of totally removing the influence of the macrocycle on the anthracene flu-

orescence. Even in the strongest hydrogen-bonding solvents, some fraction of **1** will consist of co-conformers where the macrocycle is close to the fluorophore.

Having established that the anomalous fluorescence properties of the anthracene stopper of **1** are related to the presence of the macrocycle near this fluorophore, the physical processes behind it need to be uncovered. Adding an excess of macrocycle reference (**3**) to thread **2**, has no effect on its fluorescence, again ruling out energy or electron transfer as the photophysical mechanisms. The broad, red-shifted band was furthermore not enhanced by freezing or degassing the solution, excluding a phosphorescent origin. Therefore, a singlet mechanism must underlie this emission.

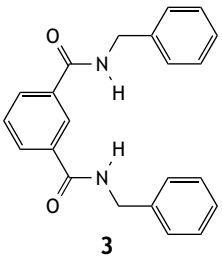

3

The fluorescence of anthracene-9-carboxamide has been studied by Werner and Rogers, who observed that the spectrum is broadened and red-shifted in the strongly hydrogen-bond-donating solvent 2,2,2-trifluoroethanol.[8] Indeed in our thread **2**, $\tilde{\nu}_c$ changes from 24000 to 22100 cm^{-1} upon going from 1,4-dioxane to 2,2,2-trifluoroethanol (see Table 4-1 and Figure 4-4b). Werner and Rogers explained their observation by assuming that in the excited singlet state the conformation changes from one in which the planes of the amide group and the anthracene ring are essentially perpendicular, to a planar configuration, in which a considerable transfer of charge from the aromatic ring to the carbonyl group occurs, leading to enhanced hydrogen bonding.

The broad, red-shifted contribution to the fluorescence spectrum of **1** in *nonpolar* solvents can thus also be induced in **2** by a strongly hydrogen-bond-*donating* solvent. However, when rotaxane **1** is placed in hydrogen-bonding solvents there is little difference between **1** and **2**, because the macrocycle is displaced from the peptide station to the hydrocarbon tail. We therefore attribute the occurrence of the rotaxane's long-wavelength emission band to fluorescence from a relaxed conformation in which the hydrogen bond donor groups of the macrocycle, *viz.* one or more of the four amide NH groups, bind to the carbonyl directly attached to anthracene. The question whether this effect is static or dynamic will be addressed in Section 4.3.3.

In nonpolar solvents such as benzene and 1,4-dioxane, the spectral changes of **1** are accompanied by a large increase of the fluorescence quantum yield relative to that of **2** (Table 4-1). This is probably due to the special photophysical properties of the anthracene chromophore. For anthracene, the first (T_1) and second (T_2) triplet levels are located at 14850 and 26090 cm^{-1} respectively.[9] The S_1 level lies 435 cm^{-1} above T_2, enabling the intersystem crossing process ($S_1 \rightarrow T_2$) to compete with fluorescence. For *A9C* the energy levels of the triplet states are not known, but the general trend holds over a range of meso-substituted anthracenes.[9]

From Figure 4-4b it can be inferred that the rotation around the anthracene-carbonyl bond and the hydrogen-bonding to the macrocycle, lowers the energy of the S_1 state of *A9C*

in **1** considerably: the broad emission has its onset at least at 1000 cm^{-1} (3 kcal/mol) lower energy. Werner and Hoffman have argued that the triplet levels are less effected by rotation around the anthracene-carbonyl bond in 9-methyl anthroate than the S_1 level.[10] If this is correct, the $S_1 \rightarrow T_2$ intersystem crossing probably becomes endothermic when the S_1 level is lowered. At the same time S_1 is still quite a bit higher in energy than T_1 so that $S_1 \rightarrow T_1$ intersystem crossing is slow due to unfavourable Franck-Condon factors. Therefore, hydrogen bonding of the macrocycle to *A9C* in **1** increases the fluorescence quantum yield by decreasing the triplet yield. Note that when a solvent such as 2,2,2-trifluoroethanol acts as the hydrogen bond donor, the fluorescence quantum yield is low (Table 4-1), which might be due to enhanced internal conversion.

4.3.3 Temperature and Matrix Effects

We have established that hydrogen bonding of the macrocycle to the *A9C* carbonyl causes the special features in the fluorescence spectrum of rotaxane **1** in nonpolar solvents. Now we should determine whether this is a static or dynamic effect. If the effect is dynamic, it should be possible to prevent it by lowering the temperature. Indeed, upon lowering the temperature the long-wavelength shoulder disappears (Figure 4-5a). The formation of the lower energy state responsible for this emission apparently involves some energetic barrier. In principle separation of the anthracene-like fluorescence quantum yield from that of the broad red-shifted emission would yield a value for the barrier, but in practice the two cannot reliably be separated.

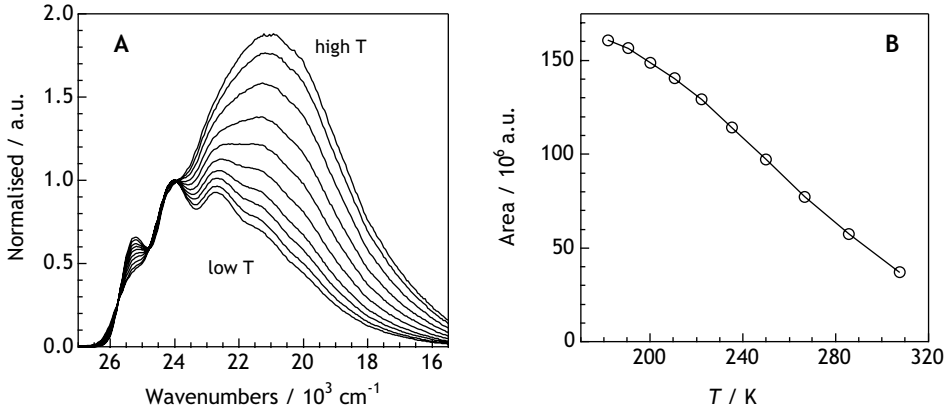

Figure 4-5. Fluorescence of **1** in CH_2Cl_2, at temperatures between 307.7 and 181.8 K, excited at 330 nm. (A) Fluorescence spectra, normalised at 24000 cm^{-1}. (B) The area under the fluorescence curves at different temperatures.

Cooling down **1** also blocks other thermally activated dark processes such as internal conversion and intersystem crossing, leading to an overall increase of fluorescence (Figure 4-5b).

An energetic barrier does not necessarily imply large amplitude motions in **1**. To test whether these were involved, we placed the rotaxane in rigid, non-hydrogen-bonding environments: D(+)-sucrose octaacetate (SOA), a room temperature organic glass and polymethyl metacrylate (PMMA), a polymer (Figure 4-6). When SOA is in the glassy state, the rotaxane emits a thread-like anthracene spectrum, whereas upon melting it to a viscous liquid the broad red-shifted band reappears. In PMMA, the fluorescence of **1** resembles that of **2**, although there is a slight broadening of the vibrational structure.

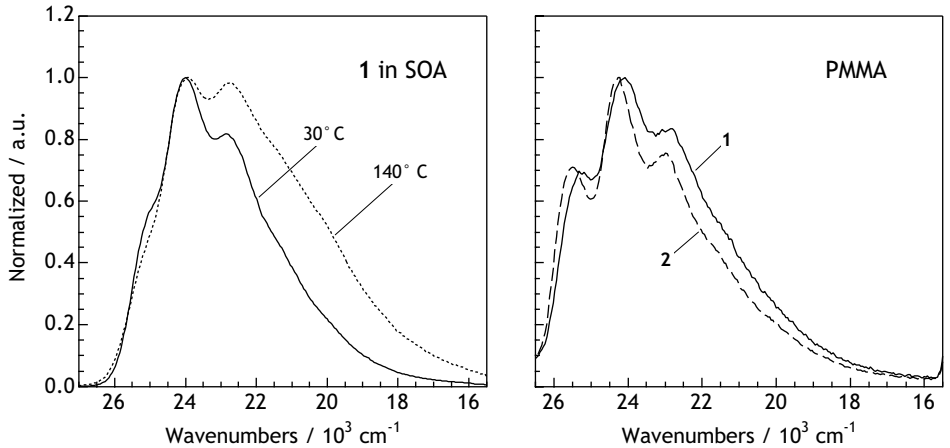

Figure 4-6. Fluorescence spectra, excited at 330 nm, normalised at 24000 cm^{-1}. (left) Rotaxane **1** in sucrose octaacetate (SOA) in the glassy state (30°C, continuous) and viscous liquid state (140°C, dotted). (right) rotaxane **1** (continuous) and thread **2** (dashed) in spin coated PMMA.

Both in glassy SOA and in PMMA the excited state processes that gives rise to the broad, red-shifted emission of **1** are prevented. Since large amplitude motions are restricted in these solid matrices, the conclusion must be that *photoexcitation leads to molecular movement.* Moreover, since in nonpolar solvents the effect is exclusively observed in rotaxane **1**, the excited state conformational changes must involve changes in interactions between macrocycle and binding station. In other words: after photoexcitation the rotaxane crosses a barrier on the S_1 potential energy surface and relaxes in a broader and lower energy minimum, associated with a conformation where the macrocycle binds the carbonyl directly attached to anthracene. Such a species will fluoresce at longer wavelength with less vibrational detail.[11]

4.3.4 Time Resolved Fluorescence

To obtain a more quantitative picture of the excited state dynamics of **1**, time-resolved fluorescence spectroscopy was performed using a picosecond Time Correlated Single Photon Counting (TC-SPC) setup. Decay traces were recorded at 14 wavelengths and globally analysed.[12] Some of the results obtained with CH_2Cl_2 as the solvent are shown in Figure 4-7.

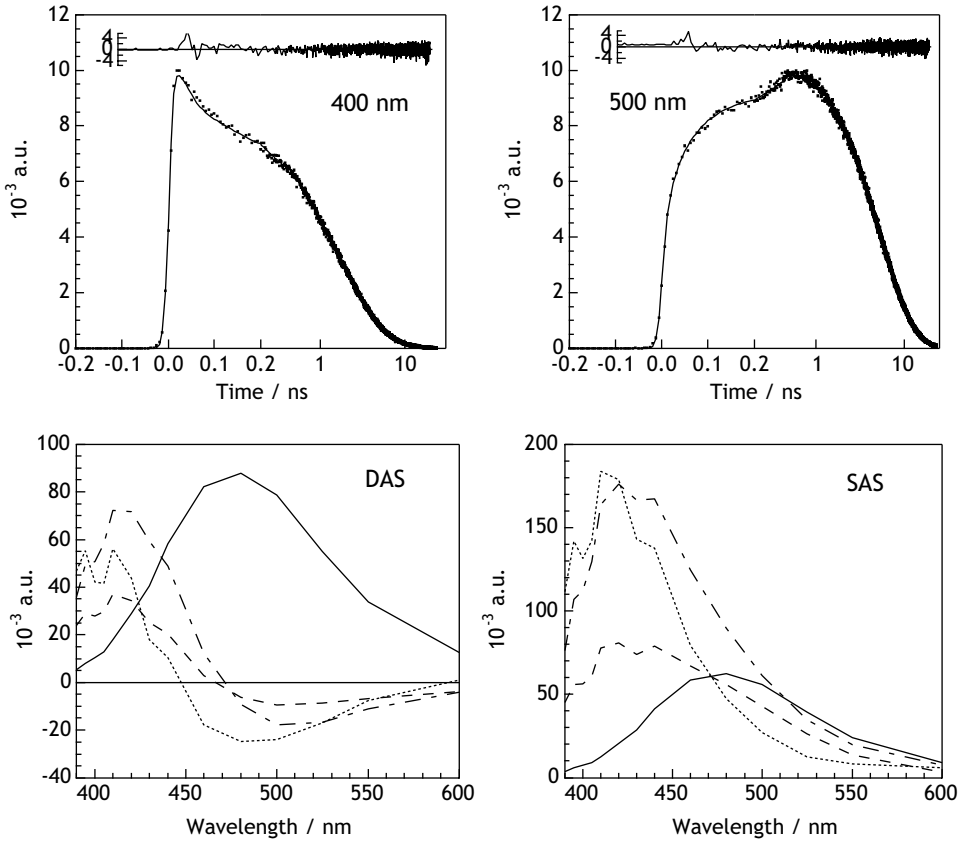

Figure 4-7. (Top) Fluorescence decay traces of **1** in CH_2Cl_2 (λ_x = 330 nm) with their fits and residuals. The time-axis is linear from -0.2 to 0.2 ns and logarithmic from 0.2 to 25 ns. Emission wavelengths: 400 nm and 500 nm. (Bottom) Results from the global and target analysis: Decay Associated Spectra (DAS), and Species Associated Spectra (SAS). Key: 36 ps (dotted), 0.26 ns (dashed), 1.82 ns (dot-dashed), 4.33 ns (continuous).

In accordance with the proposed excited state dynamics of *A9C* (Section 4.3.2), the thread **2** has a biexponential fluorescence decay (not shown). The initial perpendicular conformation relaxes in 78 ps to a more planar conformation which possesses a decay time of 3.43 ns. For rotaxane **1** such a simple kinetic scheme is not applicable: for a good fit at least 4 exponentials are required. The Decay Associated Spectra (DAS, Figure 4-7) of 36 ps, 0.26 ns and 1.82 ns possess negative amplitudes above 450 nm. Thus, it is clear that the species emitting at longer wavelength (τ = 4.33 ns) is formed from a number of precursors on time scales of 36 ps, 0.26 ns and 1.82 ns. The precursor species have anthracene-like structured emission at short wavelengths, consistent with the fact that the macrocycle does not "distort" the chromophore by hydrogen bonding.

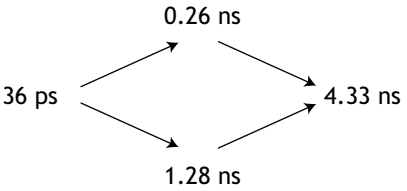

Figure 4-8. Kinetic scheme used to calculate the SAS in Figure 4-7.

The precise way in which the "precursor states" characterised by the time constants of 36 ps, 0.26 ns and 1.82 ns give rise to the final state can not be unequivocally established: different kinetic models will only differ in different Species Associated Spectra (SAS).[12] Here we assume a model (Figure 4-8) with two groups of conformations. The fastest component corresponds with the short lived state in the thread. In this t_0 state the conformations of **1** are indistinguishable and emit a spectrum with sharp anthracene-like vibrational fine structure. After 36 ps two states with a broadened anthracene spectrum have been formed which evolve with different decay times (0.26 and 1.82 ns) to the longest-lived (4.33 ns), broad and red-shifted state. The Species Associated Spectra for this model are shown in Figure 4-7 (SAS).

We believe that the emissive states with anthracene-like character correspond to conformations where the macrocycle is bound to the *AE* station (see Figure 4-3). The broad, red-shifted emission then arises from a conformation where the macrocycle forms hydrogen-bonds with the carbonyl directly attached to the anthracene (*A9C*).

4.3.5 Mechanism

The conformation of the anthracene-9-carboxamide (*A9C*) fluorophore dictates the excited state behaviour of rotaxane **1**. Because in the ground state the anthracene and amide carbonyl groups have a nearly perpendicular geometry, the macrocycle cannot bind to the *A9C* station due to unfavourable steric interactions. The macrocycle therefore forms hydrogen-bonds to the amide-ester (*AE*) station, even though the ester carbonyl cannot form hydrogen-bonds as strong as an amide carbonyl (Figure 4-9a).[13]

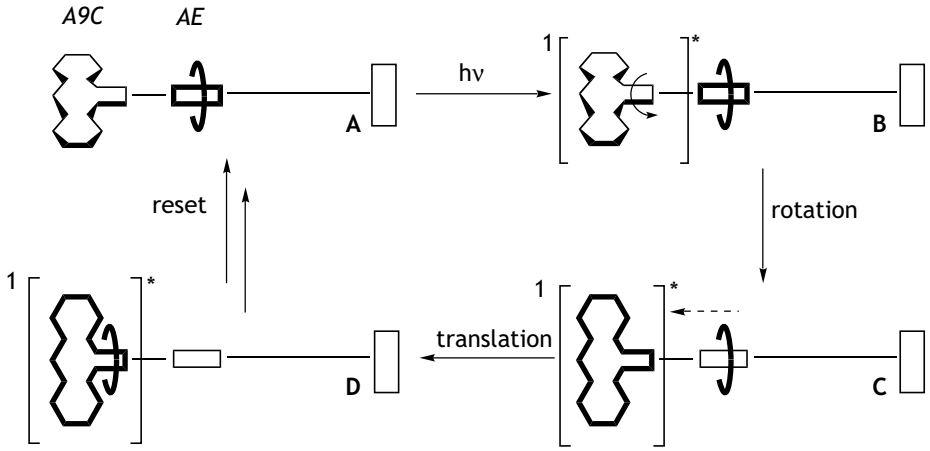

Figure 4-9. Photocycle of rotaxane **1** in nonpolar solvents (see text for explanation).

In the singlet excited state (Figure 4-9b) the anthracene-carbonyl dihedral angle gets smaller in less than 100 ps (Figure 4-9c), thus reducing anthracene's steric demands imposed onto the macrocycle. Due to increased conjugation in the *A9C* excited state, its carbonyl group also becomes a stronger hydrogen-bond-acceptor, which leads within a nanosecond to a hydrogen-bonding motif between macrocycle and thread that involves the carbonyl of the *A9C* station (Figure 4-9d). This conformation is responsible for the broad, red-shifted fluorescence that (in nonpolar solvents) is observed exclusively for **1**. In changing the H-bond pattern between the macrocycle and the binding stations, the macrocycle has effectively moved over a distance of ~3Å. After the *A9C* excited state has radiatively relaxed back to the ground state in *circa* 4 ns the macrocycle will return to its original *AE* binding position (Figure 4-9a).

Molecular modelling studies of rotaxane **1** (see Chapter 5) have shown that there are multiple hydrogen-bonding motifs possible between macrocycle and thread. We therefore attribute one of the components in the time resolved fluorescence data to a second group of conformations, rather than an extra sequential step in the dynamical process.

4.4 Conclusions

It has been demonstrated that in rotaxane **1** significant changes in macrocycle position can occur during a singlet excited state that decays in a few nanoseconds. Upon photoexcitation both geometric and electronic properties of the anthracene-9-carboxamide stopper change to allow the macrocycle to bind to the carbonyl that is directly attached to anthracene, which is easily detected by the presence of an additional broad, red-shifted band in the fluorescence spectrum. Since in the ground state in nonpolar solvents the macrocycle resides on a region of the peptide station that is further away from the anthracene stopper, photoexcitation effectively causes sub-nanosecond switching behaviour of the rotaxane. Fluorescence measurements alone can never unveil the detailed changes in H-bond pattern, which is why molecular modelling calculations were performed to test our working hypothesis. These will be described in the next Chapter.

Although in rotaxane **1** the displacement of the macrocycle is not particularly large, it occurs without the need of any additional external assistance besides photons. In **1**, the stopper's singlet excited state is not sufficiently long-lived to allow larger amplitude motions, but with other chromophores the concept of enhanced hydrogen bonding induced by optical excitation may lead to more spectacular translational phenomena in molecular shuttles designed on this principle.

Acknowledgments. We would like to thank Dr. M.A. Farrán Morales for the synthesis and characterisation of compounds **1** and **2**, and Dr. J.M. Zwier for a generous gift of reference compound **3**. Ing. D. Bebelaar is gratefully acknowledged for technical assistance with the

SPC measurements. The analysis of the time resolved fluorescence measurements would have been impossible without the help of Dr. I.H.M. van Stokkum.

4.5 References

1. Ashton, P.R., Ballardini, R., Balzani, V., Credi, A., Dress, K.R., Ishow, E., Kleverlaan, C.J., Kocian, O., Preece, J.A., Spencer, N., Stoddart, J.F., Venturi, M., and Wenger, S. A photochemically driven molecular-level abacus. *Chem.-Eur. J.* **6**, 3558-3574 (2000)
2. Benniston, A.C., Harriman, A., and Lynch, V.M. Photoactive [2]Rotaxanes - Structure and Photophysical Properties of Anthracene-Stoppered and Ferrocene-Stoppered [2]Rotaxanes. *J. Am. Chem. Soc.* **117**, 5275-5291 (1995)
3. Murakami, H., Kawabuchi, A., Kotoo, K., Kunitake, M., and Nakashima, N. A light-driven molecular shuttle based on a rotaxane. *J. Am. Chem. Soc.* **119**, 7605-7606 (1997)
4. Perrin, D., Armarego, W., and Perrin, D. *Purification of Laboratory Chemicals* 2nd ed.; Pergamon Press Ltd.: Oxford, 1980.
5. Leigh, D.A., Murphy, A., Smart, J.P., and Slawin, A.M.Z. Glycylglycine rotaxanes - The hydrogen bond directed assembly of synthetic peptide rotaxanes. *Angew. Chem.-Int. Edit. Engl.* **36**, 728-732 (1997)
6. Lane, A.S., Leigh, D.A., and Murphy, A. Peptide-based molecular shuttles. *J. Am. Chem. Soc.* **119**, 11092-11093 (1997)
7. Paolucci, F., (University of Bologna) personal communication.
8. Werner, T.C., and Rodgers, J. Studies on the fluorescence properties of meso-substituted amidoanthracenes. *J. Photochem.* **32**, 59-68 (1986)
9. Fukumura, H., Kikuchi, K., Koike, K., and Kokubun, H. Temperature Effect On Inverse Intersystem Crossing of Anthracenes. *J. Photochem. Photobiol. A-Chem.* **42**, 283-291 (1988)
10. Werner, T.C., and Hoffmann, R.M. Relation between an excited state geometry change and the solvent dependence of 9-methylanthroate fluorescence. *J. Phys. Chem.* **77**, 1611-1615 (1973)
11. Cowan, D.O., and Drisko, R.L. In *Elements of Organic Photochemistry*; Plenum Press: New York and London, 1976, pp 24-27.
12. van Stokkum, I.H.M., Scherer, T., Brouwer, A.M., and Verhoeven, J.W. Conformational dynamics of flexibly and semirigidly bridged electron donor-acceptor systems as revealed by spectrotemporal parametrization of fluorescence. *J. Phys. Chem.* **98**, 852-866 (1994)
13. Arnett, E.M., Mitchell, E.J., and Murty, T.S.S.R. "Basicity". A comparison of hydrogen bonding and proton transfer to some Lewis bases. *J. Am. Chem. Soc.* **96**, 3875-3891 (1974)

Chapter 5

Stochastic Dynamics Simulations

Analysis of hydrogen bond patterns and steric effects in an anthracene stoppered, peptide based rotaxane

I have had my results for a long time: but I do not yet know how I am to arrive at them.

– ascribed to Karl Friedrich Gauss

5.1 Introduction

In Chapter 4, the excited state dynamics of the peptide based [2]rotaxane **1** were described. In nonpolar solvents, excitation of the anthracene-9-carboxamide stopper of this rotaxane gave rise to emission that proved to be a superposition of the typical anthracene-like, structured fluorescence and a broad, red-shifted fluorescence. The latter was absent in the corresponding thread, and must be ascribed to the influence of the macrocycle. Fluorescence studies of both thread and rotaxane, revealed that this additional band was due to a rapid excited state structural change of the rotaxane.

Werner *et al.* had proposed that the almost perpendicular orientation between anthracene and the adjacent carbonyl group in the anthracene-9-carboxamide ground state changes to a parallel one in the singlet excited state.[1] Indeed, the fluorescence decay of the thread showed a biexponential decay, indicating that this conversion took place within 100 ps. In

the corresponding rotaxane, the decay showed that after this initial step a second process took place within 2 ns that was responsible for the formation of the broad, red-shifted fluorescence. We concluded that this was due to a reorganisation of the hydrogen bond pattern between thread and macrocycle. In the ground state, the macrocycle cannot approach the anthracene stopper due to steric interactions with its *peri*-hydrogens. If, however, in the excited state the anthracene-carbonyl dihedral angle becomes smaller, the macrocycle can come closer to the stopper.

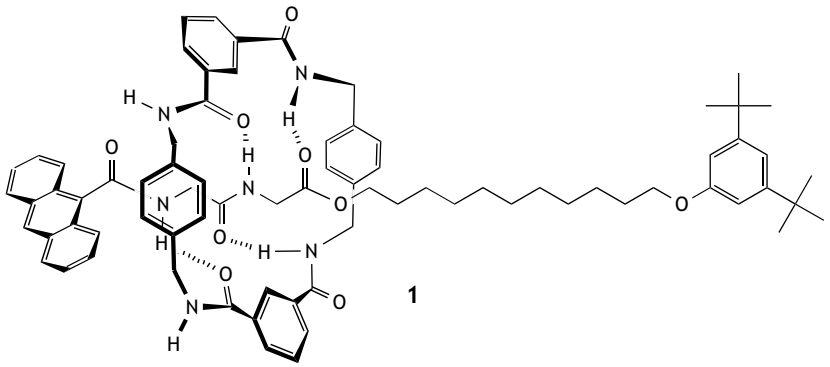

Figure 5-1. Structural formula of the rotaxane used in all calculations.

The details of the H-bond pattern in the ground state, let alone in the excited state, are difficult to obtain experimentally. Therefore, we set out to test our hypothesis by means of molecular modelling techniques. Rotaxane **1** is a promising candidate for such studies, since its functional groups and their interactions are well parametrised in force fields that are optimised for biomolecules. Compared to typical proteins, however, it is much smaller, so that long dynamics simulation times are well within reach of current computer power.

Molecular modelling can be a powerful tool in understanding the complicated experimental results that are often obtained with supramolecular systems. It has *e.g.* successfully been applied to probe the factors that determine the rate of macrocyclic ring rotation in benzylic amide [2]catenanes.[2] In other studies, computational investigations helped understanding the slippage of a macrocycle over a bulky stopper[3] or the translation of a macrocycle along a thread.[4] The binding between macrocyclic hosts and stations applied in rotaxanes was also studied by a number of researchers, calculating the structure of inclusion complexes[5,6] and their binding free energies.[7,8]

In this Chapter, the structure of rotaxane **1** (Figure 5-1) in nonpolar solution will be studied using stochastic dynamics (SD) simulations, in order to gain an understanding of the excited state dynamics that was held responsible for its anomalous fluorescence behaviour as discussed in Chapter 4. Conformational searches of **1** did not yield a satisfactory answer to the working hypothesis, *viz.* is the carbonyl group of the anthracene-9-carboxamide stopper

involved in hydrogen bonding with the macrocycle in the ground state and does this change in the excited state? It did however give some general insights into the hydrogen bond patterns in **1**, which will be discussed in detail.

In contrast to the energy minimised structures obtained from the conformational searches, SD simulations include thermal motions of the molecules. This proved to be essential for the simulation of **1** in nonpolar solution. In the energy minimised structures, hydrogen bonding of the macrocycle to the carbonyl next to the anthracene stopper was energetically favourable in many conformers. In the 10 ns SD runs, however, it was found that the macrocycle hardly binds to this carbonyl group, in accordance with the working hypothesis. The main features of the H-bond pattern were furthermore found to be independent of the choice of force field, which reinforces the confidence of our computational model.

As a first approach to mimic the anthracene-9-carboxamide excited state, only the change in anthracene-carbonyl dihedral angle was considered, leaving the electronic distribution the same as in the ground state. When this dihedral angle was constrained to 0°, the binding of the macrocycle to the carbonyl adjacent to anthracene increased dramatically. The consequences of this finding with regard to the experimentally obtained results will be discussed, and suggestions for further refinements of the computational model will be given.

5.2 Computational Details

Force Field. All calculations were performed with the Macromodel and BatchMin molecular modelling programs (V7.0 for OPLS-AA, V6.5 for the other force fields),[9] using the molecular mechanics force fields MMFF94, OPLS-AA, and AMBER* (all atom), as implemented in Macromodel.

OPLS-AA is an all-atom force field that is a faithful reproduction of Jorgensen's force field, including some unpublished parameters.[10] It is intended for use with peptides and simple organic molecules. OPLS-AA is based on OPLSA and has used a more careful reparameterisation against quantum-mechanical data. It is expected to be a better force field, particularly for peptides. Although it may do well for simple organics as well, caution should be exercised in using it for more complicated systems, such as polyfunctional organic molecules.

MMFF94 is the authentic Merck Molecular Force Field (MMFF),[11-17] which is a good force field for biopolymers (peptides and proteins) and many organic molecules. It is available in two variations: MMFF makes sp^2 delocalised nitrogens pyramidal (used in dynamics simulations) and MMFFs makes them planar (for energy minimisations).

AMBER* is a modification of AMBER(84&86),[18,19] which contains new torsional parameters for peptides, Kollman 6,12-hydrogen-bonding function, and additional parameters for organic compounds. It is a good force field for biopolymers (peptides, saccharides, nucleic acids) and simple organic molecules.

To incorporate the influence of solvent (chloroform), the continuum GB/SA model[20] was applied. Nonbonded cutoff distances were set at 8, 20, and 4Å for Van der Waals, electrostatic, and hydrogen bond interactions respectively. Atomic charges are given in Table 5-1.

The atomic charges determine mainly which hydrogen-bonding sites on the thread are most favourable to bind to. Within one force field, all N-H groups have the same charge distribution. With the carbonyl groups, each carbonyl group in the thread is different. The ester carbonyl has the

smallest bond dipole, followed by the amide carbonyl and the amide carbonyl that is attached to an aromatic group. For the OPLS-AA force field this is realised by a negative charge on C_a.

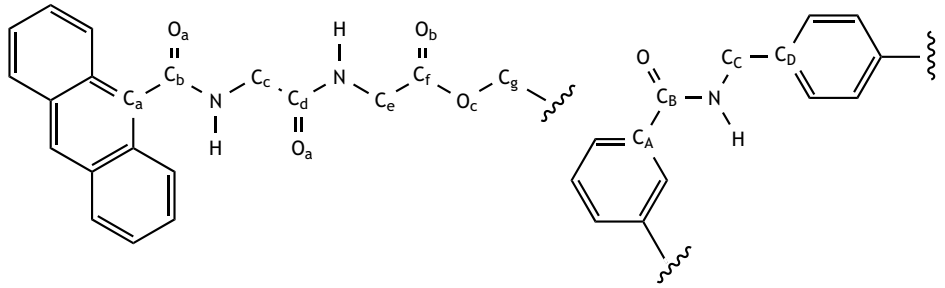

Table 5-1. Atomic charges in different force fields.

	thread		
	MMFF	OPLS-AA	AMBER*
C_a	0.086	-0.107	0.000
C_b	0.554	0.656	0.500
C_c	0.361	0.205[a]	0.246[a]
C_d	0.569	0.533	0.526
C_e	0.361	0.205[a]	0.272[a]
C_f	0.659	0.544	0.600
C_g	0.280	0.263[a]	0.250[a]
O_a	-0.570	-0.500	-0.500
O_b	-0.570	-0.430	-0.450
O_c	-0.430	-0.330	-0.400
N	-0.730	-0.500	-0.520
H	0.370	0.300	0.248

	macrocycle		
	MMFF	OPLS-AA	AMBER*
C_A	0.086	-0.105	0.000
C_B	0.554	0.666	0.500
C_C	0.444	0.207[a]	0.171[a]
C_D	-0.144	-0.105	0.100
O	-0.570	-0.500	-0.500
N	-0.730	-0.500	-0.520
H	0.370	0.300	0.248

a. Including charges on hydrogen atoms.

For rotaxane **1**, another important parameter is the potential energy dependence of the dihedral angle ϕ between anthracene and the carbonyl group that is directly attached to it. To determine this potential *N*-methyl anthracene-9-carboxamide was minimised, constraining ϕ with a force constant of 5000 kJ mol^{-1} to values between 0 an 90°. The Full Matrix Newton-Raphson (FMNR) minimisation method was used with a stringent convergence criterion for the gradient of 10^{-5} kJ mol^{-1}Å^{-1}. The potentials are shown in Figure 5-2 for the different force fields.

In all force fields the C_{ar}-C_{ar}-C=O dihedral parameter has a maximum at 90° and a minimum at 0°, reflecting the enhanced conjugation when the anthracene-9-carboxamide group is flat. Unfavourable Van der Waals interactions between the *peri*-hydrogens of anthracene and the adjacent amide, however, create a barrier at 0° that is much larger than the barrier due to a decrease in conjugation at 90° (Figure 5-2). For the MMFFs force field, the latter barrier is almost 0, while for OPLS-AA and AMBER* it is *circa* 0.7 kcal mol^{-1}.

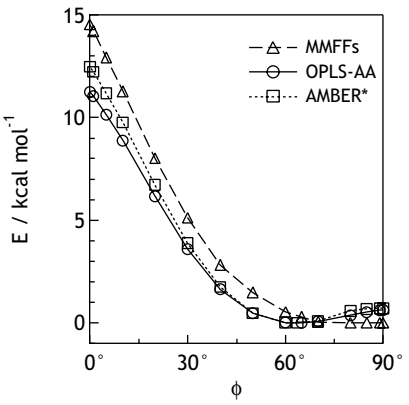

Figure 5-2. Potential energy curve for the anthracene-CO dihedral angle in *N*-methyl anthracene-9-carboxamide, using different force fields.

Conformational Search. Hand-drawn structures were subjected to a series of Low-frequency Mode Conformational Searches (LMCS),[21] a method that was found to be highly efficient for rotaxanes. Thread translation/rotation and all rotatable bonds were varied, with the exception of the alkyl chain torsional angles, for this would have resulted in many extra conformations with slightly different orientations of the tail of the thread. The amide C-N and ester C-O bonds were also varied to ensure complete coverage of conformational space. In a typical LMCS run, 250 conformational search steps were performed using the output structures of a previous run as starting structures. After each search step, the conformation was minimised with the PR Conjugate Gradient (PRCG)[22] method (maximally 1000 iterations), followed by minimisation with the Truncated Newton Conjugated Gradient (TNCG)[23] method (maximally 25 iterations). These were re-minimised to convergence (gradient < 0.05 kJ mol^{-1}Å^{-1}) with the TNCG method with all cutoff distances set to 20 Å. Duplicates due to atom numbering equivalencies (a consequence of the macrocycle's symmetry) were not removed, rather the conformers were grouped by visual inspection of the H-bond pattern.

Stochastic Dynamics. In a stochastic dynamics (SD) simulation, a randomly applied external force will act on the molecules in addition to the interactions dictated by the force field in order to maintain a constant temperature. This generates the canonical (constant temperature) ensemble. SD simulations were run for 10 ns at 350 K, with a 0.5 or 1.0 fs time step and a bath time constant of 0.2 ps. Longer time steps resulted in the frequent release of the macrocycle from the binding station towards the alkyl chain. This might be due to a build up of kinetic energy in the hydrogen-bonding groups.

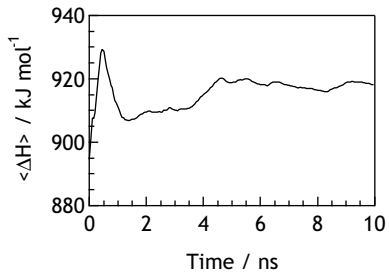

Figure 5-3. The average enthalpy of **1** in an SD run (MMFF, GB/SA $CHCl_3$).

Prior to the actual 10 ns runs, the system was equilibrated for 50 ps. In general, however, the average enthalpy $<\Delta H>$ of the system was found to converge only after ~2 ns (Figure 5-3). Every picosecond, the co-ordinates were written to an output file, which was used for further analysis, ignoring the first 2 nanoseconds.

Analysis. The output file of a typical SD simulation contained the atomic co-ordinates of 10000 structures. These were imported into Igor Pro[24] in the form of a 3D matrix (atom nr. - structure nr. - xyz). This allowed faster and more flexible analysis of the data than the MacroModel package offered. Igor works with *waves*, which are vectors to which a uniform scaling is attached.

Because the rotaxane contains a flexible thread, the position of the macrocycle on the thread is not simply given by the distance to one of the stoppers. It is more accurate to determine the position relative to the atoms in the thread. Therefore, for each structure the centre of the macrocycle was calculated by averaging the atomic co-ordinates of all macrocycle atoms. Then, the backbone atoms of the thread were defined and it was determined which backbone atom was closest to the centre of the macrocycle for each structure. This yields the relative position of the macrocycle on the thread as a function of time.

The occurrence of a hydrogen bond, was estimated by monitoring the geometry around the acceptor (O) and donor (H) atom: a hydrogen bond was considered to be present if the (N-)H···O(=C) distance was <2.5 Å, the N-H···O(=C) angle was >120°, and the (N-)H···O=C angle was >90°. For every possible combination of CO and NH a wave was created that contained 1 at times where these conditions were fulfilled, and 0 if they were not met. By combining all the waves that represented H-bonds between station and macrocycle with logical OR operations, a wave was created which contained a value of 1 at times when there was *any* H-bond between macrocycle and station. The average of this wave defines the fraction of hydrogen-bonded rotaxanes p_{bound}. Similarly the binding of any NH group from the macrocycle to a carbonyl of the station was analysed.

The average number of hydrogen bonds, <*H-bonds*>, was found by adding the waves that represented the separate hydrogen-bonding interactions. The average of this wave over all 8000 structures sampled during 8 ns gives the average number of hydrogen bonds between macrocycle and station.

5.3 Conformational Searches

5.3.1 Introduction

Intermolecular complexes in solution in general have a large conformational freedom, for the relative orientation of the separate components are only restricted by relatively weak, non-covalent interactions. For rotaxane **1** a number of conformations can be expected, because the thread contains 3 H-bond accepting and 2 H-bond donating sites which can form hydrogen bonds to the 4 NH and 4 CO groups of the macrocycle. In addition, there is considerable freedom of rotation around the bonds joining the amide and ester groups in the thread and the non-amide single bonds of the macrocycle.

We are interested in the structure of **1** in *nonpolar solution,* so all molecular modelling calculations were performed using the GB/SA $CHCl_3$ solvent model. With the force fields used in the stochastic dynamics (SD) calculations (see Section 5.4), a conformational search of **1** was performed in order to start the SD run with the global minimum.

The conformational search was set up in stages of 250 steps (see Section 5.2 for more details), each time using the resulting structures of a Low Mode Conformational Search (LMCS) as the input for a next search until no new structures in a 3 kcalmol^{-1} window were found. Care was taken to ensure complete convergence of the conformations with a large nonbonded cutoff radius in each LMCS run. For our purpose, a complete description of all

possible conformations (including *e.g.* small variations in dihedral angles) is not relevant. Rather, we would like to know the prevailing H-bond patterns in **1**, so these were used as a criterion to identify the separate conformers. The LMCS method was found to be a very efficient method for generating different rotaxane conformations, for typically no more than 1000 search steps in total were needed to find all conformers of **1** with unique H-bond patterns in a 3 kcal mol^{-1} window.

Independent of force field, in all calculated conformations the macrocycle resides on the peptide station and all the amide and ester bonds have a Z-conformation as drawn in Figure 5-4. As expected there is a large variation in the hydrogen-bond pattern of **1**. The method to uniquely label these conformers by H-bond pattern is exemplified in Figure 5-4 and will be used throughout this Chapter.

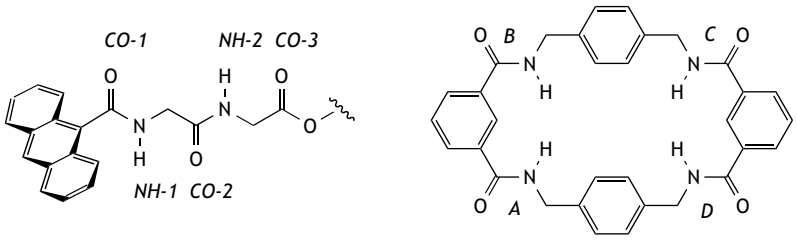

Figure 5-4. Labels used to identify the conformations of **1**. The thread's CO groups (*CO-1, CO-2, CO-3*) can form H-bonds with the macrocycle's amide NH groups; the thread's NH groups (*NH-1, NH-2*) can form H-bonds with the macrocycle's carbonyl groups. The amides of the macrocycle are labelled *A, B, C, D*. The H-bond pattern then is defined by looking along the axis of the thread to the anthracene and noting the hydrogen bonds going from *CO-1* to *CO-3* and from *A* to *D*.

Before discussing the computed conformations, let us first look at the crystal structure of an exo-pyridine analogue of rotaxane **1**. As shown in Figure 5-5, the macrocycle forms H-bonds to *NH-1* (*B*), *CO-2* (*A*), *NH-2* (*C*) and *CO-3* (*D*). The macrocycle adopts a chair-like conformation and the dihedral angle (ϕ) between anthracene and *CO-1* is 65.3°.

In the crystal, there are not only intercomponent hydrogen-bonds between thread and macrocycle, but also between molecules in adjacent unit cells. Two of the macrocycle's carbonyls are directed inwards and thus 2 NH- and 2 CO-groups point outwards, which would be favourable for packing the rotaxanes in the crystalline state. Figure 5-5 furthermore shows the nearly perpendicular orientation of the anthracene with respect to *CO-1* due to steric interactions with anthracene's *peri*-hydrogens. Apparently this also prevents H-bonding of the macrocycle to *CO-1* in the solid state.

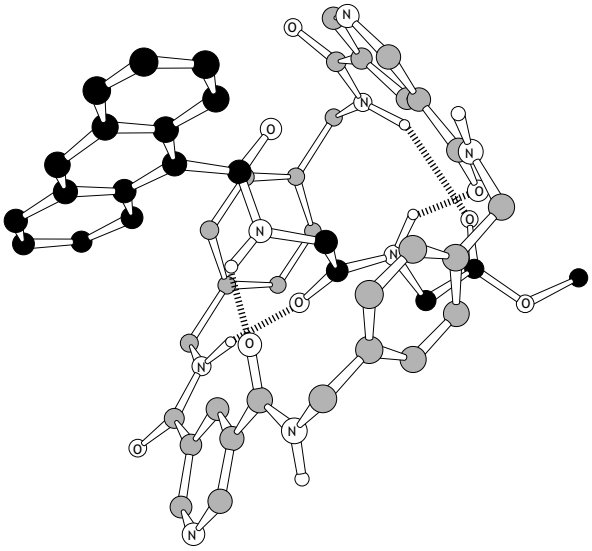

Figure 5-5. Part of the X-ray structure of the exo-pyridine analogue of **1**. C-H hydrogen atoms are omitted for clarity.

In the calculated structures the balance between two types of interactions will determine which conformations are the lowest in energy: hydrogen-bonding interactions between macrocycle and station, and steric repulsion of the anthracene stopper. The results of the conformational searches using the MMFFs, OPLS-AA and AMBER* force fields are given in Sections 5.3.2, 5.3.3, and 5.3.4 respectively. Besides the H-bond pattern, the dihedral angle, the conformation of the macrocycle and the relative steric energies of the conformations are shown and representative structures are given.

5.3.2 The MMFFs Force Field

Within a 3 kcalmol^{-1} window, only 4 conformations were found using the MMFFs force field (Table 5-2). Of these, only MMFFS-1 and MMFFS-2 will be significantly populated at room temperature and these are shown in Figure 5-6.

Clearly, with the MMFFs force field the intercomponent H-bonds dominate the outcome of the conformational search: in MMFFS-1 and MMFFS-2 all 4 amide groups of the macrocycle are involved in the H-bond pattern. In both these conformers the *CO-1* carbonyl of the thread forms a hydrogen bond to the macrocycle. This is because this aromatic amide carbonyl is parametrised to be the best H-bond accepting group (see Table 5-1). The peptide amide carbonyl is a weaker, and the ester carbonyl is the weakest H-bond acceptor, in accordance with experimental findings.[25] Thus, when other interactions are negligible, the low energy conformations will show a H-bond pattern where the macrocycle is bound to *CO-1*.

The energetic cost for the near-optimal hydrogen bond pattern in MMFFS-1 and MMFFS-2 is paid by the anthracene stopper. In *N*-methylanthracene-9-carboxamide (the stopper model compound), minimised using MMFFS and GB/SA $CHCl_3$, the dihedral angle (ϕ) between anthracene and the attached carbonyl is 80.0°. As shown in Table 5-2, in the rotaxane ϕ is smaller by almost 20°. To accommodate the macrocycle, the anthracene-9-carboxamide stopper needs to be flatter.

Table 5-2. Characteristics of the conformations found in the low mode conformational search of **1** using the MMFFs force field and GB/SA $CHCl_3$ solvent model. Given are the H-bonds to the peptide station using the notation of Figure 5-4, the dihedral angle (ϕ) between anthracene and *CO-1*, the conformation of the macrocycle and the steric energy with respect to the global minimum. The conformations in bold typeface are shown in Figure 5-6.

conformer	*CO-1*	*NH-1*	*CO-2*	*NH-2*	*CO-3*	ϕ	macro-cycle	ΔE/ kcal mol^{-1}
MMFFS-1	*A*		*B*	*D*	*C*	62.4°	chair	0.00
MMFFS-2	*A*		*B*		*C/D*	62.6°	chair	0.76
MMFFS-3			*B*	*D*	*C*	65.8°	boat	2.54
MMFFS-4		*B*	*D*	*B*	*C*	67.0°	boat	3.03

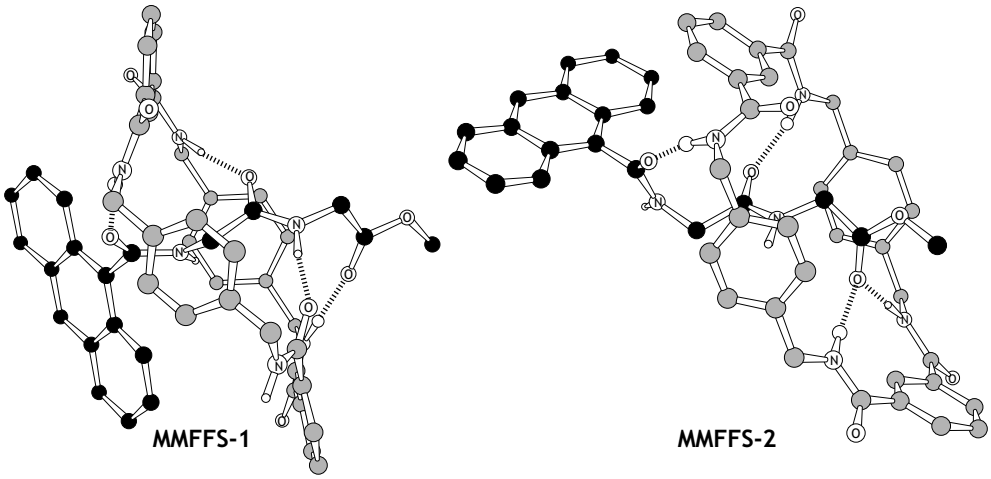

Figure 5-6. Hydrogen-bond patterns in conformations of **1** found in a low mode conformational search using the MMFFs force field and the GB/SA $CHCl_3$ solvent model. The alkyl chain and C-H hydrogen atoms are omitted for clarity. See Table 5-2 for more details.

5.3.3 The OPLS-AA Force Field

With the OPLS-AA force field, the hydrogen-bonding interactions and steric repulsion of the anthracene stopper are equally important, and consequently a large number of conformations within 3 kcal mol^{-1} was found in the conformational search (Table 5-3). This is also reflected in the variety of intercomponent H-bonds: within 3 kcal mol^{-1}, conformations with 1 to 4 intercomponent H-bonds were found, whereas the MMFFs force field gave only conformations with 4 H-bonds.

The hydrogen bond pattern of the global minimum found with the MMFFs force field (MMFFS-1) is also found with OPLS-AA (conformer OPLS-AA-6), but now it is 1.05 kcal mol^{-1} above the global minimum. In the OPLS-AA global minimum conformation there are only 3 hydrogen bonds, none of which involves *CO-1*. In the conformers where the macrocycle *does* form a H-bond to *CO-1* (OPLS-AA-2, 3, 6) this is linked to a decrease of ϕ, because the macrocycle is closer to the anthracene.

Table 5-3. Characteristics of the conformations found in the low mode conformational search of **1** using the OPLS-AA force field and GB/SA $CHCl_3$ solvent model. Given are the H-bonds to the peptide station using the notation of Figure 5-4, the dihedral angle (ϕ) between anthracene and *CO-1*, the conformation of the macrocycle and the steric energy with respect to the global minimum. The conformations in bold typeface are shown in Figure 5-7.

conformer	*CO-1*	*NH-1*	*CO-2*	*NH-2*	*CO-3*	ϕ	macro-cycle	ΔE/ kcal mol^{-1}
OPLS-AA-1			*A/B*	*D*		81.0°	chair	0.00
OPLS-AA-2	*A*		*B*			55.8°	boat	0.09
OPLS-AA-3	*B*		*C/D*			52.0°	boat	0.58
OPLS-AA-4			*A/B*	*D*	*C*	70.0°	boat	0.88
OPLS-AA-5		*B*	*D*	*B*	*C*	69.6°	boat	0.98
OPLS-AA-6	*A*		*B*	*D*	*C*	58.2°	chair	1.05
OPLS-AA-7		*B*	*D*	*B*		68.0°	boat	1.57
OPLS-AA-8			*B*			89.3°	boat	2.48
OPLS-AA-9			*B*	*D*	*C*	71.7°	chair	2.52

Some representative examples of the conformations calculated using OPLS-AA are shown in Figure 5-7. Note that the H-bond pattern of OPLS-AA-5 is also found in one of the structures from the MMFFs conformational search (MMFFS-4), albeit at a much higher energy. In this pattern, the two NH groups of the thread form a bifurcated H-bond with one macrocycle carbonyl.

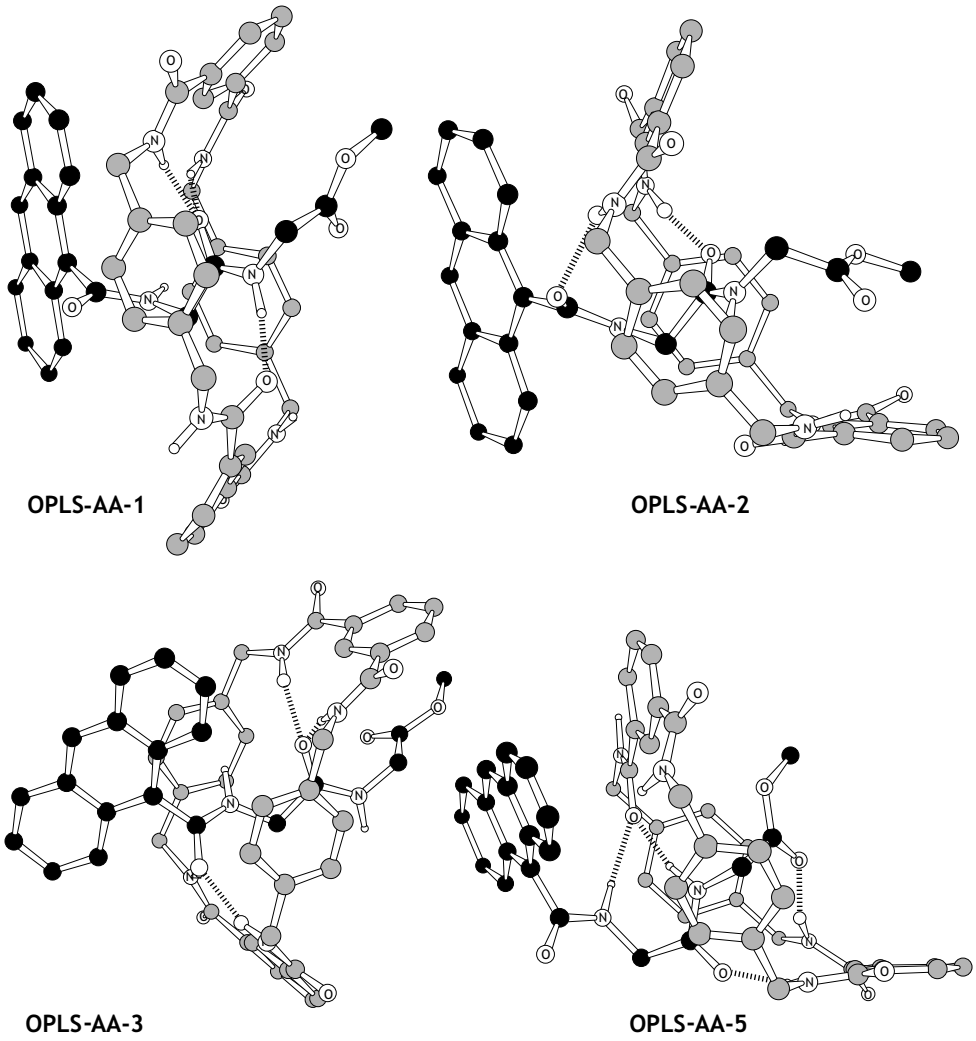

Figure 5-7. Hydrogen-bond patterns in conformations of **1** found in a low mode conformational search using the OPLS-AA force field and the GB/SA $CHCl_3$ solvent model. The alkyl chain and C-H hydrogen atoms are omitted for clarity. See Table 5-3 for more details.

5.3.4 The AMBER* Force Field

The conformations found with the AMBER* force field all have 2 or 3 intercomponent hydrogen bonds (Table 5-4). Like the OPLS-AA force field, conformations where *CO-1* is bound to the macrocycle alternate with conformations where *CO-1* is free.

Table 5-4. Characteristics of the conformations found in the low mode conformational search of **1** using the AMBER* force field and GB/SA $CHCl_3$ solvent model. Given are the H-bonds to the peptide station using the notation of Figure 5-4, the dihedral angle (ϕ) between anthracene and *CO-1*, the conformation of the macrocycle and the steric energy with respect to the global minimum. The conformations in bold typeface are shown in Figure 5-8.

conformer	*CO-1*	*NH-1*	*CO-2*	*NH-2*	*CO-3*	ϕ	macro-cycle	ΔE/ kcal mol^{-1}
AMBER*-1	*A*				*D*	56.6°	boat	0.00
AMBER*-2	*A*		*C*		*D*	51.0°	boat	0.43
AMBER*-3			*B*	*D*		85.0°	boat	0.84
AMBER*-4	*A*			*D*		62.6°	chair	1.85
AMBER*-5	*A*		*B*	*D*		84.4°	twist boat	1.91
AMBER*-6		*B*	*D*	*B*		58.8°	boat	2.68
AMBER*-7	*A*		*C*			54.0°	chair	2.89

Some of the conformations are shown in Figure 5-8 and highlight typical features only found with the AMBER* force field. In the global minimum AMBER*-1, *e.g.*, the macrocycle forms H-bonds only to *CO-1* and *CO-3* even though the latter is the weakest H-bond accepting site of the thread. AMBER*-3 is the first AMBER* conformation in which *CO-1* is not bound to the macrocycle and its dihedral angle with anthracene is almost 90°. Finally, AMBER*-5 shows a unique conformation of the macrocycle not found with the other force fields.

5.3.5 Comparison of Conformations

In contrast to the crystal structure, no conformations were found where two of the macrocycle's carbonyls were involved in the H-bond pattern for any of the force fields. Apparently, such a conformation of the ring is only favourable in the crystalline solid state. Another general trend that can be deduced from the conformational searches, is that indeed in the ground state the anthracene-9-carboxamide stopper is nonplanar, and as a consequence, the macrocycle cannot easily bind to *CO-1*. The next best H-bond accepting site is *CO-2* and here the steric repulsion of the anthracene stopper is much smaller. We therefore see that *CO-2* is bound to the macrocycle in almost all conformations, independent of force field.

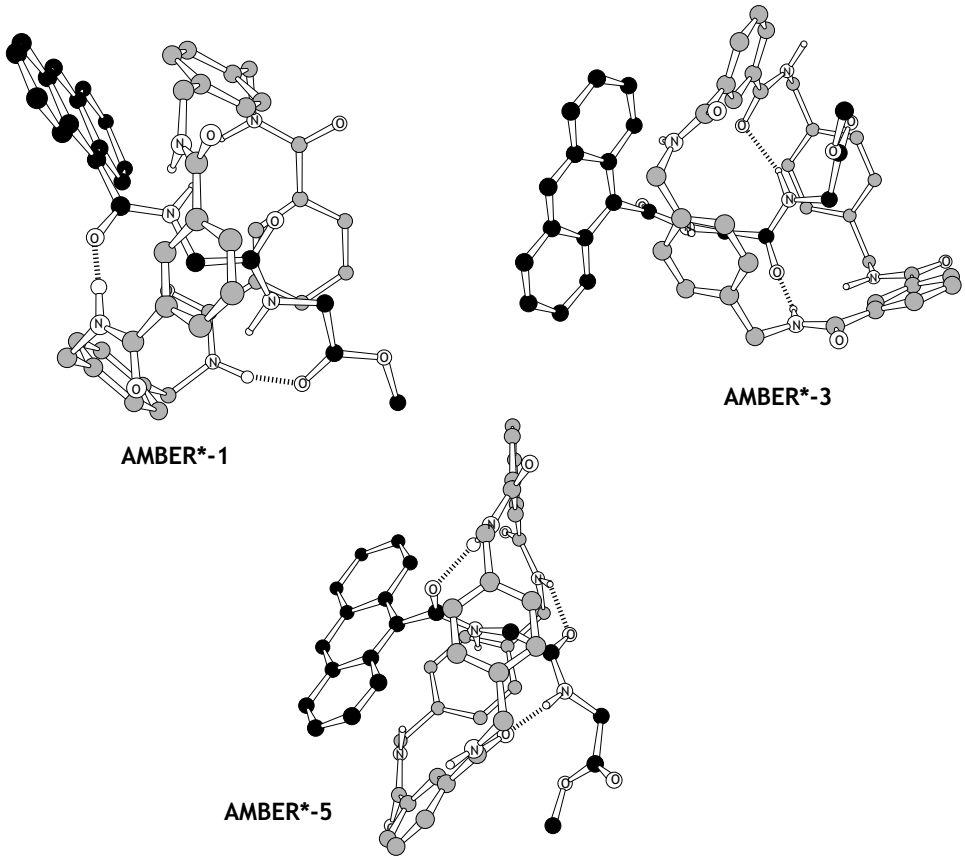

Figure 5-8. Hydrogen-bond patterns in conformations of **1** found in a low mode conformational search using the AMBER* force field and the GB/SA $CHCl_3$ solvent model. The alkyl chain and C-H hydrogen atoms are omitted for clarity. See Table 5-4 for more details.

Still, these conformational searches are not conclusive to ascertain what the detailed H-bond pattern of rotaxane **1** looks like in nonpolar solution. In particular, the question posed by the experiment (see Chapter 4) has not been answered satisfactorily: is the macrocycle bound to *CO-1* in the ground state? There must be an equilibrium between several conformations, characterised by different H-bond patterns, but which fraction of conformers will have a H-bond between *CO-1* and the macrocycle depends strongly on the force field.

Moreover, the energy minimised structures presented in this section, are static structures; thermal movement of the molecules is not taken into account. In terms of enthalpy, a large number of H-bonds is favourable, but this lowers the degrees of freedom of the system and thus lowers the entropy. Such factors might strongly influence the H-bond patterns of **1**, and can only be modelled by statistical simulations. Therefore stochastic dynamics simulations were run, which will be discussed in the next Section.

5.4 Stochastic Dynamics Simulations

Stochastic dynamics (SD) simulations of **1** were performed using the MMFF, OPLS-AA and AMBER* force fields with the GB/SA $CHCl_3$ solvent model. Typically, runs of 10 ns were performed with a step size of 1 fs at a simulation temperature of 350 K (a temperature above room temperature was chosen to sample more conformations in shorter simulation times). Such a simulation takes about 3 days, using a Silicon Graphics Octane R10000 workstation. For all runs the average enthalpy $<\Delta H>$ was taken as a measure for convergence of the simulation; it usually became stable after 2 ns.

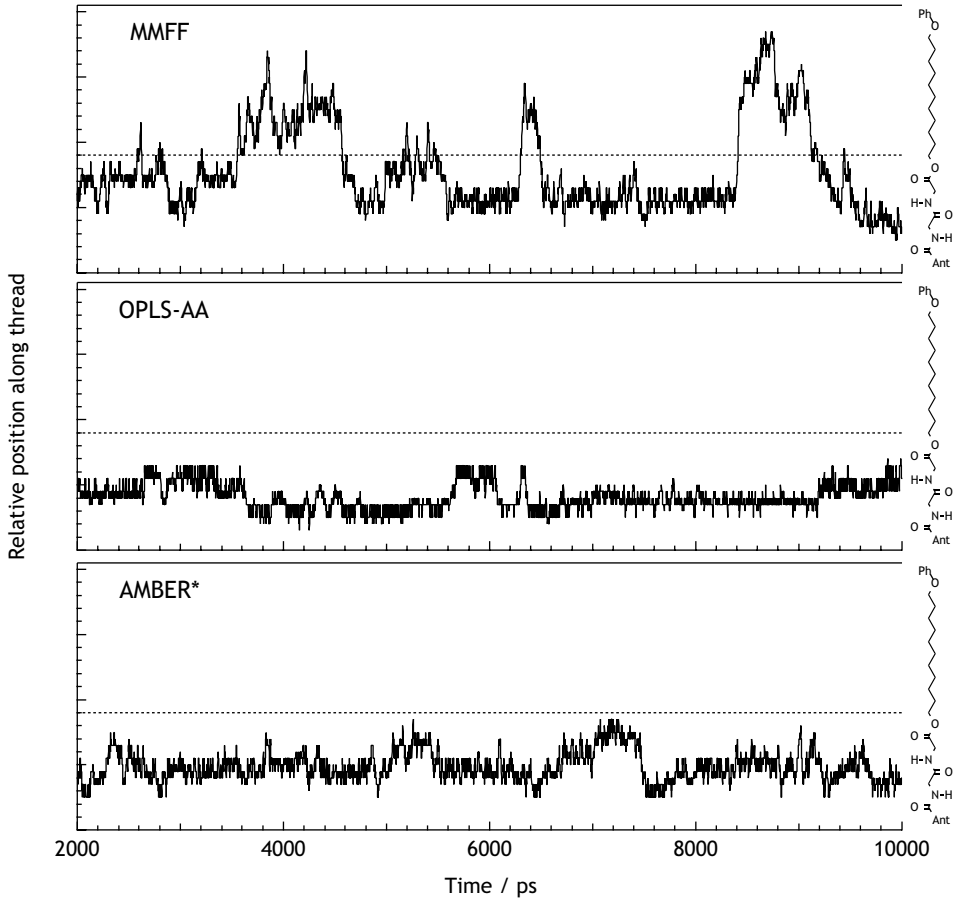

Figure 5-9. Position of the centre of the macrocycle expressed in terms of the nearest atom of the thread (right axis), during the last 8 ns of a 10 ns SD simulation, using the GB/SA $CHCl_3$ solvent model and different force fields. The dotted line marks the border beneath which the macrocycle is considered bound to the peptide station.

Analysis of the runs in terms of the conformations discussed in Section 5.3 turned out to be problematic. The specific H-bond pattern of the global minimum MMFFS-1 (see Figure 5-6) for instance was found during only ~1% of the SD simulation. This implies that although conformation MMFFS-1 is a minimum on the potential energy surface, population of this conformer is entropically unfavourable at 350 K. More generally, it seems that an analysis of the data in terms of a limited number of conformations is inappropriate, for a quick glance at the simulation results reveals many more hydrogen bond patterns. We therefore need to examine the data in a different way. The samples obtained during the SD runs were checked for the occurrences of H-bonds, using the methods described in Section 5.2. Alternatively, to follow the translation of the macrocycle along the thread, the thread atom closest to the centre of the macrocycle was calculated for each sample (see Section 5.2 for more details).

With a $CHCl_3$ continuum solvent model, the macrocycle is quite mobile. Not only the hydrogen-bond patterns change frequently, the macrocycle is observed to leave the peptide station for different periods when the MMFF force field is used (Figure 5-9). With the AMBER* and OPLS-AA force field, however, the centre of the macrocycle does not translate beyond the ester group of the peptide station during the simulation.

The graphs in Figure 5-9 can be discussed in terms of a two state model in which the macrocycle is located either *on* or *off* the peptide station. Therefore, a borderline is drawn at the carbon atom directly attached to the sp^3 ester oxygen, and the samples below this line are summed. The relative population of macrocycle bound to the station (p_{bound}) then yields the relative binding energy (ΔG) using the Boltzmann equation:

$$\Delta G = RT \ln\left(\frac{1 - p_{bound}}{p_{bound}}\right) \qquad \text{(Eq. 5-1)}$$

where R is the gas constant and T the temperature. The results of this analysis are summarised in Table 5-5 as method 1. The relative population of rotaxanes where the macrocycle is bound to the peptide station was also calculated by looking directly at the formation of hydrogen bonds (method 2). The macrocycle was considered bound if there existed at least one hydrogen bond between macrocycle and peptide station.

Table 5-5. Analysis of 8000 samples taken from the last 8 ns of a 10 ns SD run, using the GB/SA $CHCl_3$ solvent model and three different force fields. The fraction of samples is given where the macrocycle resides on the peptide station (p_{bound}) which yields the relative binding energy (ΔG). Standard deviations are given in parentheses.

	p_{bound}		ΔG / (kcal mol^{-1})	
	method 1[a]	method 2[b]	method 1[a]	method 2[b]
MMFF	0.73 (0.08)	0.79 (0.10)	-0.7 (0.3)	-0.9 (0.3)
OPLS-AA	1.00 (0.00)	0.99 (0.01)	< -3	-3.2 (0.5)
AMBER*	1.00 (0.00)	0.94 (0.03)	< -3	-1.9 (0.3)

a. Measuring the centre of the macrocycle relative to the thread.

b. Counting the occurrence of at least one hydrogen-bond between macrocycle and peptide station.

Because the precise population of rotaxanes in nonpolar solution where the macrocycle resides on the peptide station is not known experimentally, comparison of the different force fields and analyses provides an internal validation of the computational methods. With all force fields, the difference between p_{bound} for the two analysis methods is not significant, and both methods can thus be used with some confidence to analyse the SD runs. The small differences arise from structures in which the macrocycle is located on the alkyl chain, but the flexible alkyl chain still allows for a hydrogen bond between the station and the macrocycle (as witnessed with the MMFF force field), or alternatively from situations where the macrocycle is located on the GlyGly station without forming an H-bond (as occurs with AMBER*).

As expected, the peptide station is the preferred binding region for the macrocycle, but the fraction of bound rotaxanes differs per method. With the OPLS-AA and AMBER* force field, the macrocycle permanently resides at the peptide station (method 1) and forms H-bonds to the station for over 90% of the simulation time (method 2). According to the MMFF force field, however the fraction of rotaxanes, for which the macrocycle surrounds the peptide station is much smaller: 73% or 79%, depending on the method of analysis. If the macrocycle would really spend more than 20% of its time on the alkyl chain, a shielding effect of the alkyl chain protons in the ^{1}H NMR spectrum of **1** is to be expected. This however is not observed (see Figure 4-2 on page 70), and thus the MMFFs force field probably underestimates p_{bound}, and consequently $-\Delta G$ is also underestimated. The relative binding energy ΔG for the OPLS-AA and AMBER* force fields can only be determined using method 2. Since method 1 yields only *bound* conformations, ΔG must be very negative (< -3 kcal mol^{-1}).

5.5 Effect of Anthracene-Carbonyl Dihedral Angle

The conformational searches of Section 5.3 seemed to suggest that a flattening of the anthracene-9-carboxamide stopper gives room to the macrocycle to bind to *CO-1*, as was proposed for the excited state mechanism.[1] This led to the idea that the excited state of **1** might be modelled by constraining the dihedral angle (ϕ) between anthracene and *CO-1*. It therefore seems reasonable to model the excited state of the rotaxane simply by using flat bottom constraints (k = 1000 kJ mol^{-1}) for ϕ during the simulations. These were set to parallel (ϕ = 0±5°) or nearly parallel (ϕ = 30±5°) values.

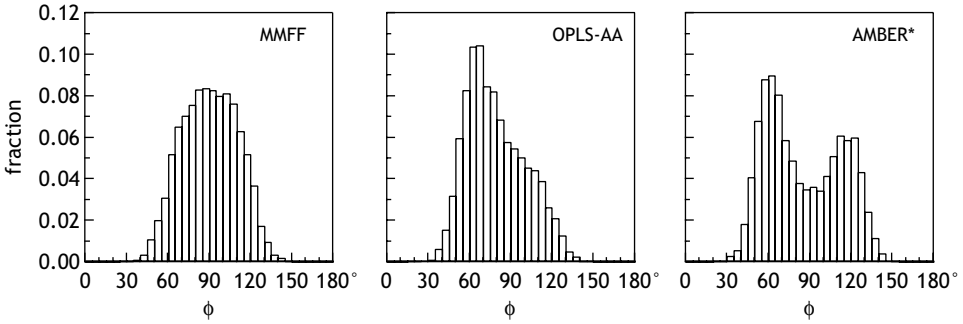

Figure 5-10. Distribution of anthracene-carbonyl dihedral angles in an *unconstrained* 10 ns SD simulation using a GB/SA $CHCl_3$ solvent model and three different force fields.

For an *unconstrained* SD simulation, the distribution of ϕ is displayed in Figure 5-10. It shows that the average dihedral angle <ϕ> between anthracene and the adjacent carbonyl is approximately 90° for all force fields, although the distributions are quite different. Rotation around the anthracene-*CO-1* bond between the local minima that are found around 60 and 120° degrees occurs only over the low 90° barrier (see also Figure 5-2). For the OPLS-AA and AMBER* force fields this barrier is not crossed frequently enough to make the distribution symmetric.

Hydrogen bond patterns of **1** during the SD runs were studied by counting binding of the macrocycle to the separate sites of the thread. Each time any of the macrocycle's amide groups (*A, B, C,* or *D*) formed a hydrogen bond to a carbonyl or NH group of the thread (using the labelling of Figure 5-4) this was recorded, giving an impression of the prevailing hydrogen bond patterns during the SD runs. It should be noted that in the MMFF simulations hydrogen bonds *not* only formed between macrocycle and peptide station, but also between *CO-1* and *NH-2* of the thread (Figure 5-11). This seven membered

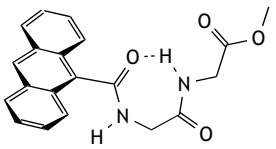

Figure 5-11. The intramolecular hydrogen bond that forms a seven membered ring in the thread.

ring formed both when the macrocycle was on and off the station during *circa* 10% of the simulation time.

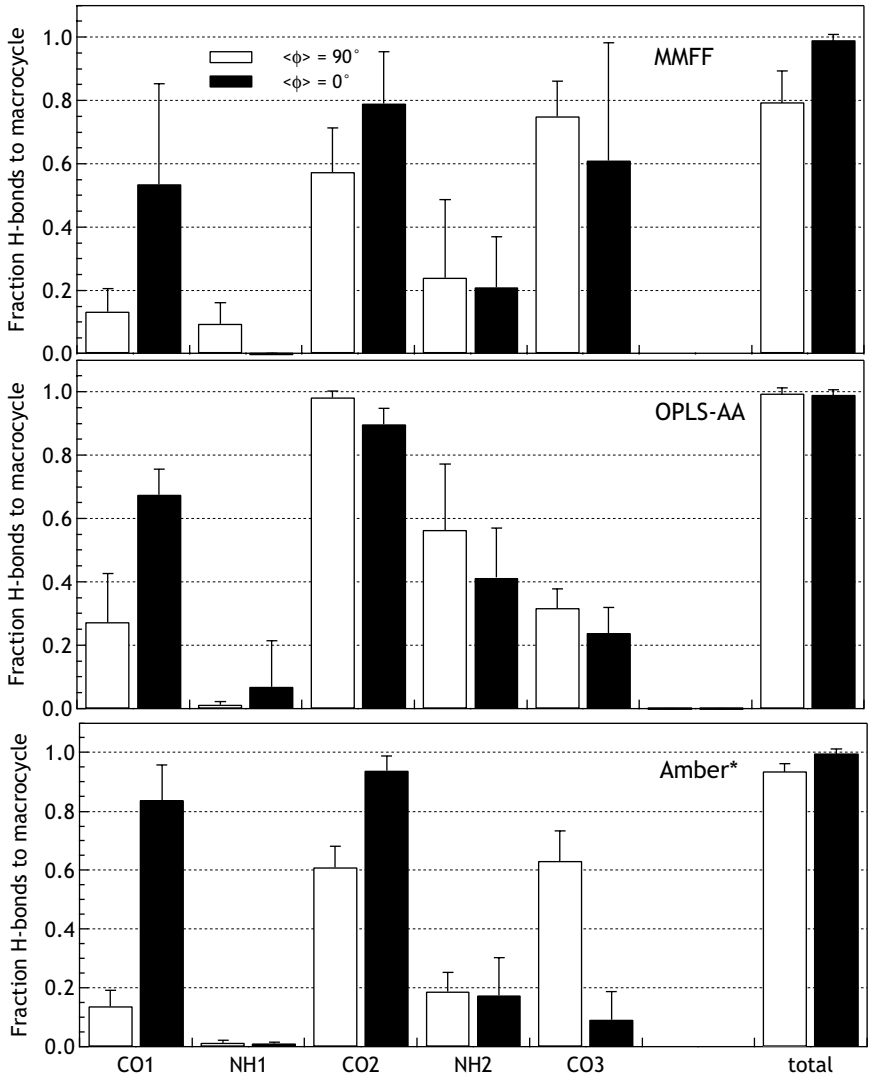

Figure 5-12. Analysis of 8000 samples taken from the last 8 ns of a 10 ns SD run, using the GB/SA $CHCl_3$ solvent model and 3 different force fields. The fraction of samples where the macrocycle forms at least one hydrogen-bond to a site on the thread are shown for different anthracene-carbonyl dihedral angles. Totals are shown separately. Error bars indicate standard deviations.

The effect of the dihedral angle ϕ on the hydrogen bond patterns between macrocycle and peptide station is shown in Figure 5-12. These bar graphs contain a wealth of information,

but the most important point to be made is that when anthracene and *CO-1* are perpendicular, there are very few H-bonds between the macrocycle and *CO-1*. However, when anthracene and *CO-1* are parallel (<ϕ> = 0°), binding of the macrocycle to *CO-1* increases dramatically. This shows that a small steric effect can have a profound influence on the hydrogen bond patterns of rotaxanes, and provides an explanation for the remarkable fluorescence behaviour (see Chapter 4) of **1**.

The three force fields differ only in the details of the H-bond patterns, the main features are force field independent which gives some confidence in the validity of these results. In the absence of constraints (<ϕ> = 90°), the macrocycle primarily forms hydrogen bonds to *CO-2*, *NH-2*, and *CO-3* (Figure 5-12), which could already be seen in the position of the centre of the macrocycle relative to the thread (see Figure 5-9). The *peri*-hydrogens of the anthracene group prevent the approach of the macrocycle, which results in very few structures where *CO-1* or *NH*-1 have formed H-bonds. This was confirmed by a separate SD run: when a C_{10} alkyl chain was placed between anthracene and *CO-1*, a much more even distribution over the separate binding sites was found: with the MMFF force field, p_{bound} = 0.70 for *CO-1*, 0.85 for *CO-2*, and 0.51 for *CO-3*.

The same effect is observed when the steric demand caused by the anthracene group is relieved by decreasing the dihedral angle <ϕ> from 90 to 0°. The fraction of conformations where the macrocycle is bound to *CO-1* increases by a factor of 3 to 4 at the expense of the *NH-2* and *CO-3* binding sites of the thread (Figure 5-12). At the same time the total number of occurrences of an intercomponent H-bond increases, except for OPLS-AA, where p_{bound} already was nearly 1. The binding of the macrocycle to the peptide station in the "excited state model" thus becomes stronger. This is also reflected by the increase of the average number of hydrogen-bonds between macrocycle and thread (Figure 5-13).

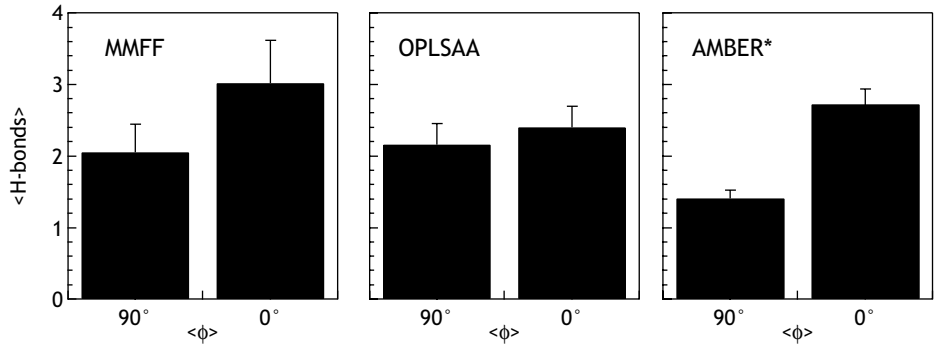

Figure 5-13. Average number of intercomponent H-bonds in the last 8 ns of a 10 ns SD run, using different force fields and the GB/SA $CHCl_3$ solvent model. The average dihedral angle <ϕ> between anthracene and CO-1 was either 90° (no constraints) or 0° (constrained). Error bars indicate standard deviations.

The results of the conformational searches (see Section 5.3) of rotaxane **1**, show a larger number of intercomponent H-bonds than is found on average in the SD runs (Figure 5-13). With the MMFF and AMBER* force fields <*H-bonds*> increases significantly upon flattening the anthracene-9-carboxamide stopper, mainly due to an increased number of H-bonds between the macrocycle and *CO-1* and *CO-2* (see Figure 5-11). For the OPLS-AA force field decreasing <ϕ> only leads to a reshuffling of the H-bond pattern: there is more binding to *CO-1* in the excited state model, but there are not more intercomponent H-bonds in general and binding to *CO-2* even decreases.

This difference between OPLS-AA and the other two force fields is also found when we look at the average position of the macrocycle with respect to the thread. For MMFF and AMBER*, the macrocycle clearly resides closer to anthracene when <ϕ> is changed from 90 to 0°, as was proposed for the excited state behaviour of **1**. As shown in Figure 5-14, the translation induced by constraining the anthracene-*CO-1* dihedral angle to 0°, amounts to almost two single bond lengths (≈ 3 Å). For OPLS-AA, even though H-bonding to *CO-1* increases, the macrocycle's location remains constant.

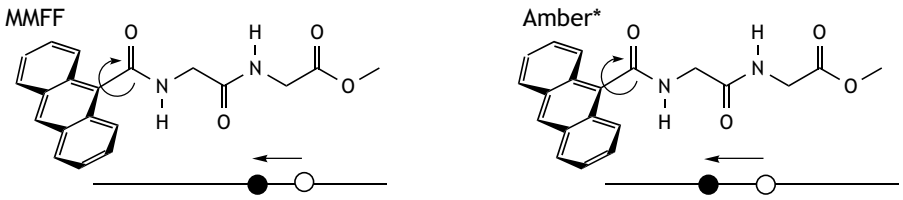

Figure 5-14. Schematic presentation of the average location of the macrocycle's centre. relative to the thread, measured during a 10 ns SD run (GB/SA $CHCl_3$, 350 K) with two force fields. The average position is given for an unconstrained (open circle) run, and a run where the anthracene-carbonyl dihedral angle is constrained to 0° (closed circles). Averaging only over samples in which the macrocycle resided on the peptide station.

The effect of the anthracene-*CO-1* dihedral angle on the intercomponent hydrogen bonds in **1**, as described in this section**,** are only manifested when <ϕ> is set to 0 ± 5°. The SD runs where this angle was constrained to 30 ± 5° showed no significant changes with respect to the unconstrained simulations.

5.6 Discussion of the Model

Independent of the force field used, the SD runs of this Chapter produce the effects that are thought to be the basis of the fluorescence phenomena observed in Chapter 4, *viz.* an increase of H-bonds between the macrocycle and *CO-1* when the anthracene-*CO-1* dihedral angle is reduced. This, however, was only observed when the anthracene-9-carboxamide stopper was constrained to flatness. Preliminary *ab initio* calculations indicate that the excited state changes are much less dramatic, so it is fair to assume that a faithful simulation of **1** in the excited state requires other factors to be taken into account.

First of all, the charge distribution of anthracene-9-carboxamide will change in the excited state, making *CO-1* a better H-bond acceptor. This could be modelled by changing the relevant atomic charges. Secondly, not only the minimum of the dihedral potential changes in the excited state, but also the barriers (see Figure 5-2 for the current potentials). The change of <ϕ> in the excited state could thus arise from a decrease of the 0° barrier. The constraints used in Section 5.5 are only a crude way to accomplish this, substitution of realistic dihedral parameters based on high level *ab initio* calculations in the force field could help to establish a more quantitative view.

Of course, the force field in combination with the solvent model is also of importance. Even though we have seen that all force fields produce the enhanced binding to *CO-1* in the excited state simulations, there are some notable differences. The MMFF force field for instance has the tendency to form the maximum number of H-bonds: all the structures of the conformational search have 4 intercomponent H-bonds (Table 5-2), and in the SD simulations it is the only force field where an H-bond within the thread is formed (Figure 5-11). The AMBER* force field on the other hand forms the smallest number of H-bonds both in the conformational search and in the SD simulations. The OPLS-AA force field is different in its behaviour when ϕ is set to 0°: the hydrogen bond pattern change is different from that of MMFF and AMBER* and the position of the macrocycle on the thread is not altered.

In the absence of detailed experimental data it is difficult to decide which force field gives the most realistic results. All three force fields are optimised for the types of interactions present in **1**, and therefore are expected to give reasonable results. The best strategy seems to be to compare different force fields as we did in this Chapter, in order to recognise force field specific results.

5.7 Conclusions

The excited state dynamics model for rotaxane **1** developed in Chapter 4 is supported by stochastic dynamics simulations. It was found that due to steric hindrance of the anthracene group, the macrocycle can not efficiently bind to the carbonyl adjacent to the anthracene. In the excited state, however, the steric demands are lower, because anthracene and the adjacent carbonyl have a more planar orientation. When the anthracene-carbonyl dihedral angle is constrained to 0° to mimic the excited state, a dramatic increase in hydrogen bonding to this carbonyl is observed in the SD runs. This binding is thought to be responsible for the anomalous fluorescence effects described in Chapter 4.

All force fields qualitatively support these findings. These force fields are well parametrised for peptides and can thus be expected to realistically model the multiple hydrogen bonds of **1**. For quantitative conclusions, a more precise parameterisation will be necessary, in particular when the modelling of the S_1 state of anthracene-9-carboxamide stopper is considered. In this Chapter it is shown that steric influences of anthracene alone can induce huge changes in hydrogen-bond patterns between station and macrocycle. However, that was only

observed when the anthracene-carbonyl dihedral angle was constrained to 0°. When the dihedral angle was set to 30°, the changes were far less dramatic. Since a complete flattening of anthracene-9-carboxamide in the excited state is unlikely (as indicated by *ab initio* calculations), other factors probably play a role. A more realistic model should therefore include electronic factors and special parameters for the anthracene-carbonyl dihedral angle in the excited state. At the same time more experimental data are needed on the structure of **1** in solution.

Supplementary Material. Three-dimensional structures of all conformations and movies showing the dynamics of H-bonding in the SD simulations will be made available on the world wide web: http://www.uba.uva.nl/nl/publicaties/wurpel/

Acknowledgement. A large number of the simulations in this Chapter have been performed by Rik van den Ende.

5.8 References

1. Werner, T.C., and Rodgers, J. Studies on the fluorescence properties of meso-substituted amidoanthracenes. *J. Photochem.* **32**, 59-68 (1986)
2. Leigh, D.A., Murphy, A., Smart, J.P., Deleuze, M.S., and Zerbetto, F. Controlling the frequency of macrocyclic ring rotation in benzylic amide [2]catenanes. *J. Am. Chem. Soc.* **120**, 6458-6467 (1998)
3. Raymo, F.M., Houk, K.N., and Stoddart, J.F. The mechanism of the slippage approach to rotaxanes. Origin of the "all-or-nothing" substituent effect. *J. Am. Chem. Soc.* **120**, 9318-9322 (1998)
4. Grabuleda, X., and Jaime, C. Molecular shuttles. A computational study (MM and MD) on the translational isomerism in some [2]rotaxanes. *J. Org. Chem.* **63**, 9635-9643 (1998)
5. Hunter, C.A., and Packer, M.J. Complexation-induced changes in ^{1}H NMR chemical shift for supramolecular structure determination. *Chem.-Eur. J.* **5**, 1891-1897 (1999)
6. Macias, A.T., Kumar, K.A., Marchand, A.P., and Evanseck, J.D. Computational studies of inclusion phenomena and synthesis of a novel and selective molecular receptor for 1,4-disubstituted benzenes and 4,4 '-disubstituted biphenyls. *J. Org. Chem.* **65**, 2083-2089 (2000)
7. Jorgensen, W.L., and Nguyen, T.B. Modeling the Complexation of Substituted Benzenes By a Cyclophane Host in Water. *Proc. Natl. Acad. Sci. U. S. A.* **90**, 1194-1200 (1993)
8. Kaminski, G.A., and Jorgensen, W.L. Host-guest chemistry of rotaxanes and catenanes: application of a polarizable all-atom force field to cyclobis(paraquat-p-phenylene) complexes with disubstituted benzenes and biphenyls. *J. Chem. Soc.-Perkin Trans. 2* 2365-2375 (1999)
9. Mohamadi, F., Richards, N.G.J., Guida, W.C., Liskamp, R., Lipton, M., Caufield, C., Chang, G., Hendrickson, T., and Still, W.C. Macromodel - an Integrated Software System for Modeling Organic and Bioorganic Molecules Using Molecular Mechanics. *J. Comput. Chem.* **11**, 440-467 (1990)
10. Jorgensen, W.L., Maxwell, D.S., and Tirado-Rives, J. Development and Testing of the OPLS All-Atom Force Field on Conformational Energetics and Properties of Organic Liquids. *J. Am. Chem. Soc.* **118**, 11225-11236 (1996)

11. Halgren, T.A. Merck molecular force field .1. Basis, form, scope, parameterization, and performance of MMFF94. *J. Comput. Chem.* **17**, 490-519 (1996)
12. Halgren, T.A. Merck molecular force field .2. MMFF94 van der Waals and electrostatic parameters for intermolecular interactions. *J. Comput. Chem.* **17**, 520-552 (1996)
13. Halgren, T.A. Merck molecular force field .3. Molecular geometries and vibrational frequencies for MMFF94. *J. Comput. Chem.* **17**, 553-586 (1996)
14. Halgren, T.A., and Nachbar, R.B. Merck molecular force field .4. Conformational energies and geometries for MMFF94. *J. Comput. Chem.* **17**, 587-615 (1996)
15. Halgren, T.A. Merck molecular force field .5. Extension of MMFF94 using experimental data, additional computational data, and empirical rules. *J. Comput. Chem.* **17**, 616-641 (1996)
16. Halgren, T.A. MMFF VI. MMFF94s option for energy minimization studies. *J. Comput. Chem.* **20**, 720-729 (1999)
17. Halgren, T.A. MMFF VII. Characterization of MMFF94, MMFF94s, and other widely available force fields for conformational energies and for intermolecular-interaction energies and geometries. *J. Comput. Chem.* **20**, 730-748 (1999)
18. Cornell, W.D., Cieplak, P., Bayly, C.I., Gould, I.R., Merz, K.M., Ferguson, D.M., Spellmeyer, D.C., Fox, T., Caldwell, J.W., and Kollman, P.A. A 2nd Generation Force-Field for the Simulation of Proteins, Nucleic-Acids, and Organic-Molecules. *J. Am. Chem. Soc.* **117**, 5179-5197 (1995)
19. Cornell, W.D., Cieplak, P., Bayly, C.I., Gould, I.R., Merz, K.M., Ferguson, D.M., Spellmeyer, D.C., Fox, T., Caldwell, J.W., and Kollman, P.A. A second generation force field for the simulation of proteins, nucleic acids, and organic molecules (vol 117, pg 5179, 1995). *J. Am. Chem. Soc.* **118**, 2309-2309 (1996)
20. Still, W.C., Tempczyk, A., Hawley, R.C., and Hendrickson, T. Semianalytical Treatment of Solvation for Molecular Mechanics and Dynamics. *J. Am. Chem. Soc.* **112**, 6127-6129 (1990)
21. Kolossvary, I., and Guida, W.C. Low mode search. An efficient, automated computational method for conformational analysis: Application to cyclic and acyclic alkanes and cyclic peptides. *J. Am. Chem. Soc.* **118**, 5011-5019 (1996)
22. Polak, E., and Ribière, G. *Revue Francaise Inf. Rech.Oper.* **16-R1**, 35 (1969)
23. Ponder, J.W., and Richards, F.M. *J. Comput. Chem.* **8**, 1016 (1987)
24. Wavemetrics, Igor Pro 3.16, Wavemetrics Inc.: Oregon, 1988-2000
25. Jeffrey, G.A. *An Introduction to Hydrogen Bonding* Oxford University Press: New York, 1997.

Chapter 6

Naphthalimide Rotaxanes

Photoinduction of Fast, Reversible Translational Motion in a Hydrogen-Bonded Molecular Shuttle[*]

We are no longer the knights who say 'Ni.' We are now the knights who say 'Ikki Ikki Ikki Ikki, P'tang Zoopdah blohlfdsjfdslkjn. (Ni!)'

– Monty Python's "The Quest for the Holy Grail"

6.1 Introduction

Ever since the discovery of template directed synthesis of rotaxanes,[1,2] scientists have strived to influence the position of the macrocycle on the thread by external stimuli, in a search for nanoscale analogues of the fundamental components of machinery from the macroscopic world.[3-5] From a plethora of possibilities to address rotaxanes (Shigekawa *et al.* even manipulated the position of the macrocycle on a polyrotaxane using scanning tunnelling microscopy[6]), photonic or electrical stimuli seem the obvious choices from a practical point of view.

Changing the oxidation state of a binding station *electrochemically* has already proven to be a viable approach to move the macrocycle from its preferred location to a second station.[7-11] It therefore seems a logical step to extend this strategy to *photoinduced* electron transfer.

---

*Brouwer, A.M., Frochot, C., Gatti, F.G., Leigh, D.A., Mottier, L., Paolucci, F., Rofia, S., and Wurpel, G.W.H. *Science* **291**, 2124-2128 (2001)

This, however, poses the problem of the lifetime of the charge separated state. When charge recombination is too fast, no macrocycle translation will be observed.[12-15] In an attempt to circumvent this problem, *sacrificial* electron donors or acceptors have been applied, which in the absence of other electrochemically active species lead to permanent reduction or oxidation of a binding station when exposed to light.[10,12,14,15] The macrocycle then has infinite time to move, but only returns upon addition of chemicals that can restore the oxidation state of the binding stations.

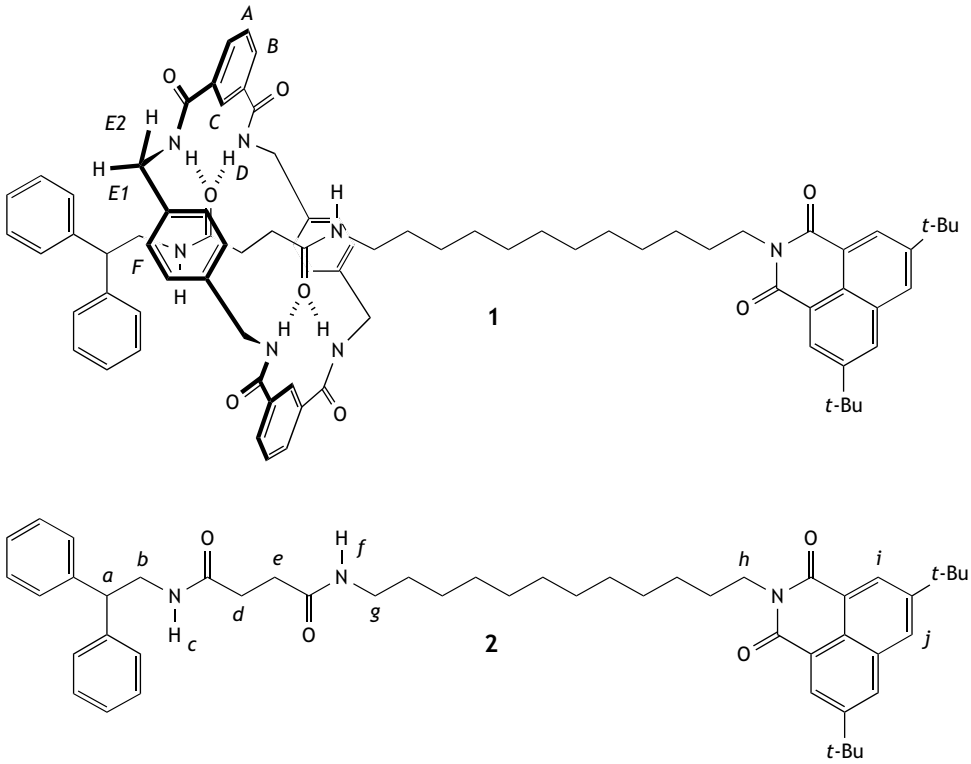

Figure 6-1. Chemical formulae of molecular shuttle **1**, shown in the preferred (*succ*-**1**) co-conformation in non-hydrogen-bond disrupting solvents, and thread **2**. The letters identify non-equivalent ^{1}H environments used in the assignment of the ^{1}H NMR spectrum (Figure 6-2). Capitals indicate macrocycle protons and lower case letters indicate thread protons.

In this Chapter, a *reversible* shuttle will be discussed, based on a hydrogen-bonded rotaxane, **1** (Figure 6-1), where for the first time shuttling over large distances (*circa* 1.5 nm) can *repeatedly* be induced by short light pulses. In the preferred conformation in the ground state, the macrocycle (which is the same as that used in Chapter 4) is hydrogen bonded to a succinamide station. Photoexcitation of the naphthalimide stopper leads to its reduction by an added external electron donor. The naphthalimide radical anion then becomes the pre-

ferred hydrogen-bonding station, and the macrocycle moves over. After spontaneous recombination of the radical cation of the donor and the naphthalimide radical anion, the system is "reset" and can be pumped again.

The kinetics of this shuttling process could be studied in detail, because binding of the macrocycle to the reduced naphthalimide group is monitored straightforwardly by time resolved optical absorption spectroscopy. Depending on solvent and temperature, shuttling of the macrocycle was found to occur within 1 μs, which is much faster than previous light driven shuttles that operate on a minute/hour time scale.[7,16]

Even though 1 μs is fast for large amplitude, submolecular motion, a charge separated state seldomly has such a long lifetime. In intermolecular donor acceptor systems, rapid back electron transfer in the geminate radical ion pair often prevents their separation. However, a high yield of separated radical ions is known to be formed in electron transfer to a triplet state.[17] This approach was successfully applied to **1**, where a high yield of naphthalimide radical anions could be observed for over 100 μs, which is more than enough to detect the translation of the macrocycle.

6.2 Experimental

Synthesis. All syntheses were carried out by F.G. Gatti in the group of D.A. Leigh at the University of Warwick. Rotaxane **1** was synthesised using the corresponding thread **2** in a five-component clipping reaction. Thus, treatment of **2** with 10 equivalents each of xylylene diamine and isophthaloyl dichloride ($CHCl_3$, NEt_3, 4 hours, high dilution) led to the formation of [2]rotaxane **1** in 59% yield.

Sample Preparation. Acetonitrile (Merck, UvaSol), propionitrile, and butyronitrile (Fluka, highest purity) were refluxed and distilled over CaH_2 under exclusion of moisture, then stored over 4 Å mol sieves. These solvents will be referred to as anhydrous. "Superdry" samples of **1** in acetonitrile were obtained by distilling previously dried MeCN off mol sieves on a high vacuum line, directly into a cell.

Fluorescence Measurements. Methods are described in Section 3.2.1 on page 45.

Cyclic Voltammetry. L. Mottier and S. Roffia in the group of F. Paolucci at the University of Bologna performed the CV Measurements. Conditions: 1.0 mM substrate concentration, 0.05 M tetrabuthylammonium hexafluorophosphate (TBAH) DMF solutions. T = 25 °C, scan rate = 1.0 Vs^{-1}, working electrode: platinum wire. A silver wire was used as quasi-reference electrode in a single compartment cell. Potentials were measured with respect to ferrocene/ferrocenium (Fc/Fc^+) as internal standard.

Transient Absorption Measurements. All samples were degassed by at least three freeze-pump-thaw cycles, unless noted otherwise. During acquisition, the cell was stirred to minimise build-up of photodegradation products in the excitation volume. For excitation, the third harmonic of a Coherent Infinity Nd:YAG laser was used (355 nm, 10 Hz, FWHM = 2 ns). The laser power was adjusted using a Glan Taylor prism to an energy of approximately 2.5 mJ $pulse^{-1}$. The laser illuminated a slit of 10 × 2 mm. Perpendicular to this the probe light, provided by an EG&G (FX504) low pressure

Xenon flash lamp, irradiated the laser-excited volume through a 1 mm pinhole, directly behind the front face of the cell.

In our lab van Ramesdonk *et al.* found that the spectral characteristics of the probe light were inhomogeneously distributed over the lamp spot. We therefore guided the probe light through a quartz plate, directing one part of the light onto the sample in such a way to overlap with the laser excited volume, and aim the other part on a reference sample holder. This is an excellent way to minimise the noise along the wavelength axis, for in this way the same part of the flashlamp arc is used for the signal and reference channels. The probe light from both the signal and reference channels is then collected in optical fibers which are connected to an Acton SpectraPro-150 spectrograph which is coupled to a Princeton Instruments ICCD-576-G/RB-EM gated intensified CCD camera. Using a 5 ns gate this camera simultaneously records the spectrally dispersed light from both optical fibers on separate stripes of the CCD.

After correction for the differences in the light collected through both fibers (by collecting signal and reference light without pumping the sample) the absorption spectrum of the transient excited state is calculated by taking the logarithm of the intensity of the light aimed at the reference sample holder (I_0) divided by the intensity of light that travelled through the excited volume of the sample (I). By varying the delay between the laser pulse and the opening of the gate of the detector, absorption spectra at different times after excitation can be obtained with a time resolution of ~5 ns.

For single wavelength measurements the probe light was provided by a continuous light source (Xe lamp, Müller lamp housing LAX1450, power supply SVX1450), again under right angle conditions. The probe light was led into an Oriel 77250 monochromator and detected by a photomultiplier connected to a digital oscilloscope.

Temperature Control. Transient absorption measurements at low temperature were performed using a home built liquid nitrogen cryostat and control unit. The samples were degassed by at least three freeze-pump-thaw cycles and allowed to thermally equilibrate for at least 30 minutes prior to data collection. An aluminium mask around the quartz cell with 2 mm holes for the probe light and 10×2 mm slits for the pump light was used for low temperature transient absorption measurements.

Analysis. All data were analysed in Igor Pro 3.16[18]. To determine the shift of the naphthalimide radical anion absorption maximum, each trace was fitted with a Gaussian function between 405 and 430 nm. The peak positions thus obtained were plotted *versus* time. The standard deviation associated with the Gaussian fit was used to perform a weighted monoexponential fit.

6.3 Results and Discussion

6.3.1 Structural Characteristics

Rotaxane **1** consists of a benzylic amide macrocycle, mechanically interlocked onto the corresponding thread **2**. It contains two potential hydrogen-bonding stations, linked by a C_{12} alkyl chain: a 3,6-di-*t*-butyl-1,8-naphthalimide (*ni*) group and a succinamide (*succ*) group. The macrocycle is prevented from slipping off the thread by the *t*-butyl substituents on the naphthalimide and the diphenylmethyl group on the other side of the thread (Figure 6-1).

X-Ray crystal structures of model succinamide rotaxanes show the *succ*-station to be an excellent binding site for the benzylic amide macrocycle, which is held in place by two sets of bifurcated hydrogen bonds from the isophthalamide groups of the macrocycle to the two

succinamide amide carbonyls. In the neutral state naphthalimide is a poor hydrogen-bond acceptor and therefore in non-hydrogen-bond-disrupting solvents the rotaxane minimises its energy by adopting the co-conformation and hydrogen-bonding motif shown as *succ*-**1** in Figure 6-1.

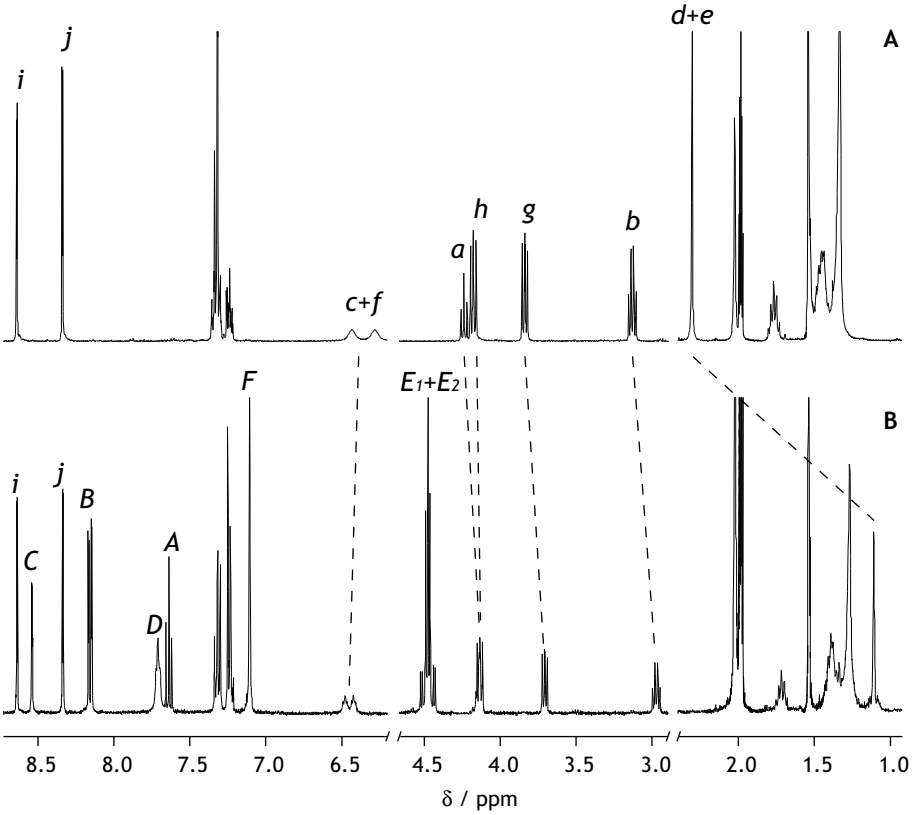

Figure 6-2. ^{1}H NMR Spectra (400 MHz) of (a) **2** and (b) **1** in CD_3CN at 329K (**1** is only sparingly soluble in CD_3CN at 298K). The letters correspond to the assignment of the resonances shown in Figure 6-1.

Structural evidence, indicating that indeed this co-conformation is predominant in solution, is found in the ^{1}H NMR spectrum of **1** in CD_3CN. It shows an upfield shift of 1.2 ppm for the methylene protons (H_d and H_e) of the succinamide station relative to the same signals in **2** due to binding of the macrocycle (the shielding is caused by the field effects of the aromatic rings of the xylylene residues). In contrast, the chemical shifts of the resonances of the naphthalimide unit (H_i and H_j) and *N*-methylene group (H_b) are virtually identical in **1** and **2**.

Similarly, the IR spectrum of **1** in MeCN shows no changes in the imide CO stretch vibrations compared to **2** (Figure 6-3). Binding of the macrocycle to the naphthalimide would lead to a weakening of this CO bond and thus shift this vibration to lower energy in **1**. On the basis of the IR spectra alone, it can however not be excluded that a small fraction of **1** resides on the *ni* station. This might escape detection, for this IR absorption would be hidden under the amide I bands (a hydrogen-bonded carbonyl stretch typically shifts 40-60 cm^{-1} to lower frequency[19]).

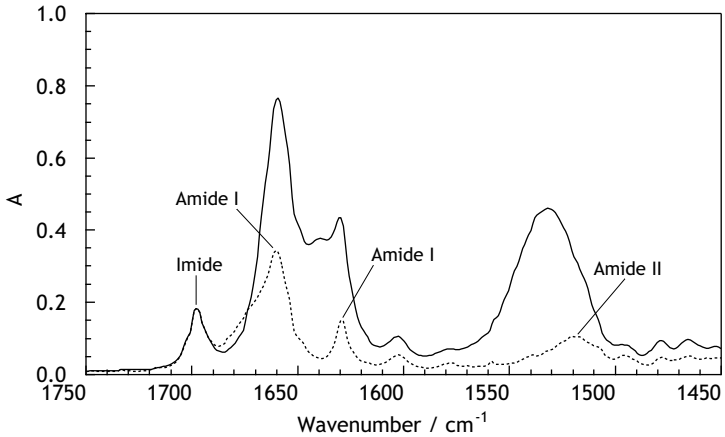

Figure 6-3. IR spectrum of rotaxane **1** (continuous) and thread **2** (dotted) in CH_2Cl_2. Spectra are baseline subtracted and scaled to the same imide absorption.

6.3.2 Electrochemistry

It has been established that the radical anion of 1,8-naphthalimide possesses much stronger hydrogen-bond accepting properties than the neutral species.[20,21] It is therefore anticipated, that after reduction of the rotaxane $ni^{\bullet-}$ becomes the preferred binding station, and the macrocycle will switch from *succ* to *ni*.

Cyclic voltammetry (CV) experiments (performed at the University of Bologna) gave strong indications for such a process. In thread **2**, the CV shows a nearly reversible one electron wave where the half wave reduction potential is located at $E_{red}^{1/2}$ = -1.61 V *vs.* ferrocene/ferrocenium (Fc/Fc^+) corresponding to the conversion of naphthalimide to its radical anion (Figure 6-4a). Significantly in rotaxane **1**, (i) the corresponding process (peak *i*) is shifted to less negative potentials, (ii) peak *i* lacks its reversible anodic counterpart (*i.e.* an oxidation peak within 60 mV), while (iii) an oxidation peak (*a*) is observed at much less negative potential (ΔE_p = 480 mV).

This behaviour suggests the conversion of pristine **1**, after reduction *i*, to a novel species, which is oxidised in *a*, and that, after the oxidation, regenerates **1** (*i.e.* a square mechanism as shown in Figure 6-5). Hydrogen bonding of the benzylic amide macrocycle to the reduced

naphthalimide moiety explains the features of the CV curve. After reduction, the macrocycle shuttles from the succinamide station to the naphthalimide group. Hydrogen bonding stabilises the radical anion resulting in the observed shift in the reoxidation peak. On the other hand, reoxidation regenerates the starting conditions and the macrocycle therefore shuttles back to its original position.

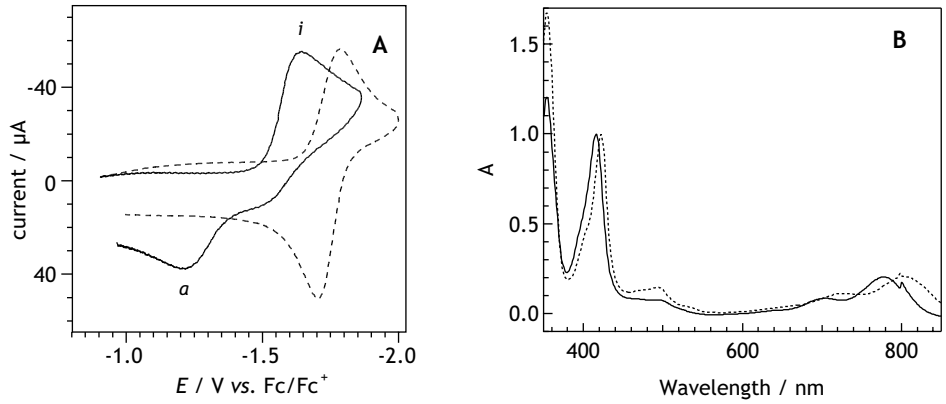

Figure 6-4. (A) cyclic voltammograms of **1** (continuous) and **2** (dashed) in DMF, scan rate 1 Vs^{-1}. (B) Electronic absorption spectra of electrochemically generated $\mathbf{1}^{\bullet-}$ (continuous) and $\mathbf{2}^{\bullet-}$ (dotted) in DMF at 298 K (corresponding to the largest charge before the isosbestic points were lost). The spectra were normalized to the intense absorption peak in the visible part of the spectrum.

The difference in ΔE_p of **1** and **2** is remarkable (redox-active host-guest complexes involving up to three hydrogen-bonds to similar naphthalimide units typically give stabilisations of around 0.2 V[20,21]) and can be taken as a measure of the intercomponent binding energy between macrocycle and $ni^{\bullet-}$. This value, 480 mV = 11.2 kcal mol^{-1}, is the equivalent of four strong, or three extremely strong, hydrogen-bonds (OCNH···O=CNR hydrogen-bond strengths are in the range 2-5 kcal mol^{-1} [22])

Furthermore, in a spectroelectrochemical experiment, rotaxane **1** displays distinctly different behaviour upon reduction than thread **2**. Both $\mathbf{1}^{\bullet-}$ and $\mathbf{2}^{\bullet-}$ show the electronic absorption spectrum that is characteristic for the radical anion of 1,8-naphthalimide (Figure 6-4),[23] but in the rotaxane all the peaks are blue-shifted compared to the thread. Since the sole difference between **1** and **2** is the presence of the mechanically interlocked macrocycle, the difference must arise from the macrocycle binding to $ni^{\bullet-}$ in the rotaxane. In $ni^{\bullet-}$ much of the negative charge is located on the carbonyl oxygens, and the electronic transitions ($D_n \leftarrow D_0$) can be described as having charge transfer character in which the negative charge on the carbonyl oxygens is decreased. Hydrogen bonds then stabilise the doublet ground state more strongly than the excited states. Thus the NH groups in the macrocycle can cause a blue shift of the $ni^{\bullet-}$ absorption by forming hydrogen bonds with the naphthalimide carbonyls.

6.3.3 Photoreduction Strategy

Reduction of rotaxanes **1** can also be accomplished photochemically, using an external electron donor in solution (See Figure 6-5). Transient absorption spectroscopy would then in principle allow monitoring of the macrocycle binding to $ni^{\cdot-}$ by a blue-shift of its absorption (see Section 6.3.2). In order to observe this shifting of the macrocycle, the lifetime of the generated radical anion should be considered: it should persist longer than the time it takes for the macrocycle to complete its translational motion. One obvious method is to use a sacrificial electron donor. After photoinduced electron transfer the donor radical cation decomposes into fragments that are no longer capable of accepting an electron of the naphthalimide radical anion. In the absence of other electron acceptors such as molecular oxygen, the radical anion will be stable. Indeed, in a transient absorption experiment where **2** in acetonitrile (MeCN) was excited in the presence of triethylamine, a build-up of $ni^{\cdot-}$ was observed, because the triethylamine cation decomposes.

For a reversible system, however, a stable radical cation is desirable, but then back electron transfer must be slow. One possible approach is to reduce the triplet state of the naphthalimide chromophore, for this makes back electron transfer spin forbidden. The 1,8-naphthalimide systems are particularly suited for this approach, because of their high triplet quantum yield.[24] The photophysics of naphthalimides, however, can be highly dependent on substitution[25] and therefore deserves some attention in order to optimise and understand the (photo)reduction cycle shown in Figure 6-5.

6.3.4 Naphthalimide Photophysics

The photophysical behaviour of substituted 1,8-naphthalimides is mainly determined by the first two close lying excited singlet states. Depending on which state is lowest in energy, efficient intersystem crossing can take place. In *N*-methyl-1,8-naphthalimide a $\pi\pi^*$ state has been reported to be the lowest singlet state.[24] This state is thought to lie very close to the second triplet state, which has $n\pi^*$ character. The different orbital occupations of S_1 and T_2 and their small energy gap promote efficient spin orbit coupling and thus deactivation of the excited singlet state *via* intersystem crossing readily occurs.

A $\pi\pi^*$ state is likely to be the lowest singlet excited state in thread **2** as well, as can be seen from the absorption and fluorescence spectrum (Figure 6-6). The high molar absorption coefficient of the first absorption band (13.1×10^3 $M^{-1}cm^{-1}$ at 353 nm) and the mirror image shape of the fluorescent band are indicative of this.

Although the photophysical properties of the naphthalimide rotaxanes can be expected to be quite similar to those of *N*-methyl-1,8-naphthalimide, some deviations are anticipated due to the two *t*-butyl groups. A summary of some photophysical properties of **2** in MeCN is given in Table 6-1. In acetonitrile, rotaxane **1** shows the same photophysical behaviour as thread **2**. This means that rotaxanation does not influence the excited states of the 1,8-naph-

thalimide stopper, in accordance with the predominance of the *succ*-**1** co-conformer (see Section 6.3.1).

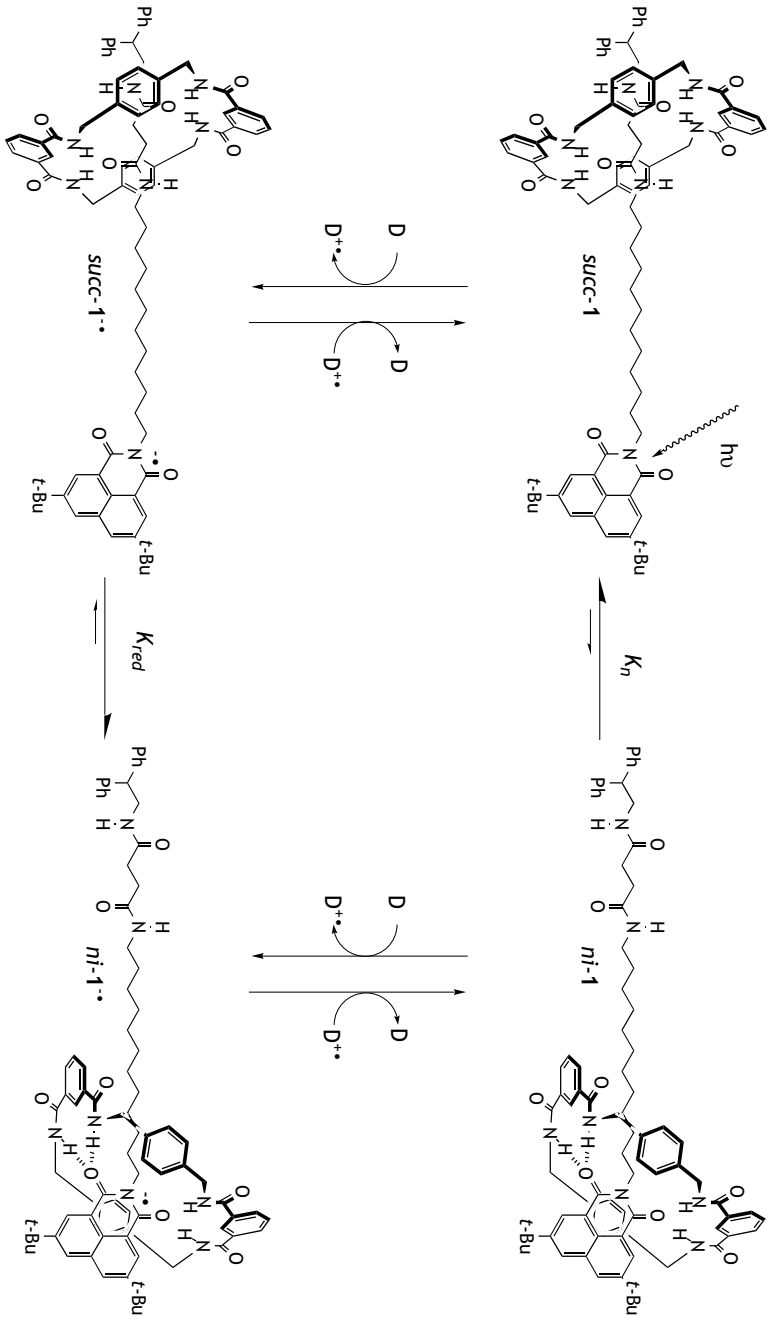

Figure 6-5. Photoreduction cycle of rotaxane **1**.

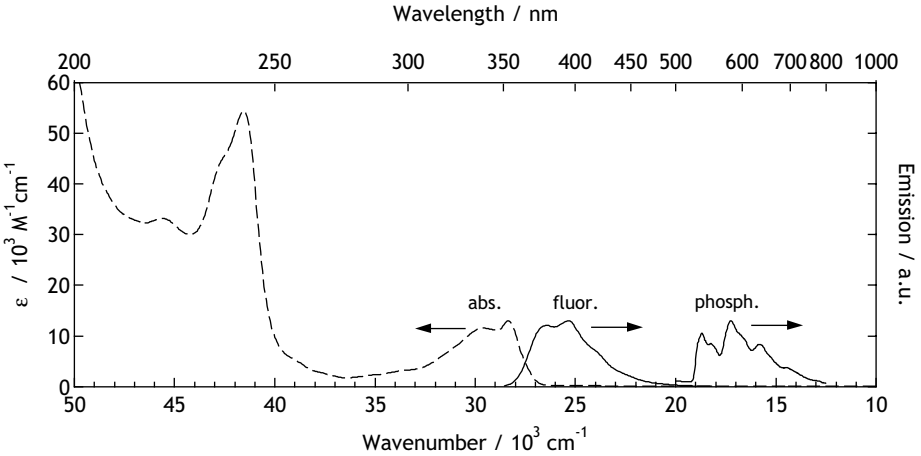

Figure 6-6. Electronic absorption (dashed) and emission (continuous) spectra of **2**. Excitation at 330 nm, absorption and fluorescence in MeCN, phosphorescence in MeTHF (77 K).

Table 6-1. Photophysical properties of **2** in MeCN, compared to unsubstituted *N*-alkyl-1,8-naphthalimides.

	this work	literature
E_{00} (S) / eV	3.41	3.63[26]
E_{00} (T)/ eV	2.32[a]	2.29[26]
$E_{red}^{1/2}$ / V *vs.* SCE	-1.16[b]	-1.34[23]
Φ_f	0.15	0.027[24]
τ_f / ns	1.6	0.145[24]
τ_T / μs	43.9[c]	

a. from phosphorescence in MeTHF at 77 K

b. in DMF

c. from transient absorption

The electron donating *t*-butyl substituents lower the energy of S_1 relative to T_2. This leads to a longer fluorescence lifetime and a larger fluorescence quantum yield. In acetonitrile rotaxane **1** shows the same photophysical behaviour as thread **2**. This means that rotaxanation does not influence the excited states of the 1,8-naphthalimide chromophore, again confirming the presence of a *succ*-**1** co-conformer (See Section 6.3.1).The energy of the singlet

state of **2** is lowered even further by increasing the polarity of the surrounding medium as is evident from the red-shifted fluorescence (Table 6-2).

Table 6-2. Solvent dependence of fluorescence of **2**

solvent	ε_r	λ_{max}	Φ_f
cyclohexane	2.0	367, 383	0.018
dichloromethane	8.9	375, 395	0.12
acetonitrile	37.5	376, 394	0.15
ethanol (95%)	24.6	386, 398	0.20

When the singlet state is lowered in energy, intersystem crossing becomes less favourable and a higher fluorescence quantum yield is observed. This mechanism implies that in the absence of other decay pathways, the triplet yield of **2** should be lower. This of course limits the efficiency of the photoreduction step *via* a triplet mechanism in MeCN to maximally 85%.

Selective excitation of thread **2** in MeCN with a 355 nm laser pulse (fwhm= 2 ns), leads to the prompt appearance of the characteristic $^3ni^*$ absorption (Figure 6-7), with peaks at 370, 442 and 468 nm. The decay of this triplet is non-exponential due to triplet-triplet annihilation, but becomes nearly monoexponential when using the lowest possible laser power on a diluted sample. Under these conditions, the triplet state has a decay time of 43 µs in MeCN.

The time resolution of our transient absorption setup (5 ns) does not allow for the detection of the short lived singlet state. Time correlated Single Photon Counting, however, afforded a value for the fluorescence decay time of $\tau_f = 1.6$ ns for **2** in acetonitrile (Table 6-1). The radiative decay rate $k_f = \Phi_f/\tau_f \approx 10^8\ s^{-1}$ (Φ_f= 0.15, see Table 6-1) is in reasonable accordance with the radiative rate of $2\times10^8\ s^{-1}$ calculated from the absorption spectrum.*

In degassed samples of thread **2** in MeCN, a long lived, weak but sharp transient around 416 nm is formed within the duration of the laser pulse. This transient is absent in aerated solutions. The shape of the absorption band and the oxygen sensitivity are indicative for a naphthalimide radical anion (see Section 6.3.2). The relative initial absorption of this peak is dependent on concentration, but independent of laser intensity. We tentatively ascribe this absorption to excimers formed via ground state complexes of **2**; the radical cation of *ni* is

*Calculated using a modified Einstein relation[27,28]: $1/\tau_R = 8\times2303\pi c\tilde{\nu}_{ul}^2 n^2 N_A^{-1}(g_l/g_u)\int\varepsilon d\tilde{\nu}$, where c is the speed of light in vacuo (in cm^{-1}), $\tilde{\nu}_{ul}$ is the wavenumber of the first vibronic transition (28325 cm^{-1}), n is the refractive index of the medium, N_A is Avogadro's constant, ε is the molar absorption of the transition (in $M^{-1}cm^{-1}$ *vs.* wavenumber, integrated between 25000 and 33000 cm^{-1}), g_l and g_u denote the degeneracies of the ground and excited states respectively.

thought to have a very low molar absorption coefficient and thus is not observed.[29] Ground state aggregation of 1,8-naphthalimides is known to occur[30] as well as excimer formation.[29,31] Since the amount of naphthalimide radical anions produced in a typical intermolecular electron transfer process as described below, is at least an order of magnitude larger, this excimer formation can be neglected.

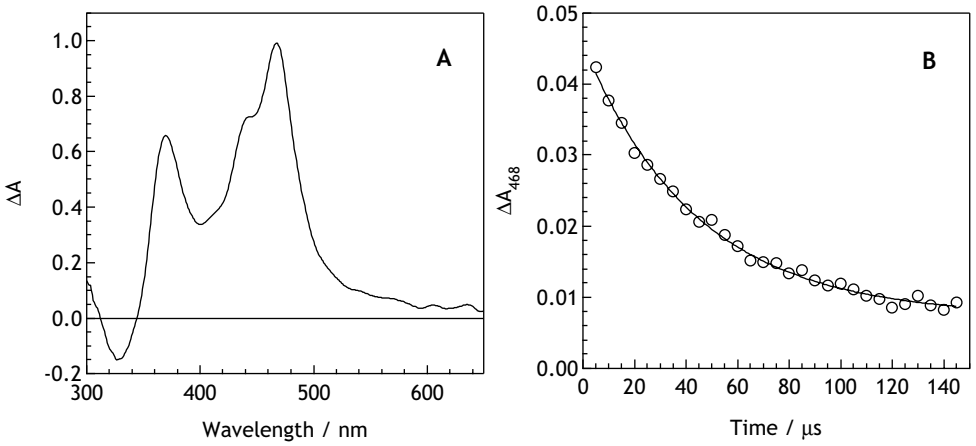

Figure 6-7. (A) Triplet-triplet absorption spectrum of **2** in MeCN taken directly after the laser pulse. (B) The decay at 468 nm with a mono-exponential fit, including a baseline. The baseline is due to a small amount of long lived naphthalimide radical anions presumably formed *via* an exciplex (see text).

6.3.5 Electron Transfer to Triplet Naphthalimide

The basic photophysical properties of *ni* being known, an electron donor can be selected that is capable of reducing $^3ni^*$ in order to create long lived $ni^{\cdot-}$ species. For that, both k_{et} and k_{sep} must be large, while k_{bet} must be small (Scheme 6-1).

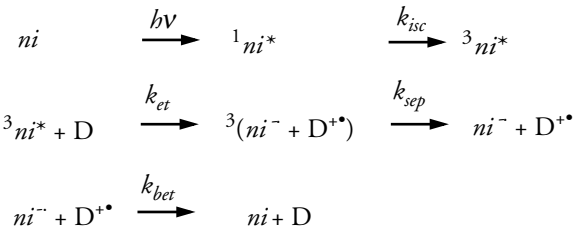

Scheme 6-1. Mechanism of triplet electron transfer, indicating the relevant rates

In a polar solvent such as MeCN, Coulombic interactions can be neglected and the driving force, ΔG_{et}, for electron transfer is:

$$\Delta G_{et} = e(E_{ox}^{1/2} - E_{red}^{1/2}) - E_{00} \qquad \text{(Eq. 6-1)}$$

Using E_{00}(T) and $E_{red}^{1/2}$ from Table 6-1, it follows that the oxidation potential of the electron donor must be +1.16 V *vs.* SCE or lower to make electron transfer from the triplet state thermodynamically favourable. Indeed a number of electron donors were found to be able to reduce $^3ni^*$: *N,N*-dimethylaniline (DMA; $E_{ox}^{1/2}$ = 0.81 V *vs.* SCE[32]), *N,N,N,'N'*-tetramethylphenylenediamine (TMPD; $E_{ox}^{1/2}$ = 0.17 V *vs.* SCE[33]), and 1,4-diazabicyclo[2.2.2]octane (DABCO; $E_{ox}^{1/2}$ = 0.57 V *vs.* SCE[34]). It is also possible to create $ni^{\cdot-}$ from the singlet state, *e.g.* using biphenyl, but its short lifetime requires a high concentration of electron donors.

Requirements for the radical cation of the electron donor are: (i) stability, to ensure reversibility of the photoreduction, and (ii) a low molar absorption coefficient, particularly at the wavelength where $ni^{\cdot-}$ absorbs. This will allow unperturbed monitoring of changes in the $ni^{\cdot-}$ absorption. Both DMA and DABCO meet these requirements.

The forward electron transfer rate was determined by measuring the triplet decay rate of **1** with DMA added in different concentrations. The triplet decay was recorded at 468 nm and had to be fitted with a sum of two exponentials, because the longer lived radical anion also absorbs at this wavelength. The fast component of this fit is taken as the triplet decay rate. A weighted, linear fit of k_T *vs.* [DMA] (Figure 6-8) directly yields the quenching constant for the naphthalimide rotaxane and the electron donor DMA in MeCN: k_{et} = $2.2 \pm 1.6 \times 10^8$ $M^{-1}s^{-1}$. The large uncertainty in this rate is partly due to the limited number of data points, but is also a reflection of the crude approximation to model the triplet decay with an extra exponential for the underlying, second order radical anion decay.

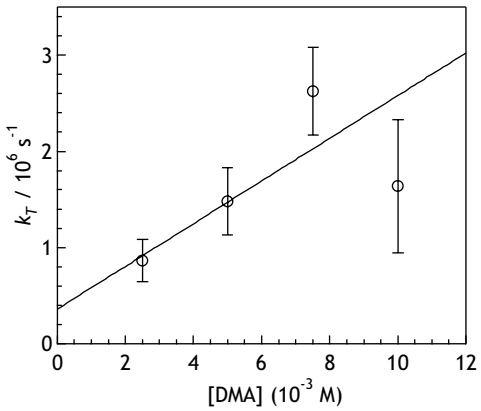

Figure 6-8. $^3ni^*$ decay rates of **1** in the presence of DMA, with a weighted linear fit. Error bars indicate a 95% confidence interval, based on the standard deviations of the triplet decay fits.

In the presence of 1-10 mM donor, $ni^{\cdot-}$ with characteristic absorptions at 416, 490, 730, and 820 nm rises at the same rate as the decay of $^3ni^*$, which proves that indeed the radical anion is formed *via* the triplet state. If TMPD is employed as electron donor, also the donor radical cation is clearly observed (λ_{max} = 388, 600 nm), confirming that $^3ni^*$ indeed is quenched by an electron transfer mechanism.

The decay kinetics of $ni^{\bullet-}$ were measured with single wavelength transient absorption at 416 nm. As can be seen in Figure 6-9, both **1** and **2** show a decay that can be fitted by a second order rate law.

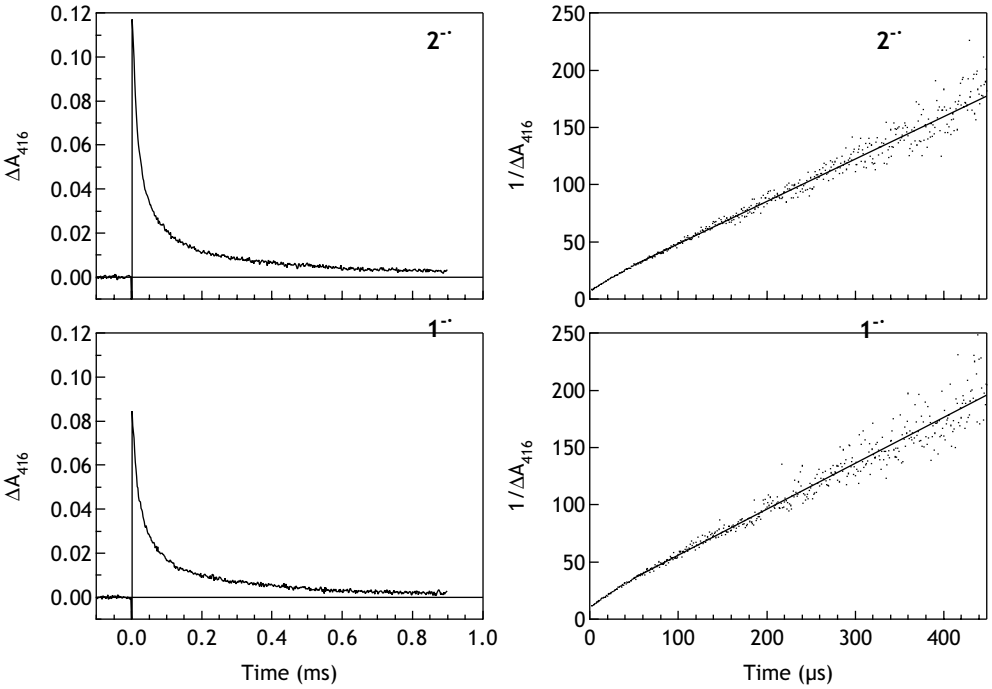

Figure 6-9. (left) Decay of the naphthalimide radical anion of **1** and **2**, generated by photoreduction with 10 mM DABCO in MeCN, recorded at 416 nm. (right) Plots of $1/\Delta A_{416}$ *vs.* time with a weighted linear fit between 50 and 500 μs.

Most probably, $ni^{\bullet-}$ is converted back to *ni* upon bimolecular charge recombination with a donor radical cation. Using the molar extinction coefficient of $ni^{\bullet-}$ (23550 $M^{-1}cm^{-1}$)[23], the recombination rate can be obtained from the slope of $1/[ni^{\bullet-}]$ *vs.* time: $k_{bet} = 9 \pm 2 \times 10^9$ $M^{-1}s^{-1}$ for both **1** and **2**. After charge recombination (*circa* 100 μs) the system returns to the ground state and can be pulsed again, giving the same result.

The quantum yield of radical ion formation (Φ_{ri}) was determined by measuring the absorption of the naphthalimide radical (A_{ri}) directly after the laser pulse and comparing this to the absorption maximum of triplet benzophenone in benzene (A_{BP}), generated by excitation with an equally intense laser pulse. Since both the molar absorption coefficient of $ni^{\bullet-}$(ε_{ri} = 23550 $M^{-1}cm^{-1}$)[23] and $^3BP^*$ (ε_{BP} = 7220 $M^{-1}cm^{-1}$)[35] at their maximum are known, Φ_{ri} can be calculated using,

$$\Phi_{ri} = \frac{1 - T^{x}_{BP}}{1 - T^{x}_{ri}} \frac{A_{ri}/\varepsilon_{ri}}{A_{BP}/\varepsilon_{BP}} \qquad \text{(Eq. 6-2)}$$

Where T^{x}_{BP} and T^{x}_{ri} are the ground state transmittances of BP and *ni* at the excitation wavelength (355 nm). For a 5×10^{-5} M solution of **1** in MeCN in the presence of 10 mM DABCO, this yielded a quantum yield of formation of radical anions of 0.20. This value of Φ_{ri} can be used to estimate the efficiency of the switching process (see Section 6.3.8).

6.3.6 Transient Absorption Shift

When the 1,8-naphthalimide stopper in **1** was reduced *electrochemically*, the absorption maxima of its radical anion were found to be blue shifted with respect to those of the thread **2** (Section 6.3.2). This effect must arise from the presence of the macrocycle, using its 4 N-H groups to bind to the two carbonyls of $ni^{\cdot-}$.

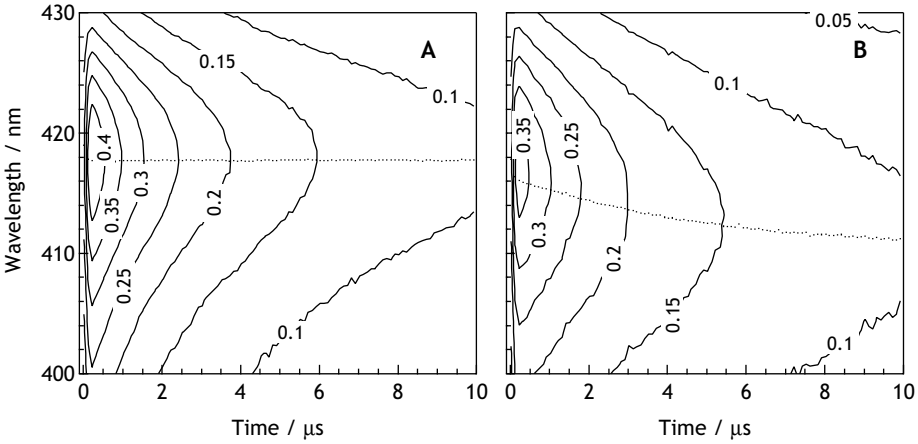

Figure 6-10. Contour plots of 100 transient absorption spectra of (A) thread **2** and (B) rotaxane **1** in PrCN with 10 mM DABCO, taken with 100 ns increments after the laser pulse. Numbers indicate the optical densities. The absorption maximum of $ni^{\cdot-}$ is indicated by the dots.

If we now *photoreduce* the 1,8-naphthalimide stopper in MeCN by selective excitation (355 nm, fwhm = 2 ns) in the presence of an electron donor, we observe that during the lifetime of the radical anion the position of its absorption maximum located around 416 nm stays constant for the thread **2**. In the corresponding rotaxane **1**, however, *a blue shift of several nanometers occurs on a microsecond timescale* (Figure 6-10). This phenomenon is independent of which electron donor is used, and the shift rate is furthermore constant over a range of donor concentrations (Figure 6-11).

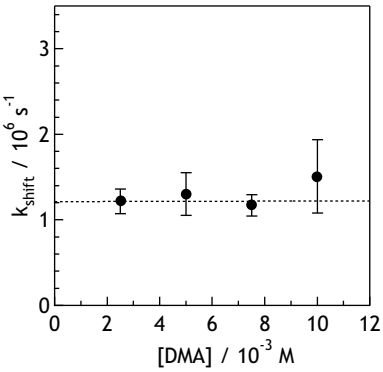

Figure 6-11. The shift rate of the absorption maximum of *ni*$^{\cdot-}$ as a function of donor (DMA) concentration. Error bars indicate a 95% confidence interval, based on the standard deviations of fitting the absorption maximum shift.

Since this spectral shift occurs only in the rotaxane, it must be caused by the macrocycle. The magnitude of the photoinduced spectral shift (~ 5 nm) furthermore corresponds well with the difference in absorption maximum of **1**$^{\cdot-}$ and **2**$^{\cdot-}$ measured spectroelectrochemically. The same binding motifs and multiple hydrogen-bonds are thus present in both experiments and therefore the photoinduced shift must also result from the macrocycle binding to the *ni*$^{\cdot-}$ station. In general a blue shift of the *ni*$^{\cdot-}$ absorption appears to be associated with an increased polarity of its environment as evidenced by the solvent behaviour of the thread (see Section 6.3.7).

The transient nature of the blue shift of the radical anion absorption maximum in the rotaxane is apparently caused by the translation of the macrocycle along the thread to its new equilibrium position, characterized by K_{red}. If so, then the rate at which the new equilibrium is established (*i.e.* the rate of shuttling) should be related to the rate at which the absorption maximum shifts.

Let us define the separation between the absorption maxima of free and complexed naphthalimide radical anion as $\Delta\lambda$. Since $\Delta\lambda$ is approximately 5 nm and the absorptions have a fwhm > 25 nm, a coalesced band is observed characterized by its maximum λ_{max}. As the relative intensities of the underlying bands change in time, λ_{max} will also change. It can be shown (see Appendix, Section 6.5) that λ_{max} is linearly correlated to the intensity changes of the separate bands when $\Delta\lambda$ is small compared to the width of the separate bands. Since that is the case here, the measured shift rate of the radical anion absorption maximum (k_{shift}) equals the rate at which the equilibrium for the reduced state is established. Because this lies almost completely towards *ni*-**1**$^{\cdot-}$, the rate observed is the macroscopic rate for the translation of the macrocycle along the thread. Indeed, plots of λ_{max} *versus* time for **1**$^{\cdot-}$ show perfect monoexponential behaviour (Figure 6-12).

6.3.7 Solvent and Temperature Effects

If, as expected, the rate determining step in the translational process involves the breaking of the hydrogen-bonds between the macrocycle and the *succ* station, then, since hydrogen-bonding is stronger in less polar solvents, the macrocycle should shuttle more slowly in solvents with a lower dielectric constant (ε). When **1** was photoreduced in the presence of DABCO in alkylnitriles of different polarities, the shift rate indeed followed the predicted trend (Figure 6-12), *i.e.* $k_{shift} = 1.35 \times 10^6$ s^{-1} in MeCN ($\varepsilon = 37.5$), 0.45×10^6 s^{-1} in EtCN

($\varepsilon = 27.2$), and 0.21×10^6 s^{-1} in PrCN ($\varepsilon = 23.3$). Note further that in a mechanism in which hydrogen-bond *formation* would be rate limiting, such as *e.g.* a folding mechanism, the trend would be exactly opposite.

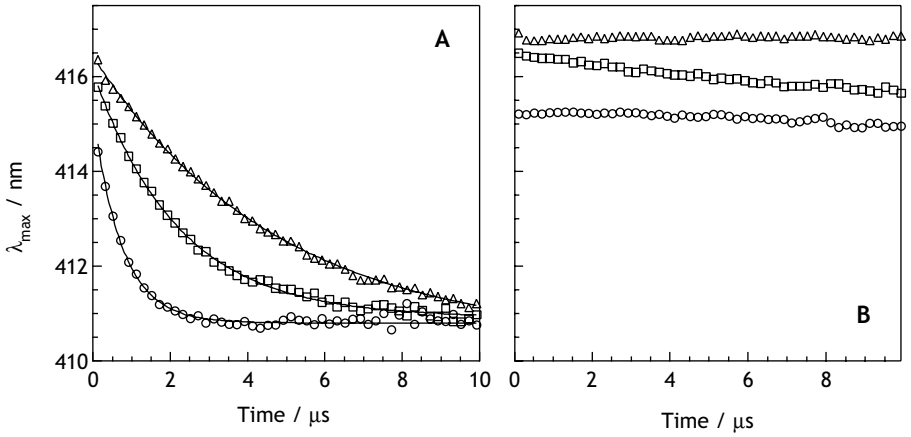

Figure 6-12. Changes in the absorption maximum (λ_{max}) of $ni^{\bullet-}$, formed after photoexcitation of **1** (A) or **2** (B) in the presence of 10 mM DABCO measured in three different solvents: triangles are for butyronitrile (PrCN), squares for propionitrile (EtCN) and circles for acetonitrile (MeCN). For clarity half of the data points are omitted. The data for **1** were fitted to a weighted mono-exponential function in order to obtain the shift rate k_{shift}.

Similarly, a co-solvent can be used to specifically weaken the hydrogen-bond interaction between the macrocycle and the *succ* station. Using up to 2% water in MeCN the rate increases by a factor of 1.5 compared to superdry MeCN (Figure 6-13a).

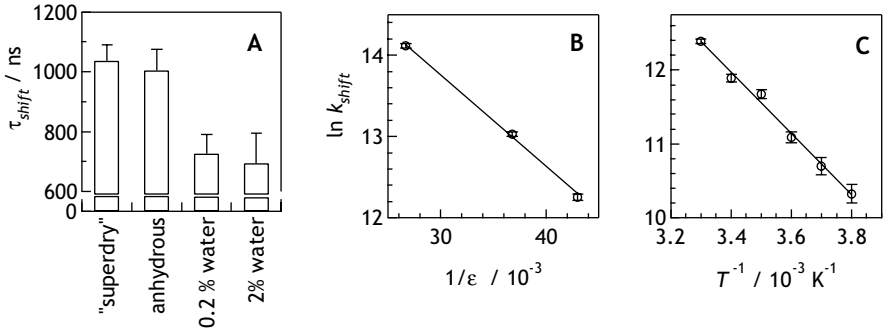

Figure 6-13. The shift rate of the $ni^{\bullet-}$ absorption maximum in rotaxane **1** depends (A) on the water content in acetonitrile (see Experimental section for the definition of "superdry" and "anhydrous"), (B) on the relative dielectric constant, ε, of the surrounding medium, and (C) on the temperature (in butyronitrile). Error bars indicate a 95% confidence interval. The straight lines are weighted fits.

Hydrogen-bonds are largely electrostatic in nature and the free energy of binding of the macrocycle to a station should be inversely proportional to the dielectric constant of the surrounding medium. Therefore, a plot of $\ln(k_{shift})$ versus $1/\varepsilon$ might yield a linear relationship. As demonstrated in Figure 6-13b, this is indeed the case.

By measuring k_{shift} at different temperatures in PrCN and applying Eyring's transition state theory (Equation 6-3), the barrier $\Delta G^{\ddagger}$ for the photoinduced translational process in **1** could be determined.

$$k = \kappa \frac{k_B T}{h} \exp(-\Delta G^{\ddagger}/RT) \qquad \text{(Eq. 6-3)}$$

$$\Delta G^{\ddagger} = \Delta H^{\ddagger} - T\Delta S^{\ddagger} \qquad \text{(Eq. 6-4)}$$

In Equation 6-3, κ is the transmission coefficient, k_B is Boltzmann's constant, h Planck's constant, R the gas constant, and T the temperature. A straight line fit of $\ln(k_{shift})$ *vs.* T^{-1} (Figure 6-13c) yielded $\Delta H^{\ddagger}$ = 7.6 ± 0.5 kcal mol^{-1}, and $\Delta S^{\ddagger}$ = -8.8 ± 1.6 cal mol^{-1} for activation enthalpy and activation entropy respectively (assuming κ = 1). According to Equation 6-4, the Gibbs free energy barrier then is: $\Delta G^{\ddagger}$ = 10.2 ± 0.7 kcal/mol at 298 K. Similar barriers have been determined by NMR measurements ($\Delta G^{\ddagger}_{298K}$ = 12.4 ± 0.3 kcal/mol) for a rotaxane with two glycylglycine hydrogen-bond accepting stations (which has a similar binding motif to succinamide) separated by a fourteen atom spacer.[36] The similarity in temperature dependence of shuttling in **1** and previously studied molecular shuttles, thus strongly suggest a similar motion on a molecular level, *i.e.* a translation of the macrocycle along the thread.

The negative entropy of activation is somewhat puzzling, since the transition state is thought to involve a weakening of the macrocycle-succinamide interactions, and hence an increased number of low energy vibrational modes, which would suggest an increase of entropy. The observed negative apparent $\Delta S^{\ddagger}$ may be explained by considering the shuttling as a two-stage process: initial breaking of the H-bonds between macrocycle and *succ* station, followed by a diffusive migration towards the *ni*$^{\cdot-}$ stopper. In some attempts the macrocycle might overcome the energetic barrier to arrive at the alkyl chain, but *not* diffuse toward the naphthalimide stopper. In other words the transmission coefficient κ, that was assumed to be unity, might be less, giving rise to an apparent negative activation entropy.

6.3.8 Mechanism

Having measured the rate of photoinduced shuttling in **1** by direct observation, the remainder of the photoreduction cycle (Figure 6-5) can be inferred by Occam's Razor. The radical anion absorption lasts for ~100 μs following which the sample can be reproducibly pulsed again with the laser to regenerate the original transient absorption spectrum. Clearly, the strong intercomponent binding will hold the macrocycle on the *ni*$^{\cdot-}$ station until it is reox-

idised. In the neutral state, however, a strong driving force exists for the macrocycle to shuttle back to the succinamide site, *vide supra,* and the system is reset.

Thusfar we have focused on the (transient) changes of the *ni* station, for these unequivocally prove that reduction to $ni^{\cdot-}$ leads to complexation with the macrocycle. How this complexation comes about on a molecular level cannot be inferred as directly, because the flexible alkyl chain in principle allows for other mechanisms: the macrocycle could *e.g.* remain bound to the *succ* station and the alkyl chain could fold so as to allow the macrocycle to form a complex with $ni^{\cdot-}$.

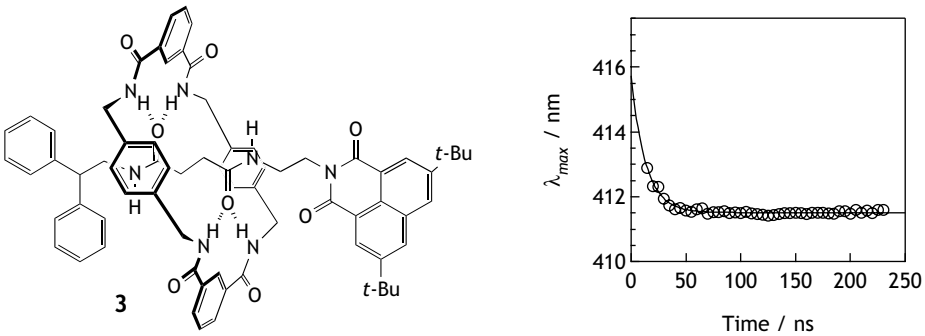

Figure 6-14. Changes in the absorption maximum (λ_{max}) of $ni^{\cdot-}$ with time, formed after photoexcitation of **3**, a C_2 chain analogue of **1** in MeCN in the presence of 10 mM

Although such motions can certainly occur during the lifetime of the naphthalimide radical anion, it is very unlikely that they are *responsible* for the changes observed in the electronic absorption spectrum of $ni^{\cdot-}$, because: (i) a similar process could also take place in the thread, and it evidently does not (See Figure 6-10), (ii) the observed solvent effect (See Figure 6-13) indicates that breaking of hydrogen-bonds is rate-limiting, not formation of hydrogen-bonds, again not consistent with any kind of folding mechanism, (iii) rotaxane **3**, a shorter (C_2 instead of C_{12} spacer) version of **1** which is much too rigid to fold and form multiple H-bonds to the *ni* station also shows the same optical shifts as **1**, but the changes take place on the same timescale as the electron transfer step (< 20 ns), reflecting the shorter shuttling distance required for the macrocycle (Figure 6-14), (iv) alkyl chains fold some two orders of magnitude faster than the dynamics observed here,[37] (v) folding a long alkyl chain is entropically very unfavourable, whereas shuttling does not freeze out low-energy motions of the chain (See *e.g.* Gellman amides).[38] It is thus justified to ascribe our observations to a gliding motion of the macrocycle over the thread.

Having established the mechanism, the question that remains to be answered is: how efficient is this shuttling process? In Section 6.3.5, the quantum yield of radical anion formation was determined to be 0.20. This value is dependent of donor concentration, but can serve as a typical value for the experiments conducted in this Chapter. Knowing the yield of radical

anions, the fraction of **1**$^{\bullet-}$ that shuttles needs to be determined in order to obtain an estimate of the efficiency of the complete switching process.

The naphthalimide radical anion in the rotaxane is formed when it resides mainly in the *succ*-**1**$^{\bullet-}$ co-conformation. Shuttling of the macrocycle to form the *ni*-**1**$^{\bullet-}$ co-conformation then competes with back electron transfer to donor radical cations. These processes are a combination of first and second order reactions. To determine the yield of *ni*-**1**$^{\bullet-}$, a numerical solution was sought using Chemical Kinetics Simulator, a computer program that uses a stochastic method, based on reaction probabilities, to calculate the time history of a chemical system using the reaction's mechanism and the initial conditions specified.[39]

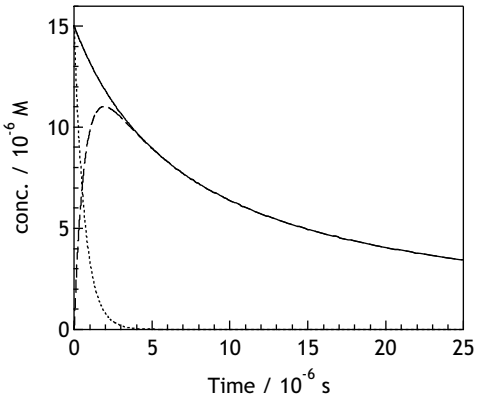

succ-**1**$^{\bullet-}$ $\xrightarrow{k_{shift}}$ *ni*-**1**$^{\bullet-}$

ni-**1**$^{\bullet-}$ + D$^{+\cdot}$ $\xrightarrow{k_{bet}}$ *ni*-**1** + D

succ-**1**$^{\bullet-}$ + D$^{+\cdot}$ $\xrightarrow{k_{bet}}$ *succ*-**1** + D

[*succ*-**1**$^{\bullet-}$] = [D$^{+\cdot}$] = 1.5× 10^{-5} M

k_{shift} = 1.35× 10^{6} s^{-1}

k_{bet} = 9 × 10^{9} M^{-1}s^{-1}

Figure 6-15. Simulation of the shuttling process in reduced **1**, using the kinetic scheme and reaction conditions shown on the right. The calculated radical anion decay (continuous) is the sum of the contributions of *succ*-**1**$^{\bullet-}$ (dotted) and *ni*-**1**$^{\bullet-}$ (dashed) co-conformers.

As shown in Figure 6-15, shuttling is fast compared to recombination of the radical anion. The quantum yield of *shuttling* (Φ_{shift}) is given by the ratio between the area under the *ni*-**1**$^{\bullet-}$ decay curve and the total decay area. Using the experimentally found rates in MeCN, Φ_{shift} = 0.999 is found. Thus the efficiency of the overall switching process is only limited by the yield of radical anions, Φ_{ri} = 0.20.

6.4 Conclusions

The naphthalimide rotaxane **1** is a fast, reversible shuttle, that can be addressed with nanosecond laser pulses. In less than 1 μs the macrocycle moves from its preferential binding site to a second station at a distance of 1.5 nm. Previous light driven shuttles function on the minutes/hours timescale and could only switch once.[7,16] By employing the triplet state of the 1,8-naphthalimide stopper we succeeded in generating long lived radical anions, thus circumventing the need for sacrificial electron donors and creating a system that is cyclable.

The shuttling process could furthermore be measured directly by monitoring the absorption maximum of the photogenerated naphthalimide radical anion ($ni^{\cdot-}$). This allowed us to determine the rates, barriers and solvent dependence of the system. It also permitted an estimate of the quantum yield of the total switching process.These kinetic data support the mechanism as outlined in Figure 6-5 where the macrocycle *glides* between the two binding stations.

Tuning of the binding properties and lifetime of the radical anion (by altering the station, macrocycle or environment) may allow faster switching times and even more efficient analogues to be produced. Since breaking the hydrogen-bonds between macrocycle and preferential binding station is found to be the rate limiting process, weakening these interactions seems to be essential to get faster switching times, without changing the chain length. This, however, also reduces the ground state equilibrium between the two stations and hence a smaller shift of the radical anion absorption maximum will be observed. A careful trade-off between these two effects must be made in order to optimise this shuttle.

Because in the present system shuttling of the macrocycle already is much faster than the reset by bimolecular back electron transfer, the overall quantum yield of switching is limited only by the yield of radical anions. This yield could be improved by using a naphthalimide derivative with a higher triplet yield and an electron donor that would give faster forward electron transfer. Ideally the donor acceptor couple would be part of an intramolecular electron transfer system, for that would cancel out the restriction to operate the shuttle in liquid solution and bring a real-world application one step closer. The necessary long lived charge separated state could be realised using a stepwise electron transfer mechanism. The trichromophores studied by Wasielewski and co-workers in that respect are promising candidates for incorporation in these types of rotaxanes, for they are based on naphthalimide chromophores and reach lifetimes of approximately 300 ns for the charge separated state.[40]

6.5 Appendix: Relation Between Peak Shift and Population Change

Following Figure 6-5, when the rotaxane is reduced a new equilibrium, characterized by the equilibrium constant (K_{red}), has to set in with a typical time constant τ_{shift}. The populations $p(t)$ of free and complexed naphthalimide radical anion (Equation 6-5) are a function of τ_{shift} and the new equilibrium constant K_{red} as long as the radical anions recombine much more slowly than τ_{shift} and the difference for the recombination rate between complexed and free radical anions is negligible.

$$p_{complex}(t) = \frac{K_{red}}{1 + K_{red}}(1 - e^{-t/\tau_{shift}})$$
$$p_{free}(t) = \frac{1}{1 + K_{red}}(1 + K_{red}e^{-t/\tau_{shift}}) \qquad \text{(Eq. 6-5)}$$

If we call the functions describing the two absorption spectra $s_{complex}(\lambda)$ and $s_{free}(\lambda)$, the complete translational process is described as:

$$T(\lambda, t) = s_{free}(\lambda)p_{free}(t) + s_{complex}(\lambda)p_{complex}(t) \qquad \text{(Eq. 6-6)}$$

Unfortunately, the transient absorption spectra are too complicated to obtain the spectra and time profiles directly, using *e.g.* Singular Value Decomposition or global fitting. Instead, we decided too look at one parameter of the absorption spectra, which is easily obtained experimentally: the absorption maximum of the radical anion (λ_{max}).

The task now is to obtain this parameter out of $T(\lambda,t)$ as a function of time. In order to do so we have to simplify the problem. The absorption spectra of complexed and free naphthalimide radical anion can be described by a Gaussian function, called $g(\lambda)$. This is a reasonable approximation as can be seen in Figure 6-16. We furthermore assume that $g_{free}(\lambda)$ and $g_{complex}(\lambda)$ have the same fwhm and molar absorption, so they differ only in the location of their maximum.

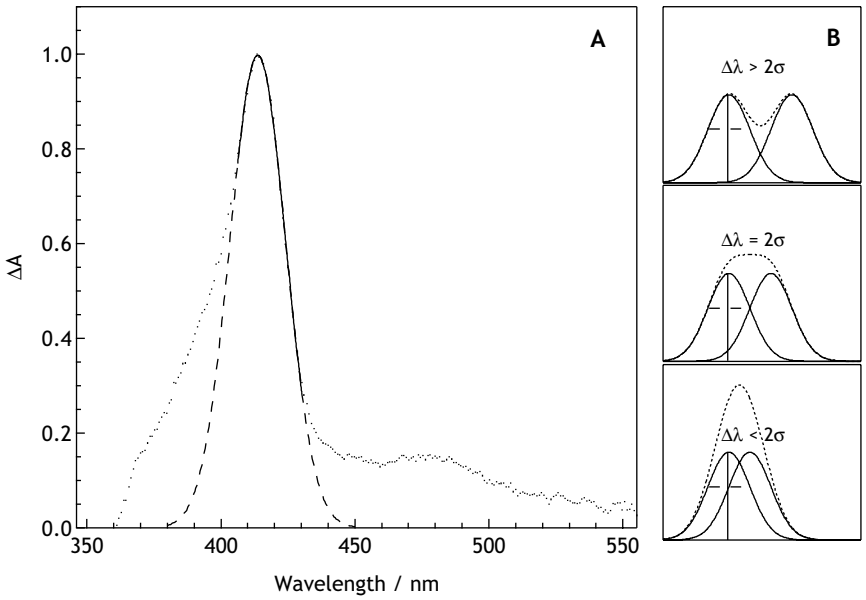

Figure 6-16. (A) A trace from a typical transient absorption spectrum, showing the characteristic naphthalimide radical anion absorption peak of **1** (dots), together with a gaussian fit (continuous inside, dashed outside the fit region). (B) Three examples, showing that two gaussian curves of equal width and height will coalesce when they are displaced by less than 2σ.

To determine the maximum of a linear combination of two displaced gaussians is not trivial, but we need only to consider the situation where the two bands coalesce. Coalescence will

occur when the displacement $|\Delta\lambda|$ is smaller than 2σ, as is shown in Figure 6-16. In our case, the fwhm of the radical anion absorption is approximately 25 nm, which corresponds to $\sigma \approx 11$ nm. A typical shift of the absorption maximum is 5 nm, which is well under 2σ.

We now need to find the maximum of a linear combination Ψ of these two displaced gaussians (Equation 6-7).

$$\Psi(\lambda, t) = c_1(t)g(\lambda) + c_2(t)g(\lambda - \Delta\lambda) \qquad \text{(Eq. 6-7)}$$

The derivative $\partial\Psi/\partial\lambda$, however is a complicated function, which is not easily solved to find the maximum. Therefore, a simulation was done: c_1 and c_2 were varied linearly as:

$$\begin{aligned} c_1 &= t \\ c_2 &= 1 - t \end{aligned} \qquad 0 \le t \le 1 \qquad \text{(Eq. 6-8)}$$

Then, on each t, the peak maximum was determined. This was repeated for several displacements $\Delta\lambda$ (Figure 6-17).

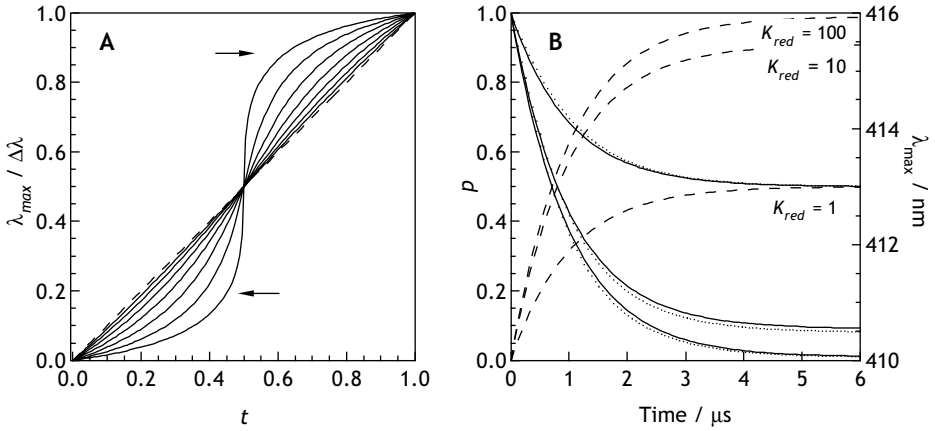

Figure 6-17. (A) The variation of the peak maximum, when t is varied linearly (Equation 6-8), where the ratio $\Delta\lambda$ / σ runs from 2.00 to 0.50 insteps of 0.25. (B) The relative populations p of free (continuous) and complexed (dashed) compound as function of time (Equation 6-5) against the left axis for different values of K_{red}. The corresponding shift of the absorption maximum (dots) is plotted against the right axis. Parameters: fwhm = 25 nm, $\Delta\lambda$ = 6 nm, τ_{shift} = 1 µs.

As is evident from Figure 6-17, the peak maximum does not vary linearly with t. The deviation from linearity however becomes negligible when the ratio $\Delta\lambda$ / σ decreases. In our experiments $\Delta\lambda$ / $\sigma \approx 0.5$, so the approximation that the peak maximum varies linearly with t is justified.

Indeed, if we substitute c_1 and c_2 for the more realistic time profiles from Equation 6-5, and use experimental values for $\Delta\lambda$ and σ, we observe a curve for the change in the peak maximum that is almost indistinguishable from the shift profile $p_{complex}$ (Figure 6-17). So as long as $\Delta\lambda$ / σ is small, the change in the peak maximum represents the change in relative population of free naphthalimide radical anion.

Acknowledgements. The work described in this Chapter is the result of a collaboration with Prof. Dr. D. A. Leigh of the Centre for Supramolecular and Macromolecular Chemistry at the University of Warwick and Dr. F. Paolucci of the Dipartimento di Chimica "G. Ciamician", Università degli Studi di Bologna. F.G. Gatti (Warwick), performed the synthesis, and L. Mottier and S. Roffia (Bologna) carried out the electrochemical experiments. Their valuable contributions are gratefully acknowledged. In our own group we are indebted to Drs. S.A. Zoon, Dr. C. Frochot and to H.J. van Ramesdonk who offered assistance and advice with the photophysical measurements.

6.6 References

1. Anelli, P.L., Ashton, P.R., Ballardini, R., Balzani, V., Delgado, M., Gandolfi, M.T., Goodnow, T.T., Kaifer, A.E., Philp, D., Pietraszkiewicz, M., Prodi, L., Reddington, M.V., Slawin, A.M.Z., Spencer, N., Stoddart, J.F., Vicent, C., and Williams, D.J. Molecular Meccano. 1. [2]Rotaxanes and a [2]catenane made to order. *J. Am. Chem. Soc.* **117**, 193-218 (1992)
2. Anelli, P.L., Spencer, N., and Stoddart, J.F. A molecular shuttle. *J. Am. Chem. Soc.* **113**, 5131-5133 (1991)
3. Balzani, V., Gomez-Lopez, M., and Stoddart, J.F. Molecular machines. *Acc. Chem. Res.* **31**, 405-414 (1998)
4. Sauvage, J.P. Transition metal-containing rotaxanes and catenanes in motion: Toward molecular machines and motors. *Acc. Chem. Res.* **31**, 611-619 (1998)
5. Balzani, V., Credi, A., Raymo, F.M., and Stoddart, J.F. Artificial molecular machines. *Angew. Chem.-Int. Edit.* **39**, 3349-3391 (2000)
6. Shigekawa, H., Miyake, K., Sumaoka, J., Harada, A., and Komiyama, M. The molecular abacus: STM manipulation of cyclodextrin necklace. *J. Am. Chem. Soc.* **122**, 5411-5412 (2000)
7. Armaroli, N., Balzani, V., Collin, J.P., Gavina, P., Sauvage, J.P., and Ventura, B. Rotaxanes incorporating two different coordinating units in their thread: Synthesis and electrochemically and photochemically induced molecular motions. *J. Am. Chem. Soc.* **121**, 4397-4408 (1999)
8. Anelli, P.L., Asakawa, M., Ashton, P.R., Bissell, R.A., Clavier, G., Gorski, R., Kaifer, A.E., Langford, S.J., Mattersteig, G., Menzer, S., Philp, D., Slawin, A.M.Z., Spencer, N., Stoddart, J.F., Tolley, M.S., and Williams, D.J. Toward controllable molecular shuttles. *Chem.-Eur. J.* **3**, 1113-1135 (1997)
9. Asakawa, M., Ashton, P.R., Balzani, V., Credi, A., Mattersteig, G., Matthews, O.A., Montalti, M., Spencer, N., Stoddart, J.F., and Venturi, M. Electrochemically induced molecular motions in pseudorotaxanes: A case of dual-mode (oxidative and reductive) dethreading. *Chem.-Eur. J.* **3**, 1992-1996 (1997)

10. Ballardini, R., Balzani, V., Gandolfi, M.T., Prodi, L., Venturi, M., Philp, D., Ricketts, H.G., and Stoddart, J.F. A Photochemically Driven Molecular Machine. *Angew. Chem.-Int. Edit. Engl.* **32**, 1301-1303 (1993)
11. Bissell, R.A., Cordova, E., Kaifer, A.E., and Stoddart, J.F. A Chemically and Electrochemically Switchable Molecular Shuttle. *Nature* **369**, 133-137 (1994)
12. Ashton, P.R., Ballardini, R., Balzani, V., Credi, A., Dress, K.R., Ishow, E., Kleverlaan, C.J., Kocian, O., Preece, J.A., Spencer, N., Stoddart, J.F., Venturi, M., and Wenger, S. A photochemically driven molecular-level abacus. *Chem.-Eur. J.* **6**, 3558-3574 (2000)
13. Benniston, A.C., Harriman, A., and Lynch, V.M. Photoactive [2]Rotaxanes - Structure and Photophysical Properties of Anthracene-Stoppered and Ferrocene-Stoppered [2]Rotaxanes. *J. Am. Chem. Soc.* **117**, 5275-5291 (1995)
14. Ashton, P.R., Balzani, V., Kocian, O., Prodi, L., Spencer, N., and Stoddart, J.F. A light-fueled "piston cylinder" molecular-level machine. *J. Am. Chem. Soc.* **120**, 11190-11191 (1998)
15. Ashton, P.R., Ballardini, R., Balzani, V., Constable, E.C., Credi, A., Kocian, O., Langford, S.J., Preece, J.A., Prodi, L., Schofield, E.R., and Spencer, N. Ru-II polypyridine complexes covalently linked to electron acceptors as wires for light-driven pseudorotaxane-type molecular machines. *Chem.-Eur. J.* **4**, 2413-2422 (1998)
16. Murakami, H., Kawabuchi, A., Kotoo, K., Kunitake, M., and Nakashima, N. A light-driven molecular shuttle based on a rotaxane. *J. Am. Chem. Soc.* **119**, 7605-7606 (1997)
17. Haselbach, E., Vauthey, E., and Suppan, P. Comparison of Photoinduced Electron-Transfer Reactions of Aromatic Carbonyl Vs Cyano Compounds With Electron-Donors in Condensed Phase - the Importance of the Spin State of the Geminate Ion-Pair For Obtaining High Ion Yields. *Tetrahedron* **44**, 7335-7344 (1988)
18. Wavemetrics, Igor Pro 3.16, Wavemetrics Inc.: Oregon, 1988-2000
19. Williams, D.H., and Fleming, I. In *Spectroscopic methods in organic chemistry* 4th ed.; McGraw-Hill Book Company: London, 1989, p 51.
20. Niemz, A., and Rotello, V.M. From enzyme to molecular device. Exploring the interdependence of redox and molecular recognition. *Acc. Chem. Res.* **32**, 44-52 (1999)
21. Ge, Y., Lilienthal, R.R., and Smith, D.K. Electrochemically-controlled hydrogen bonding. Selective recognition of urea and amide derivatives by simple redox- dependent receptors. *J. Am. Chem. Soc.* **118**, 3976-3977 (1996)
22. Jeffrey, G.A. *An Introduction to Hydrogen Bonding* Oxford University Press: New York, 1997.
23. Van Dijk, S.I., Groen, C.P., Hartl, F., Brouwer, A.M., and Verhoeven, J.W. Long-lived triplet state charge separation in novel piperidine-bridged donor-acceptor systems. *J. Am. Chem. Soc.* **118**, 8425-8432 (1996)
24. Wintgens, V., Valat, P., Kossanyi, J., Biczok, L., Demeter, A., and Berces, T. Spectroscopic Properties of Aromatic Dicarboximides .1. N-H and N-Methyl-Substituted Naphthalimides. *J. Chem. Soc.-Faraday Trans.* **90**, 411-421 (1994)
25. Wintgens, V., Valat, P., Kossanyi, J., Demeter, A., Biczok, L., and Berges, T. Spectroscopic properties of aromatic dicarboximides .4. On the modification of the fluorescence and intersystem crossing processes of molecules by electron-donating methoxy groups at different positions. The case of 1,8-naphthalimides. *New J. Chem.* **20**, 1149-1158 (1996)
26. Korol'kova, N., Val'kova, G., Shigorin, D., Shigalevskii, V., and Vostrova, V. Luminescence-spectroscopic properties of naphtalimide derivatives. *Russ. J. Phys. Chem.* **64**, 206-209 (1990)
27. Lewis, G.N., and Kasha, M. Phosphorescence in fluid media and the reverse process of singlet-triplet absorption. *J. Am. Chem. Soc.* **67**, 994-1003 (1945)

28. Strickler, S.J., and Berg, R.A. Relationship between absorption intensity and fluorescence lifetim of molecules. *J. Chem. Phys.* **37**, 814-822 (1962)
29. Aveline, B.M., Matsugo, S., and Redmond, R.W. Photochemical mechanisms responsible for the versatile application of naphthalimides and naphthaldiimides in biological systems. *J. Am. Chem. Soc.* **119**, 11785-11795 (1997)
30. Szadowski, J., Malinowski, W., and Wojciechowski, K. Influence of intermolecular interactions on the physical properties of phthalimide and naphthalimide and their N-substituted derivatives. *Pol. J. Chem.* **52**, 737-742 (1978)
31. Barros, T.C., Berci, P., Toscano, V.G., and Politi, M.J. Intramolecular Excimer Formation From 1,8-N- Alkyldinaphthalimides. *J. Photochem. Photobiol. A-Chem.* **89**, 141-146 (1995)
32. Murov, S., Carmichael, I., and Hug, G. *Handbook of photochemistry* 2nd ed.; Marcel Dekker: New York, 1993.
33. Lauteslager, X.Y. "Charge transfer fluorescence as a tool to investigate the dynamics of donor-bridge-acceptor compounds," Ph.D. Thesis, Universiteit van Amsterdam, 1998.
34. Nelsen, S.F., and Hintz, P.J. Electrochemical oxidation of tertiary amines. The effect of structure upon reversibility. *J. Am. Chem. Soc.* **94**, 7114-7117 (1972)
35. Carmichael, I., and Hug, G. Triplet-triplet absorption spectra of organic molecules in condensed phases. *J. Phys. Chem. Ref. Data* **15**, 1-250 (1986)
36. Lane, A.S., Leigh, D.A., and Murphy, A. Peptide-based molecular shuttles. *J. Am. Chem. Soc.* **119**, 11092-11093 (1997)
37. Zachariasse, K.A., Macanita, A.L., and Kuhnle, W. Chain length dependence of intramolecular excimer formation with 1,n-bis(1-pyrenylcarboxy)alkanes for n=1-16, 22, and 32. *J. Phys. Chem. B* **103**, 9356-9365 (1999)
38. Gellman, S.H., Dado, G.P., Liang, G.-B., and Adams, B.R. Conformation-directing effects of a single intramolecular amide-amide hydrogen bond: variable-temperature NMR and IR studies on a homologous diamide series. *J. Am. Chem. Soc.* **113**, 1164-1173 (1991)
39. Hinsberg, W., Houle, F., Allen, F., and Yoon, E., Chemical Kinetics Simulator™ 1.01, IBM: Almaden Research Center, 1996
40. Greenfield, S.R., Svec, W.A., Gosztola, D., and Wasielewski, M.R. Multistep photochemical charge separation in rod-like molecules based on aromatic imides and diimides. *J. Am. Chem. Soc.* **118**, 6767-6777 (1996)

Summary

Rotaxanes consist of at least two molecular units –a macrocycle and a thread– that are mechanically bonded. The macrocycle is locked onto the thread, and prevented from slipping off by bulky stopper groups at the ends of the thread. Such a special molecular assembly might be used to construct nanoscale analogues of components of machinery from the macroscopic world: so-called molecular machines. This explains the strong increase of scientific interest for this class of supramolecular structures.

An obvious function for rotaxane based molecular machines is found in the translation of the macrocycle along the thread. Thermal energy can cause this shuttling to occur spontaneously, but it would be more interesting to induce this macrocyclic motion by an external stimulus. In this Thesis we have shown that photons can form an excellent "fuel" for such a process. In hydrogen-bonded rotaxanes in which the thread contains two different binding stations we have succeeded in translating the tetraamide macrocycle from one station to the other under the influence of light. Subsequently the macrocycle returns to its original equilibrium position. The scope of this Thesis, however, is broader: in a general sense we studied how rotaxanation leads to changes in the photophysical behaviour of incorporated chromophores.

In Chapter 2, for instance, a rotaxane is described in which the thread contains a natural polyene, bixin. The electronic absorption of this chromophore, responsible for its deep orange red colour, was found to be sensitive towards the presence of the macrocycle: in the rotaxane the absorption was red shifted compared to that of the thread. Its solvatochromism was also altered: the absorption maximum of bixin shifts to the red with increasing polarisability of the solvent, as is expected for polyenes. The sensitivity towards this solvent effect, however, was smaller in rotaxanes than in the thread. Thus, in a way, the macrocycle can "protect" the thread against the solvent.

Electron transfer is another photophysical phenomenon that was studied in rotaxanes. In Chapter 3 two rotaxanes are discussed in which the macrocycle contains electron accepting units. One of the stoppers is an anthracene fluorophore that after photoexcitation can donate an electron to the macrocycle. This causes quenching of the anthracene fluorescence. Electron transfer rates normally depend exponentially on the distance between electron donor and acceptor. They should therefore be related to the average distance between stopper and macrocycle. This average distance is determined by the properties of the surrounding sol-

vent, since these determine the preferential position of the tetraamide macrocycle: on the peptide station, close to the fluorescent stopper where the macrocycle can form hydrogen bonds to the thread, or on the hydrophobic part of the thread which is further away from the stopper.

We found that in polar, hydrogen-bond disrupting solvents the macrocycle is located at the hydrophobic part, at larger distance from the stopper. In nonpolar solvents, formation of hydrogen-bonds between the tetraamide macrocycle and the peptide station is energetically more favourable and thus the macrocycle resides more closely to the stopper. In the latter case the anthracene fluorescence is almost completely quenched. However, even in the most polar, hydrogen-bond disrupting solvents the fluorescence is not completely restored, which indicates that in those solvents the average distance between stopper and macrocycle increases less than expected. Time resolved fluorescence measurements showed that the rotaxane in solution can adopt at least three different groups of conformations which have different distances between stopper and macrocycle. This could provide an explanation for the observed fluorescence behaviour.

The principle of fluorescence quenching by electron transfer between stopper and macrocycle was furthermore employed in a photocleavable rotaxane. Because the thread is short, the macrocycle is always located close to the anthracene stopper and thus its fluorescence is permanently quenched. In this rotaxane, however, photocleavage of the second stopper causes dethreading thereby restoring the anthracene fluorescence. It was shown that this principle works in solution, but also on a solid support, provided that some solvent is present. This allowed us to make a fluorescent imprint.

The first photoinduced movement of a macrocycle along a thread is described in Chapter 4. The rotaxane which displays this phenomenon was originally intended as a reference system for the compounds of Chapter 3: it contains the same thread, but the macrocycle is unable to quench the fluorescence of the anthracene stopper. The fluorescence of this rotaxane was expected to be identical to that of the corresponding thread. Emission spectra in nonpolar solvents, however, showed an extra broad, long wavelength band that was absent in the thread. Fluorescence measurements indicated that in the anthracene excited state a dynamical change in hydrogen-bond pattern between macrocycle and station occurs which is held responsible for the anomalous fluorescence.

We hypothesised that in the ground state the macrocycle does not form the usual hydrogen-bond pattern with the peptide station due to steric hindrance of the anthracene stopper. The carbonyl group directly bound to the anthracene group therefore is hardly involved in the hydrogen-bonding network. In the excited state this carbonyl group becomes a stronger hydrogen-bond acceptor. Furthermore, because the anthracene-carbonyl dihedral angle becomes smaller, the steric demand decreases. This makes hydrogen bonding of the macrocycle to the carbonyl next to anthracene more favourable in the excited state, causing an effective translation of the macrocycle along the thread of *circa* 3 Å.

To obtain a more detailed view of the pattern of hydrogen bonds between macrocycle and peptide station, molecular mechanics simulations were performed (Chapter 5). Using different force fields conformational analyses and stochastic dynamics simulations were carried out. These showed that the macrocycle scarcely forms hydrogen bonds to the carbonyl group directly attached to anthracene, in accordance with the hypothesis of Chapter 4.

By constraining the anthracene-carbonyl dihedral angle to 0° during the simulations an excited state model was formed. In these simulations the number of hydrogen-bonds between the macrocycle and this carbonyl dramatically increased and the average position of the macrocycle was closer to the anthracene stopper. This oversimplified model of the excited state again supports the experimental findings and shows the importance of steric interactions for hydrogen-bond patterns in rotaxanes.

Within the limited excited state lifetime of the anthracene fluorophore (nanoseconds) the macrocycle cannot translate over large distances. For this, the binding strength of a station needs to be altered for a longer period of time. In Chapter 6 we discuss a system in which long lived, photoinduced changes in binding strength leads to reversible shuttling over *circa* 15 Å. This is realised by reduction of one of the binding stations in its triplet excited state with an external electron donor that is present in solution. Thus, upon photoexcitation, a long lived radical anion (~ 100 μs) is formed that has a much larger affinity for the macrocycle than the neutral form has, causing the macrocycle to shuttle from its original station towards the radical anion. When the extra electron present in the radical anion is returned to the donor radical cation, the station returns to its neutral form. Thereupon the ring shuttles back and the cycle can start all over again.

The shuttling kinetics could be studied in detail by following the changes of the radical anion absorption in time, since complexation of the macrocycle to the radical anion using hydrogen bonds leads to a blue shift of the absorption maximum. The rate of this absorption shift is directly related to the shuttling rate of the macrocycle along the thread. Depending on temperature and solvent this translation occurs on a timescale of 1 microsecond.

Until recently, the focus in rotaxane research was mainly synthetic, and the stimuli for dynamical processes were mainly chemical or electrochemical in nature. This Thesis shows that the same effects can be accomplished using light which has the advantage that faster spectroscopic techniques can be employed. By using those, a detailed picture of the structure and dynamics of hydrogen-bonded rotaxanes in solution has emerged.

Samenvatting

Een rotaxaan bestaat uit tenminste twee moleculaire eenheden –een ring en een draad– die mechanisch met elkaar verbonden zijn. De draad steekt door de ring en kan daar niet af glijden door de aanwezigheid van grote stoppergroepen aan de uiteinden van de draad. Zo'n bijzondere moleculaire samenstelling kan mogelijk gebruikt worden voor de constructie van machine-onderdelen op nanoschaal: zogenaamde moleculaire machines. Dit verklaart de sterk toegenomen wetenschappelijke aandacht voor deze klasse van supramoleculaire verbindingen.

Een voor de hand liggende functie voor moleculaire machines die op rotaxanen gebaseerd zijn, is de translatie van de ring over de draad. Dit pendelen (*shuttling*) van de ring kan door thermische energie spontaan plaatsvinden, maar interessanter is het om de beweging van de ring door middel van een externe impuls te sturen. In dit Proefschrift hebben we laten zien dat fotonen hiervoor een uitstekende "brandstof" kunnen vormen. We zijn erin geslaagd om met behulp van licht in rotaxanen waar de draad twee verschillende bindingsstations bevat, de ring van het ene station naar het andere station te schuiven waarna de ring terugkeert naar de uitgangspositie. De interacties tussen de stations en de tetra-amide ring zijn daarbij gebaseerd op waterstofbruggen. Het onderzoek dat beschreven wordt in dit Proefschrift bestrijkt echter een breder gebied. In algemene zin is bekeken hoe rotaxanering leidt tot veranderingen in fotofysisch gedrag van de in het systeem opgenomen chromoforen.

In Hoofdstuk 2 bijvoorbeeld, wordt een rotaxaan beschreven waarin de draad wordt gevormd door een natuurlijk polyeen, bixine. De elektronische absorptie van deze chromofoor die verantwoordelijk is voor een sterke rood-oranje kleur bleek beïnvloedbaar door de ring: vergeleken met de losse draad was de absorptie van het rotaxaan naar het rood verschoven. Verder bleek ook de solvatochromie veranderd te zijn: zoals gebruikelijk voor polyenen, schuift het absorptiemaximum van bixine naar het rood onder invloed van een toenemende polariseerbaarheid van het oplosmiddel. Dit oplosmiddeleffect bleek echter kleiner te zijn in de rotaxanen dan in de draad. In zekere zin kan de ring de draad dus "beschermen" tegen de invloed van het oplosmiddel.

Elektronenoverdracht is een ander fotofysisch verschijnsel dat bestudeerd is in rotaxanen. In Hoofdstuk 3 worden twee rotaxanen besproken waarbij de ring elektronaccepterende groepen bevat. De stopper bevat een antraceen fluorofoor die na foto-excitatie een elektron kan overdragen aan de ring waardoor zijn fluorescentie wordt gedoofd. De elektronenover-

drachtssnelheid neemt in het algemeen exponentieel af met toenemende afstand tussen elektron donor en acceptor zodat dit proces in principe gebruikt kan worden om de gemiddelde afstand tussen de ring en de stopper af te schatten. Deze gemiddelde afstand wordt bepaald door de eigenschappen van het omringende oplosmiddel, aangezien deze bepalen waar de tetra-amide ring zich bij voorkeur bevindt: op het peptide station naast de fluorescerende stopper waar de ring waterstofbruggen kan vormen met de draad, of op het verder gelegen hydrofobe deel van de draad.

We vonden dat in polaire, waterstofbrug vormende oplosmiddelen de ring zich op het hydrofobe deel bevindt, ver van de antraceen stopper. In apolaire oplosmiddelen is het vormen van waterstofbruggen tussen tetra-amide ring en peptidestation energetisch gunstiger en bevindt de ring zich dus dichter bij de stopper. Dit laatste resulteert in een nagenoeg volledige doving van de antraceenfluorescentie. De fluorescentie blijft echter voor een aanzienlijk deel gedoofd in de polairste, sterkst waterstofbrug vormende oplosmiddelen, wat erop duidt dat de gemiddelde afstand tussen stopper en ring in dergelijke oplosmiddelen minder toeneemt dan verwacht. Tijdopgeloste fluorescentiemetingen toonden aan dat de rotaxanen in oplossing ten minste drie groepen van conformaties kunnen aannemen met verschillende afstanden tussen stopper en ring, hetgeen een verklaring vormt voor het waargenomen fluorescentiegedrag.

Het principe van fluorescentiedoving door elektronenoverdracht tussen stopper en ring werd verder toegepast in een fotolabiel rotaxaan. Doordat de draad kort is, is de ring altijd dicht bij de antraceen stopper en is de fluorescentie dus permanent gedoofd. In dit rotaxaan kan echter de tweede stopper met behulp van licht afgesplitst worden waarna de ring van de draad kan glijden en de antraceen fluorescentie wordt hersteld. Er werd getoond dat dit principe werkt in oplossing, maar ook op een vaste drager mits er nog enig oplosmiddel aanwezig is. Het laatste stelde ons in staat een fluorescerende afbeelding te maken.

De eerste fotogeïnduceerde beweging van een ring over een draad staat beschreven in Hoofdstuk 4. De rotaxaan waar dit in optreedt was oorspronkelijk bedoeld als referentiesysteem voor de verbindingen uit Hoofdstuk 3: hij bevat dezelfde draad, maar de ring is niet in staat de fluorescentie van de antraceen stopper te doven. De verwachting was dat de fluorescentie van deze rotaxaan overeen zou komen met die van de corresponderende draad. In apolair oplosmiddel werd echter een extra langgolvige, brede band in het emissiespectrum waargenomen die afwezig was in de draad. Verschillende fluorescentiemetingen gaven aan dat in de aangeslagen toestand van de antraceenchromofoor een dynamische verandering in het patroon van waterstofbruggen tussen ring en draad optreedt die verantwoordelijk is voor deze bijzondere fluorescentie.

De hypothese werd geformuleerd dat in de grondtoestand de ring een ongebruikelijk patroon van waterstofbruggen met het peptidestation vormt door sterische hindering van de antraceen stopper. De carbonylgroep die direct verbonden is met de antraceengroep is daardoor nauwelijks betrokken in het netwerk van waterstofbruggen. In de aangeslagen toestand

wordt deze carbonylgroep een sterkere acceptor voor waterstofbruggen. Verder wordt de antraceen-carbonyl tweevlakshoek kleiner waardoor de sterische hindering afneemt. Hierdoor kan in de aangeslagen toestand van de rotaxaan, de ring beter waterstofbruggen vormen met de carbonyl die direct gekoppeld is aan de antraceen stopper. Effectief levert dit een translatie van de ring over de draad van *circa* 3 Å op.

Om een gedetailleerder inzicht te krijgen in de waterstofbrugpatronen tussen ring en peptide station in deze rotaxaan werden moleculaire mechanica berekeningen uitgevoerd (Hoofdstuk 5). Met behulp van verschillende parametersets voor atomaire interacties (force fields) werden zowel conformatieanalyses als stochastische dynamica simulaties uitgevoerd. Hieruit bleek dat de ring nauwelijks waterstofbruggen vormt met de carbonylgroep die direct is verbonden met antraceen, in overeenstemming met de in Hoofdstuk 4 gevormde hypothese.

Door gedurende de simulaties de antraceen-carbonyl tweevlakshoek tot 0° te beperken, werd een model voor de aangeslagen toestand gemaakt. In deze simulaties nam het aantal waterstofbindingen van de ring met deze carbonyl sterk toe en lag de gemiddelde positie van de ring dichter bij de antraceen stopper. Dit sterk versimpelde model voor de aangeslagen toestand ondersteunt opnieuw de experimentele waarnemingen en toont het belang van sterische interacties op waterstofbrug patronen in rotaxanen.

De beperkte levensduur (nanoseconden) van antraceen's aangeslagen toestand staat niet toe dat de ring zich over grotere afstanden verplaatst. Hiertoe dient de bindingssterkte van een station voor langere tijd te worden veranderd. In Hoofdstuk 6 bespreken we een systeem waar langduriger fotogeïnduceerde verandering in bindingsterkte leidt tot reversibel pendelen van de ring over ongeveer 15 Å. Dit wordt gerealiseerd door één van de bindingsstations vanuit de triplettoestand te reduceren met een in oplossing aanwezige, externe elektrondonor. Door fotoexcitatie ontstaat zodoende een langlevend radicaal anion (~ 100 μs) dat de ring vele malen sterker bindt dan aanvankelijk waardoor de ring van zijn oorspronkelijke station naar het radicaal anion schuift. Wanneer het radicaal anion station recombineert tot het neutrale station, schuift de ring terug en kan de cyclus opnieuw beginnen.

Door de verandering in de absorptie van het radicaal anion in de tijd te volgen kan een gedetailleerd kinetisch beeld gevormd worden van de dynamica van het pendelen. Complexatie van de ring aan het radicaal anion door middel van waterstofbruggen leidt namelijk tot een blauwverschuiving van het absorptiemaximum. De snelheid van deze absorptieverschuiving is direct gerelateerd aan de pendelsnelheid van de ring over de draad. Afhankelijk van de temperatuur en het oplosmiddel vindt deze translatie plaats op een tijdschaal van 1 microseconde.

Tot voor kort had onderzoek aan rotaxanen een sterk synthetische invalshoek, waarbij dynamische processen vooral werden bewerkstelligd door chemische en elektrochemische impulsen. Dit Proefschrift laat zien dat hetzelfde bereikt kan worden met licht, wat als voordeel heeft dat daarmee snellere spectroscopische technieken gebruikt kunnen worden. Hier-

door is een gedetailleerd beeld ontstaan van de structuur en dynamica van waterstofgebrugde rotaxanen in oplossing.

Dankwoord

In de ruim vier jaar dat ik promotie-onderzoek heb mogen verrichten als lid van de Organic Photonic Materials werkgroep (OPM), is er geen dag geweest dat ik met tegenzin naar het lab ging. Het onderzoek ging –zoals dat hoort– met ups en downs, maar er was nooit een reden om níet te zingen of te fluiten. Ik heb dan ook altijd enige moeite gehad om wat ik deed "werk" te noemen, daarvoor had ik veel te veel schik in wat ik deed. Dankzij, of misschien wel ondanks, de gezellige werksfeer is dit proefschrift uiteindelijk gereed gekomen. Daar zijn een heleboel mensen bij betrokken geweest en tegen al diegenen wil ik op deze plaats zeggen: bedankt lieve mensen, zonder jullie was het nooit gelukt.

Allereerst wil ik Fred Brouwer bedanken, mijn dagelijkse begeleider en co-promotor. Beste Fred, toen jij me in oktober 1996 een promotieplaats aanbood konden we geen van beiden vermoeden dat het met een rotaxanenproefschrift en een artikel in Science zou eindigen; twee-laser experimenten, weet je nog? In die moeizame beginperiode vol falende lasers en ander ongemak wist je steeds nieuwe projecten te verzinnen tot je op een dag vroeg of ik misschien wat metinkjes aan rotaxanen uit het DRUM-project wilde doen. Vanaf dat moment kreeg mijn onderzoek vleugels. Je gaf me alle vrijheid, maar bleef altijd zorgvuldigheid eisen. Je gezonde wantrouwen tegen mijn dit-is-te-mooi-om-waar-te-zijn resultaten hebben me steeds gemotiveerd om nog betere experimenten te doen.

Dan wil ik uiteraard mijn promotor, Jan Verhoeven, bedanken. Beste Jan, jouw indrukwekkende vakkennis en enthousiasme voor de wetenschap hebben mij altijd enorm geïnspireerd. Menigmaal heb je met wat simpele krabbels op een servet of schoolbord een flits van inzicht weten te bewerkstelligen.

Mijn promotie-onderzoek in de OPM-groep begon ik niet als *tabula rasa*. Doordat ik eerder een hoofd- en bijvakstage had gelopen, had ik al enige ervaring en kennis op fotofysisch gebied opgedaan. Alle oud-OPMers uit die tijd, maar in het bijzonder natuurlijk mijn begeleider Xavier Lauteslager, wil ik daarvoor hartelijk bedanken.

In de afgelopen jaren zijn er verder een groot aantal mensen in de OPM-groep geweest die een bijzondere bijdrage aan mijn onderzoek hebben geleverd. Om te beginnen, John van Ramesdonk, die mij wegwijs maakte in het laserhok (use brains!) en me daarna nog vele malen heeft geholpen met de onvermijdelijke technische problemen van de laserspectroscopie. John, bedankt. Then, I would like to thank Céline Frochot. We both started to work with rotaxanes around the same time, and for long we were the only ones working with

rotaxanes in our group. I enjoyed doing experiments together, but also the singing and partying.

Dan ben ik veel dank verschuldigd aan al die andere OPMers die er voor zorgden dat promoveren nooit een saaie bedoening werd: Martijn Werts, naar eigen zeggen de uitvinder van de lunchclub, maar ook nooit te beroerd om al je data aan singuliere-waarde-ontbinding te onderwerpen; Mattijs Koeberg, cool, maar altijd vriendelijk, en tevens mijn redder in nood bij alle Mac-problemen; Marijn Goes, altijd de juiste wijn bij de betere klassieke muziek; Lene Hviid, met al haar prachtige Deens-Hollandse spreekwoorden, je moet me de bek niet openbreken; Jurriaan Zwier, de master; (Bischop) Piet Wiering; Stijn Berkhout, inmiddels versie 8.0.02; en verder Herman Fennema, Bert Bakker, Sandro Fazio, Natalia Haraskiewicz en Jacob Baggerman. Daarnaast alle studenten die ons lab bevolken en bevolkten: Katrien, Niels, Lucy, Marcel D., Marcel B., Kees, Jelle, Roel, Bregje, Jochem, Dirkjan, Mattijs, Peter, Lou, Ron.

Ik heb verder het genoegen gehad om een aantal studenten te mogen begeleiden: Emile Rienks, Bas Zoon, Joost van Lier, Rik van den Ende, Rudi van der Laan, en Robin Leguijt. Het was ontzettend leuk en leerzaam om jullie aio te zijn. Helaas staat lang niet alles wat jullie gedaan hebben in dit proefschrift, maar jullie experimenten en berekeningen zijn bijzonder waardevol geweest voor ons begrip van die rare rotaxanen.

The research described in this thesis is only a small part of a large European network: the DRUM project (Development of Rotaxane-based Unconventional Materials). At the heart of this network is David Leigh, the leader of the synthetic group at the University of Warwick. I would like to thank him for supplying us with all these beautiful rotaxanes. Needless to say, I am forever indebted to the people working in his group, the mama's and the papa's of these wonderful molecules: Angeles Farrán Morales, Francesco Gatti, and Thomas Futterer, who did a magnificent job, synthesising these compounds. Within the network, we furthermore co-operated with the electrochemistry group of Francesco Paolucci at the Univerity of Bologna. I would like to thank him and his group for sharing their results on the naphthalimide rotaxanes and for the many discussions that followed.

I have very dear memories of all the DRUM meetings in beautifull places like Lipari and Nice. Not many Ph.D.'s get the chance to regularly meet so many young scientist from such different places and disciplines. It was both scientifically stimulating and great fun. Thank you all.

Twee andere Nederlandse *principle investigators* van het DRUM team wil ik op deze plaats ook bedanken: Wybren Jan Buma voor zijn bijdragen aan hoofdstuk 2, en Hans Hofstraat (Philips) voor zijn hulp met de fotolabiele rotaxanen uit hoofdstuk 3.

Bij de SPC metingen heb ik veel technische ondersteuning gekregen van Dick Bebelaar. De analyse van die data zou onmogelijk geweest zijn zonder de geavanceerde, mathematische analyses van Ivo van Stokkum.

Verder heb ik vaak en dankbaar gebruik gemaakt van de kennis en kunde van een groot aantal UvA-medewerkers: Marijke Duyvendak, Ankie Koeberg en Rickey Tax (bibliotheek), Gerrie Braspenning en Ron Groenestein (glasblazerij), de mannen van de technische werkplaats, Mohammed en later Jaap van de kantine, Willem, opgevolgd door Iwan van het magazijn, Hans (bestelbonnen en declaraties), Jan Geenevasen (NMR), Joep voor alle electronica, en Ronald onze portier.

Er zijn uiteraard nog meer mensen die mijn dank verdienen: de leden van mijn promotiecommissie, Paula van der Heijdt voor het ontwerpen van het fraaie omslag, alle fotonische collega's uit de anorganische en fysische stallen en de collega's van de synthetisch organische en bio-organische werkgroepen.

Aan het einde van deze lange opsomming wil ik alle mensen buiten de muren van de faculteit bedanken: vrienden, bekenden, familie en dan in het bijzonder mijn lieve ouders en zus. Jullie vriendschap, liefde en steun zijn altijd heel belangrijk voor me geweest. Tot slot, lieve Theo, wil ik jou bedanken voor je humor, je aanmoedigingen, maar bovenal voor de liefde die je in mijn leven bracht.

Sjors Wurpel
Amsterdam, 1 mei 2001